School of Civil, Environmental and Land Management Engineering
Master of Science in Civil Engineering

POLITECNICO
MILANO 1863

A CONDENSATION PROCEDURE FOR CREEPING LANDSLIDES DESCRIPTION IN NATURALLY CEMENTED MATERIALS

Supervisor: Prof. Claudio Giulio di Prisco
Assistant supervisor: Ing. Luca Flessati

Master thesis of:
Orfano Maria Matr. 894078

Academic year 2019-2020

Contents

Acknowledgments

At the very end of my way at Politecnico I am still uncertain about who I want to thank. Maybe I only need to thank all the obstacles I met, all the defeats and people who tried to hinder me and to make me feel mediocre. Thanks to all these things I realized who I don't want to be and I focused on my weak points, so I gained a lot of strength to move on when life does not go as expected.
Anyway, certainly, I am very grateful to Professor Claudio di Prisco and Ing. Luca Flessati, because they guided me in this complex and stimulating work, that gave me the possibility to exploit a little bit of my creativity and because they have infused me passion for geotechnics, starting from the third year of my course of study.

A Marcella e a chi non ha mai smesso di credere nella mia creatività

Abstract

Creeping landslides in naturally bonded soils need a careful study, due to the complexity of this class of materials, characterized by a strain softening and viscous behaviour. In particular, after crack propagation occurring locally in the material, a progressive failure, leading to an unexpected slope collapse may occur.
In literature models for creeping landslides description exist, but they cannot reproduce the landslide inception phase; for this reason a new model capable of reproducing the onset of instability was developed in this thesis.
The reference point for the model development and calibration is a numerical model integrating strain softening elastic-plastic and elastic-viscoplastic constitutive relationships under simple shear conditions. The equivalent model will be developed in the elastoplastic case and then extended to the strain softening viscoplastic case, considering a stress path deriving from water table level change.
Particular attention will be given to the role played by the structural hardening in a constrained soil element. Its influence on the slope response will be remarked and it will be introduced in the new model.
Finally, the influence of the soil parameters spatial variability will be studied.

Introduction

Creeping landslides are characterized by slow downward movements and, in most cases, their evolution is governed by seasonal phenomena (e.g. seasonal rainfalls, snow melting...) periodically taking place. These perturbations are often the cause of unexpected collapses.
The class of landslides analyzed in this thesis is typical of cemented materials, which are characterized by interparticle bonds, conferring to the material both cohesion and tensile strength.
Locally a loss of cohesion may verify in the material and, when the local failure occurs, the stresses are transferrred to the surrounding portions of the domain, that subsequently may reach failure. This chain of events, which is delayed in time due to the viscoplastic nature of cemented materials, is called progressive failure mechanism and may bring to an instability phenomenon characterized by strains and displacements acceleration. This kind of catastrophic events may occur after different mechanical perturbations: one of the most typical, that will be subject of this thesis, is the water table level change. The increase and decrease of the water table level promotes in time the onset of material damage and cohesion degradation.
Some 1D rigid-viscoplastic models for creeping landslides description exist, but they are capable only to describe the reactivation phase and not the landslide inception phase.
The aim of this thesis is the development of a new 1D viscoplastic equivalent model capable of reproducing the creeping landslide evolution, from the inception phase to the reactivation phases. In the new 1D model the hypothesis of rigid-viscoplastic model is removed: the new model is a strain hardening elastic-viscoplastic model and the system will be studied at the REV scale.
The idea of this approach is providing a simple way of studying slope stability problems deriving from creeping landslides in naturally bonded materials. In the 1D equivalent model the constitutive equations do not have to be integrated and the number of static parameters needed for slope stability analyses is reduced.
The model is conceived and calibrated on the basis of numerical simulations, in which both elastoplastic constitutive model and strain softening visoplastic constitutive model are integrated under simple shear conditions (SSC).
All the analyses are based on a stress path deriving from water table level change. The problem is studied by following two steps: the first step implies the use of an elastoplastic constitutive law. For the sake of simplicity, the model has been initially defined and calibrated by considering an elastic-perfectly plastic case.

The second step is the extension of the 1D elastoplastic code to the strain softening viscoplastic case: the removal of consistency law, according to the viscoplastic theory, makes possible also the study of softening regime.
As it was previously mentioned, the model is 1D, meaning that is capable of reproducing the response of infinite long slopes. In this case, along the slope direction, the material properties and the material response do not change. Actually, along the slope direction the material parameters are not homogeneous, so the influence of their spatial variability will be shown, in order to understand the difference between the response of the slope with the parameters mean values and the mean slope response. To do so some analyses under simple shear conditions will be performed with an elastic law, an elastic perfectly-plastic law, a strain softening elastoplastic law and a strain softening viscoplastic law.
In Chapter1 an overview of i) cemented materials microstructural and mechanical features and ii) of the constitutive models used to reproduce their behaviour is provided. In particular the time-dependent behaviour of this class of materials is remarked, highlighting the time evolution of microcracks.
In Chapter2 creeping landslides are described and the displacement trends characterizing their evolution are reported. The process of shear band propagation bringing to the slope collapse will be analyzed. Moreover, the already existing 1D lumped models are described.
Chapter3 is devoted to the description of the elastoplastic slope response, with particular attention to structural hardening phenomenon. The SSC model is described and the passages for 1D model construction, calibration and validation are shown. All these passages are extended to the viscoplastic law and to the strain-softening viscopalstic law in Chapter 4. In addition, in Chapter4, the comparison between the 1D equivalent model object of this thesis and the already existing 1D lumped model for creeping landslides description is shown.
In Chapter6 the influence of the parameters spatial variability is shown.

Chapter 1

Bonded materials: relevance of microstructure on the mechanical behaviour

Cemented materials have many substantial microstructural differences with respect to a unbonded assembly of grains forming a soil.
Cemented materials and soft rocks often have a more rigid structure than remoulded soils: diagenetic bonds develop between grains, so that a material with a matrix, a solid skeleton and relatively stable structure is formed. In general, these bonds are formed naturally, through diagenesis or geological processes of temperature/pressure increase. They affect the behaviour of such kind of soils in various ways: they can be subjected to changes in time due to hydraulic, chemical or physical processes. Moreover, thanks to chemical bonds, soil acquires tensile strength. Since bonds are often fragile in nature, they also develop a collapsable structure that may give rise to unexpected instabilities.
The study of cemented materials microstructure is very important for the understanding of their behaviour, which does not only depend on the loading history but also on the chemical processes. Chemical reactions are actually governing the formation and destruction of the intergranular bonds, even in absence of perturbations.
In this chapter, the main features of cemented materials bahaviour will be outlined. Their degradation in time will be conceptually explained, referring to the constitutive relationship proposed in [Nova et al., 2003], conceived for cemented materials, considering the bonds as an internal variable evolving while the material is progressively damaged. For sake of simplicity, it is assumed that degradation, whatever its cause may be, affects internal variables and not other material properties, such as elastic moduli or critical state line.
In this chapter cemented materials microstructure, modes of failure, damage phenomenon and creep behaviour will be described.

1.1 Intergranular bonds

Cemented materials are natural soils that possess a structure deriving from processes taking place in their geological life. The term "structure" was firstly introduced in clays as being the combination of bonding and fabric. For a coarse-grained soil, bonding can only take the form of interparticle cementing, since interparticle forces are negligible.
Naturally cemented materials, such as calcarenites and silica sandstones, can be also classified as soft rock, because they have a solid structure, but less strength with respect to an hard rock.
Calcareninte consists of a medium carbonate sand of biogenetic origin bonded by calcium carbonate and represents a material with weak grains bonded by a quite strong cement. The grains of these soft rocks are formed by dead calcareous organisms (shells, corals and other calcareous organic structures) accumulated at the same marine environment. The cement precipitated from the saturated sea water during or soon after deposition, preventing large strains from developing in the soil under the increase of overburden stress: the result is a soil having low density and open fabric.
As an example of silica sandstone, the one described in [Coop and Cuccovillo, 1997] will be reported. It is a medium quartz sand bonded with ion oxide and is thus characterized by strong grains bonded by relatively weak cement. This weak rock was deposited in a shallow water marine environment, the cement is formed in the later stages of the diagenesis, when the environmental conditions favoured the precipitation from the groundwater flowing through the sediments. Prior to the cement deposition, high overburden pressure had caused a substantial increase in density leading to the development of a well defined fabric that can be seen in the scanning electron micrographs in Figure1.1. This fabric is characterized by the large area of the intergranular contacts. The iron oxide appears white and, for the grains in contact, the cement coating is likely to weld the grains together. [Dapples, E., 1972] observed that iron oxide in silica sands provides only weak bonding because of its poor adherence to the quartz grains.

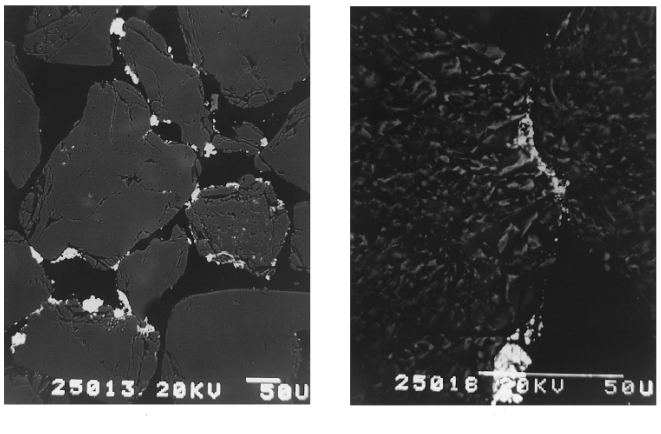

Figure 1.1: Scanning electron micrographs of the silica sandstone with different degrees of magnification

[Ciantia and Castellanza, 2016], through a microstructural analysis, individuated the main kinds of intergranular bonds that could be found in a structured soil. To individuate the microscopic bonds nature ([Ciantia and Di Prisco, 2016]) performed a complete set of microinvestigations by means of X-ray micro-computer-tomography (MTC) scanning electron microscope (SEM) analyses. In Figure1.2 a typical thin-section obtained from samples hardened with epoxy resin are photographed by means of an high resolution camera connected to an optical microscope, while in Figure1.3 SEM images of 3D microstrucures of different Calcarenites are reported.

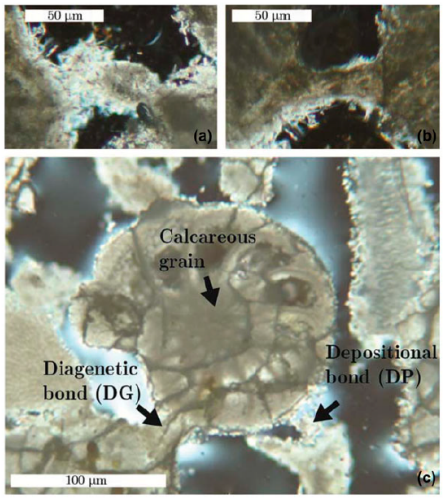

Figure 1.2: Typical thin-section obtained at an optical microscope where diagenetic bonds (DG) and depositional bonds (DP) are clearly visible

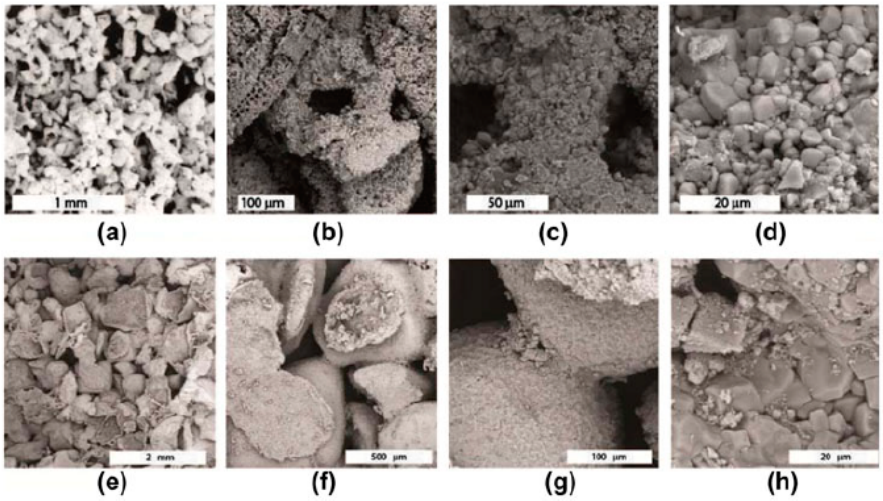

Figure 1.3: SEM images of 3D microstructure with different magnifications: (a-d) Calcarenite from Gravina di Puglia,(e-h) Calcarenite from Gallipoli

By observing the material at the miscro scale two different types of bonds between grains can be recognized:

1. *diagenetic bonds (DG)*, identified as the bonds formed during diagenesis. During the sedimentation process, the grain themselves are filled with the same calicite crystals forming DG. For this reason, at the polarized light microscope these bonds usually appear totally similar to the grains (Figure1.2);

2. the second type of bonds, named *depositional bonds (DP)* is composed by less densely packed material formed by small calcite micrograins.

Often a bond is the result of the superimposition of these two kinds of miscrostructures, as the surface of DG is usually covered by a layer of loosely packed microcrystals.
From what already observed comparing calcarenites and silica sandstones, emerges that the behaviour of the material is strictly dependent on the mineralogy and on the type of interparticle bonds. Nevertheless, for sake of simplicity, such a dependence will be neglected in this thesis.

1.2 Local failure mechanisms

In cemented materials the fundamental microstructural variables are: porosity, directional characteristics of the structure (i.e. inherent anisotropy) and bonds stability. Differently from soils, cemented materials have their own shape, even if

confining pressure is not applied. Each microstructural evolution and the consequent development of irreversible strains are necessarily linked to the intergranular bonds damage.
Structured materials have three fundamental modes of failure:

- *Tensile failure*: this fragile mode of failure can be also called splitting mode, as it is characterized by fractures development: during the process grains lose contact and cannot contrast the evolution of instability (Figure1.4a);

- *Shear failure*: it develops when the state of stress bringing to instability is characterized by a slightly larger confining pressure with respect to the splitting mode. The shear mode is characterized by the developing of strain localization which induces the formation of a shear band and the damage of the material (Figure1.4b).
  In Figure1.5 samples after triaxial compression tests on uncemented soils (a) and artificially cemented sands (b) ([Amini and Hamidi, 2014]) can be seen at three different confining pressure ($p_c = 50, 100, 150kPa$). All cemented samples show barreling mode of failure without shear plane formation. In cemented samples initially the mode of failure is a combination of barreling shape and shear plane, but increasing the confining pressure, the shear band is more evident and inclined with respect to the horizontal plane;

- *Volumetric instability*: in case of very porous materials, if the confining pressure increases, the grains can damage and, to reach a new equilibrium condition, a reduction of macro voids volume is necessary. This brings to an unstable process characterized by a sharp decrease of void ratio associated with the formation of a compaction band (Figure1.4c). An example of compaction band after a triaxial test on calcarenite can be seen in Figure1.6.

For the sake of simplicity, in this thesis only the case of an infinite slope is considered and, therefore, only shear failure mode is considered.

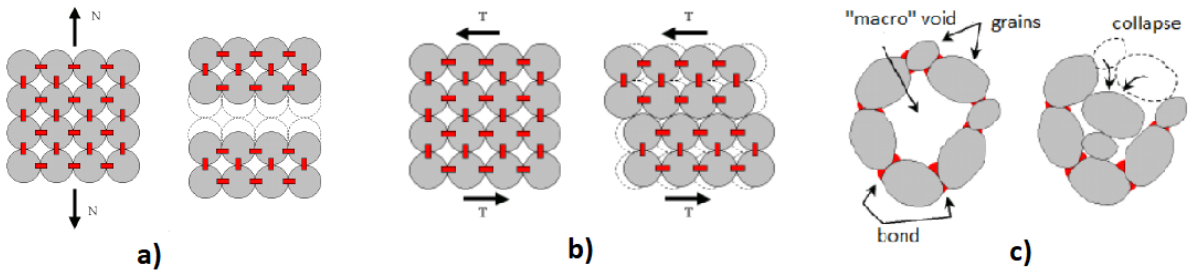

Figure 1.4: Microstructural evolution for a) tensile mode of failure b) shear mode of failure c) volumetric mode of failur

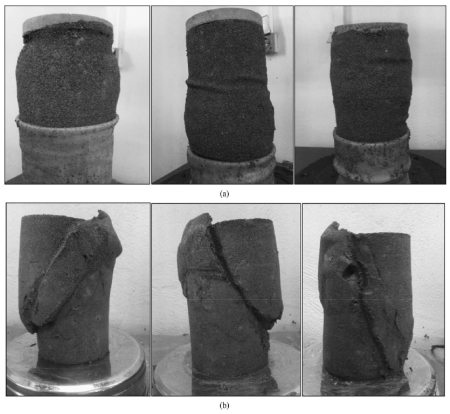

Figure 1.5: Failure modes of tested samples. (a) Barreling mode in the uncemented samples; (b) shear zone in the cemented samples

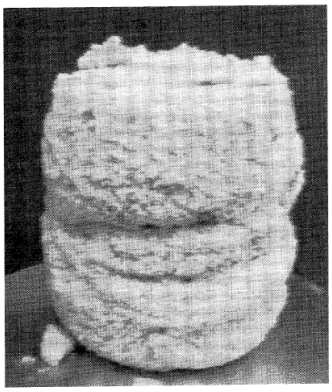

Figure 1.6: Sample with a compaction band after a triaxial test on calcarenite ([Lagioia and Nova, 1995b])

It can be experimentally shown that there is a relationship between confining pressure, imposed stress path and the mode of failure and it will be shown later on. It is possible to study experimentally the damage phenomenon recording during the tests acoustic emissions associated to a generic loading path ([di Prisco, 2012b]). These emissions are due to the progressive failure of bonds and to the release of the accumulated elastic energy. Damage modifies the material response: for instance, referring to a uniaxial compression test (Figure1.7) it is evident that along the loading-unloading paths, in the post peak phase, a progressive reduction of material stiffness verifies.
During the loading process initial elastic deformation involves the stretching of molecular bonds and frictional sliding between surfaces of any existing small cracks. New cracks appear as the peak stress is approached and continue to open and grow at the peak shear strength until they link together to form a major plane of failure.

The shear resistance abruptly decreases to a residual value determined by sliding friction angle along the new failure plane.

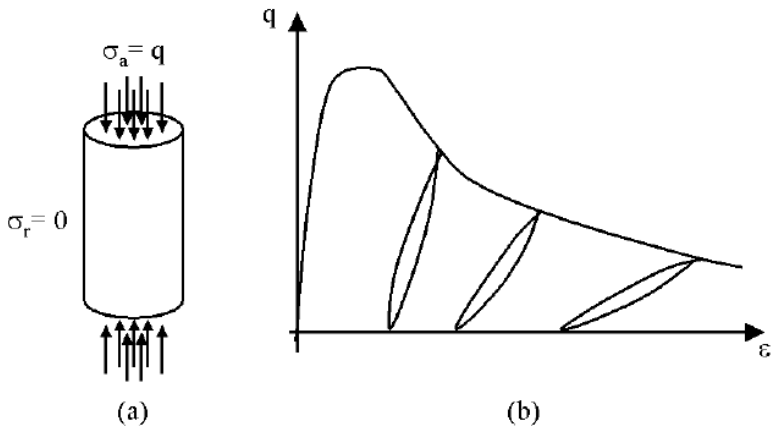

Figure 1.7: (a) sketch of a uniaxial compression test (b) stress-strain curve for a cyclic uniaxial compression test in displacement control conditions

The material damage can be also translated in a decrease in shear stiffness with strains. This aspect is shown in some monotonic triaxial tests performed in [Sharma and Fahey, 2003]. G_0 is the initial tangent stiffness and the secant shear modulus G_{sec} in a monotonic test is defined as the gradient of the straight line passing through the origin and the point corresponding to a particular stress or strain amplitude on the $q - 3\varepsilon_s$ curve (Figure1.8a)), where $q = (\sigma_1 - \sigma_3)$ is the deviator stress and $\varepsilon_s = 2/3(\varepsilon_1 - \varepsilon_3)$ is the deviatoric strain.
In Figure1.8b) the variation of G_{sec} with ε_s obtained from undrained triaxial tests performed on cemented sands at $p_0 = 200, 600\, kPa$ respectively can be seen. The samples are consolidated below the isotropic yield stress, so no significant breakage of bonds during the consolidation phase occurs. The data show that there is a threshold yield strain $\varepsilon_{s,yield}$, which separates the plateau of initial constant stiffness from the start of substantial stiffness degradation. As previously observed, a decrease of stiffness with shearing occurs. This decrease is also influenced by the confining pressure: the sample consolidated at $p'_0 = 600kPa$ shows more gradual degradation of stiffness compared with the sample consolidated ad $p'_0 = 200kPa$, although ε_y was about 0.0002 for both samples. This suggests that even for samples consolidated below the yield stress, the consolidation pressure has an effect on the mechanism of bond degradation and stiffness degradation during shearing.

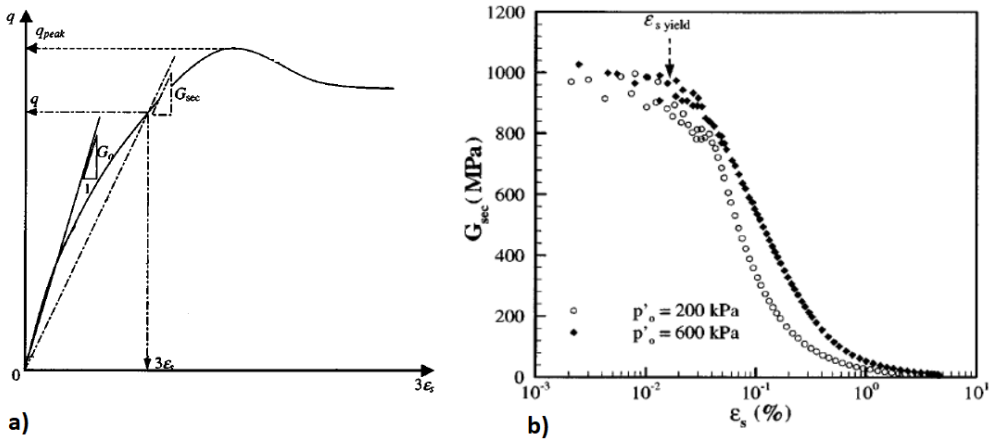

Figure 1.8: a) Symbols and definitions for a monotonic test b) variation of G_{sec} with deviatoric strain amplitude for cemented samples

1.2.1 Mathematical modelling of cemented material behaviour

To better understand the previously cited modes of failure, [Nova et al., 2003] constitutive model for cemented materials is reported as a reference.
For the sake of simplicity, the material is assumed to be isotropic. The constitutive relationship is elastic plastic and characterized by a strain hardening.
As suggested by [Nova, 1992],[Nova, 1986] the main difference between an intact soft rock and a granular soil lies in that for soft rocks, contrary to soils, the initial elastic domain is not related to the previous loading history (i.e preconsolidation) but rather exists by itself and its size is linked to the strength of bonds.
The second hypothesis is that the additivity holds: strains are given by the sum of an elastic reversible component and a plastic irreversible component

$$\dot{\varepsilon} = \dot{\varepsilon}_{ij}^{el} + \dot{\varepsilon}_{ij}^{pl}. \tag{1.1}$$

The elastic behaviour of the material is defined postulating that a strain energy function $\psi(\varepsilon^e)$ exists such that:

$$\sigma_{ij}\left(\varepsilon_{ij}^{el}\right) = \frac{\partial \psi}{\partial \varepsilon_{ij}^{el}}\left(\varepsilon_{ij}^{e}\right), \tag{1.2}$$

from which, by differentiation, the following law can be obtained.

$$\dot{\sigma}_{ij} = D_{ij,hk}(\varepsilon_{hk}^{e})[\dot{\varepsilon}_{hk} - \dot{\varepsilon}_{hk}^{p}], \tag{1.3}$$

where the elastic stiffness $D_{ij,hk}^{e}$ is given by:

$$D_{ij,hk}^{e} \equiv \frac{\partial^2 \psi}{\partial \varepsilon_{ij}^{el} \otimes \partial \varepsilon_{ij}^{el}}. \tag{1.4}$$

The elastic moduli are assumed not to be affected by accumulated plastic strains (which means by mechanical destructuration), by weathering or by non mechanical actions. This is clearly another very strong assumption, introduced again for sake of simplicity.
Irreversibility is introduced by requiring the state of the material, defined in terms of the stress components σ_i and the set of internal variables q_i,to belong to the set:

$$E_\sigma := \{(\sigma_{ij}, q_i) | f(\sigma_{ij}, q_i) \leq 0\}. \tag{1.5}$$

where f is the yield (or loading) function. The internal variables q_i, are assumed to depend on the history of the material element, via the accumulated plastic strain tensor ε^p_{ij}, and a set of scalar internal variables θ_i taking into account the degradation caused by all the non-mechanical effects, like chemical degradation, temperature. Neglecting for sake of simplicity the chemical actions, the internal variable vector will be only a function of accumulated plastic strains:

$$q_i = q_i(\epsilon^p_{ij}). \tag{1.6}$$

The evolution of internal variables is provided by the following generalized hardening law

$$\dot{q}_{ij} = \frac{\partial q_i}{\partial \varepsilon^p_{ij}} \dot{\varepsilon}^p_{ij}. \tag{1.7}$$

According to the standard theory of plasticity, plastic strain rates are defined by the following non-associative flow rule:

$$\dot{\varepsilon}^p_{ij} = \dot{\Lambda} \frac{\partial g}{\partial \sigma_{ij}}, \tag{1.8}$$

where $g(\sigma_{ij}, q_i)$ is the plastic potential and $\dot{\Lambda} \geq 0$ is the plastic multiplier. The loading/unloading conditions are prescribed in terms of the so-called Kuhn Tucker complementary conditions:

$$\dot{\Lambda} \geq 0 \qquad f(\sigma_{ij}, q_i) \leq 0 \qquad \dot{\Lambda} f(\sigma_{ij}, q_i) = 0, \tag{1.9}$$

which imply that plastic loading can occur only for states on the yield surface $(f = 0)$. In the plastic loading (i.e for $\dot{\Lambda} = 0$) the following consistency condition holds:

$$\dot{f}(\sigma_{ij}, q_i) = 0. \tag{1.10}$$

Combining Equation1.10 with the elastic constitutive Equation1.3 and the flow rule 1.8, the following expression of plastic multiplier is obtained:

$$\dot{\Lambda} = \frac{1}{K_p} \frac{\partial f}{\partial \sigma_{ij}} D^e_{ij,hk} \dot{\varepsilon}_{ij}, \tag{1.11}$$

where

$$K_p \equiv \frac{\partial f}{\partial \sigma_{ij}} D^e_{ij,hk} \frac{\partial g}{\partial \sigma_{ij}} + H > 0 \qquad H \equiv -\left(\frac{\partial f}{\partial q_i}\frac{\partial q_i}{\partial \varepsilon^p_{ij}}\right)\frac{\partial g}{\partial \sigma_{ij}}. \tag{1.12}$$

In Equation1.12 H is the so-called hardening modulus, which can be either positive (hardening regime) or negative (softening regime), while K_p must be always positive by hypothesis, this apect will be better discussed in Appendix B. Imposing the constraint of K_p positiveness a condition on the hardening modulus can be found:

$$H > -\frac{\partial f}{\partial \sigma_{ij}} D^e_{ij,hk} \frac{\partial g}{\partial \sigma_{ij}} = H_c, \tag{1.13}$$

where H_c is the subcritical softening modulus, as defined by [Maier, 1966]. As also outlined in Appendix B, when $H = H_c$ the determinant of the compliance matrix is zero, which implies the loss of uniqueness of the incremental response even under full strain control.
The yield function and the plastic potential are isotropic, thus depends on three invariants defined as:

$$p \equiv \frac{1}{3} tr(\sigma_{ij}) \qquad q \equiv \sqrt{\frac{3}{2}} ||s_{ij}|| \qquad S \equiv sin\big(3\theta\big) = \sqrt{6}\frac{tr(s^3_{ij})}{\big[tr\big(s^2_{ij}\big)\big]^{3/2}}, \tag{1.14}$$

where p is the mean pressure, q is the stress deviator, proportional to the norm of the deviatoric part of the stress tensor s_{ij}, and S is a trigonometric function of the Lode angle θ.
The yield surface and the plastic potential of this model have the following expression:

$$\begin{cases} f = A_f^{K_{1f}/C_f} B_f^{-K_{2f}/C_f} p^* - p^*_{cf} = 0 \\ g = A_g^{K_{1g}/C_g} B_g^{-K_{2g}/C_g} p^* - p^*_{cf} = 0 \end{cases} \tag{1.15}$$

where, considering $h = f$ or $h = g$

$$\begin{cases} K_{1h} = \frac{m_h\left(1-a_h\right)}{2\left(1-m_h\right)}\left[1 + \sqrt{1 - \frac{4a_h\left(1-m_h\right)}{m_h\left(1-a_h\right)}}\right] \\ K_{2h} = \frac{m_h\left(1-a_h\right)}{2\left(1-m_h\right)}\left[1 - \sqrt{1 - \frac{4a_h\left(1-m_h\right)}{m_h\left(1-a_h\right)}}\right] \end{cases} \tag{1.16}$$

$$A_h \equiv 1 + \frac{1}{K_{1h} M_h(S)} \frac{q}{p^*} \tag{1.17}$$

$$B_h \equiv 1 + \frac{1}{K_{2h} M_2(S)} \frac{q}{p^*} \tag{1.18}$$

$$C_h \equiv \big(1 - m_h\big)\big(K_{1h} - K_{2h}\big) \tag{1.19}$$

$$p^* \equiv p + p_t \qquad p^*_{cf} \equiv p_s + p_m + p_t \qquad p_t = k p_m. \tag{1.20}$$

The function $M_h(S)$ appearing in Equations1.17 and 1.18 are given by [Van Eekelen, 1980]:

$$M_h(S) = M_{ch} c_{1h} \big(1 + c_{2h} S\big)^{nh} \tag{1.21}$$

$$c_{1h} \equiv \frac{1}{2^{n_k}} \big[1 + (c_{Mh})^{1/n_h}\big]^{n_h} \tag{1.22}$$

$$c_{2h} \equiv \frac{1 - (c_{Mh})^{1/n_h}}{1 + (c_{Mh})^{1/n_h}}. \tag{1.23}$$

In the above expressions $k = p_t/p_m$, the quantities a_h, m_h, M_{ch}, c_{Mh} and n_h are material constants. In Equations 1.22 and 1.23. c_{Mh} represents the ratio between M_{eh}/M_{ch}, between the values of the function M_h in triaxial extension ($S = -1$) and compression ($S = 1$), respectively.
The yield function shape is shown in Figure1.9.
So the surface is defined in the triaxial plane with q-p variables, while there is a dependence also on the Lode angle. This surface is not passing from the axes origin as cemented materials have a certain amount of tensile resistance due to the intergranular bonds. The scalar quantities p_c, p_m and p_t represent the internal (hardening) variables describing the effects of the previous (mechanical) loading history. The hardening variable p_c defines the size of the yield function that the material would have in absence of intergranular bonds, so it plays the role of pre-consolidation pressure, p_t represents the increment in isotropic traction resistance due to the bonds and p_m is the increment in isotropic compression resistance. It is reasonable to assume that p_t and p_m are related by the following expression:

$$p_t = \frac{p_m}{10}. \tag{1.24}$$

The yield surface dimension is thus governed by the hardening variables p_t and p_c. It is important to remark that owing to p_t and p_m:

1. the material is characterized by a non-negligible traction resistance;

2. the material is characterized by a certain shape (even for nil confining pressuers);

3. initially the image point of the state of stress is expected to lie inside the yield surface.

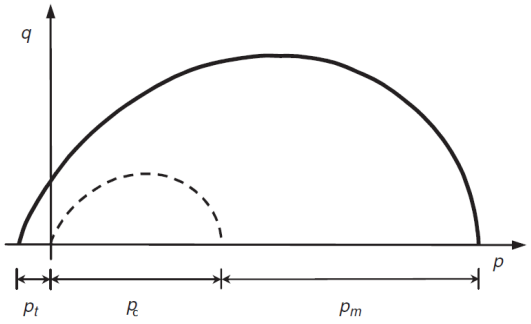

Figure 1.9: Reference failure surface for cemented materials

At the microscopic level, there are many agents causing a progressive destruction of intergranular bonds ([Castellanza, 2002]), such as weathering and the development of irreversible strains. By collecting qualitatively all the information about structured materials [Castellanza et al., 2002] show in the triaxial plane the failure loci for different degrees of weathering of granite (Figure1.10a) and it is possible to conclude that the most relevant consequence of damage is the progressive reduction of the size of the initial elastic domain (Figure1.10b).

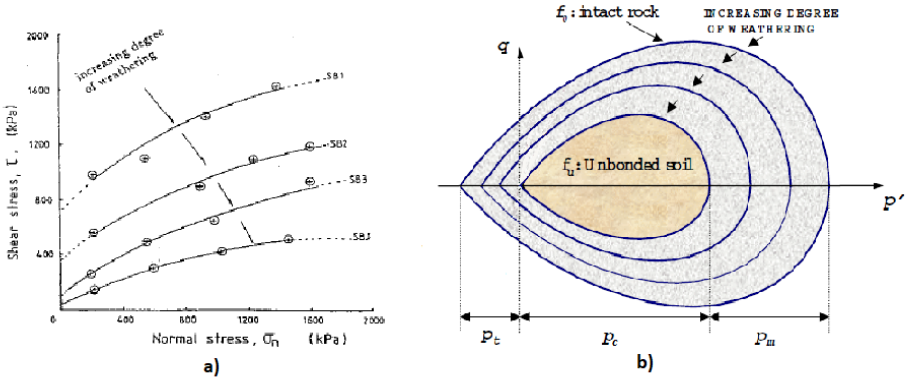

Figure 1.10: a) Failure loci in direct shear tests for different dergess of weathering of granite (after [Kimmance, 1988]); b) decay of uniaxial strength with respect to weathering degree (after [Baynes and Dearman, 1978]); c) yield loci for rock at different degree of weathering (after [Castellanza et al., 2002])

The microscopic destructuring of bonds is translated with the evolution of scalar variables p_t, p_c and p_m, decreasing as plastic strains are accumulated. Under the assumed hypothesis of material isotropy, the evolution of p_c is associated with the invariant of the plastic strain rates $\dot{\varepsilon}_v^p$ is the volumetric part of plastic deformation and $\dot{\varepsilon}_s^p$ is the deviatoric part of plastic deformation, which reflect the macroscopic effects of irreversible fabric modification. As in [Nova, 1977] it is assumed that the

following hardening law holds for p_c:

$$\dot{p}_c = \rho_s p_c\big(\dot{\varepsilon}_v^p + \xi_s \dot{\varepsilon}_s^p\big), \tag{1.25}$$

where ρ_s is the plastic logarithmic volumetric compliance and ξ_s is the dilatancy $d = \frac{\dot{\varepsilon}_v^p}{\dot{\varepsilon}_s^p}$ at the critical state i.e. for $H = 0$.
This hardening law can predict either hardening response (ductile) or softening response (fragile). The increment in plastic deviatoric strains $\dot{\varepsilon}_s^p$ is necessarily positive: it always gives a positive contribution to Equation1.25; the increment in deviatoric deformation $\dot{\varepsilon}_v^p$ is positive on the right of the peak of the plastic potential, giving a positive contribution bringing to hardening behaviour, while it is negative on the left. In this case, thanks to this negative contribution, given by the dilatancy developing on the left of the peak, Equation1.25 predicts a softening behaviour and so a decrease in the variable p_c.
The parameter p_m accounts for the effects of the interparticle bonding. The degradation of the bonds can occur for both mechanical and non-mechanical effects, like grain rearrangement or chemical dissolution (hereafter disregarded). The following evolution equation for the internal parameter p_m is reported:

$$\dot{p}_m = -\rho_m p_m\big(|\dot{\varepsilon}_v^p| + \xi_m \dot{\varepsilon}_s^p\big), \tag{1.26}$$

where ρ_m and ξ_m are material parameters controlling the rate of mechanical degradation of bonding.
According to the previously done considerations on $\dot{\varepsilon}_v^p$ and $\dot{\varepsilon}_s^p$ and due to the minus sign of Equation1.26, the variation of p_m always predicts a softening behaviour.
The combination of the two hardening laws given by Equations 1.25 and 1.26 permits to predict the previously cited modes of failure. For instance, under high confining pressure, yielding occurs for a stress state such that $\dot{p}_m < 0$, $\dot{p}_c > 0$, so the hardening modulus is positive. As a consequence, the degradation effect of debonding is compensated by the hardening of the material. Despite this, it may happen that the hardening of the material cannot compensate the degradation of bonds: in this case volumetrc instability occurs (compaction bands). In contrast, for low confining pressures, $\dot{p}_m < 0$ and $\dot{p}_c < 0$, so that $H < 0$: debonding and softening both contribute to the loss of strength ([Lagioia and Nova, 1995a]).
This model is capable of reproducing the experimental evidence showing that it is possible to define three different mechanical behaviours for three different zones of the yield surface (Figure1.11). Until the point representing the state of stress is inside the surface, the material behaviour is assumed linear and reversible, once the surface is reached, the structure of the material changes, according to the evolution of internal variables p_c, p_t and p_m. Zone A and C are respectively associated to tensile and volumetric mode of failure, while zone B is related to the mode of failure typical of the infinite slope configuration in cemented materials: shear failure.
If the stress path reaches the yield surface in zone B, strain localization and material damage is observed, but a part of the contact forces released by the bonds is

taken by the friction forces that directly develop between the grains. The hardening modulus, depending on the variation of the internal variables $\dot{p}_c$ and $\dot{p}_m$, is in this zone in between positiveness and negativeness, as can be seen in Figure1.12, which means that the behaviour may be either fragile or ductile. The higher the contact pressure, the more the system response progressively passes from fragile to ductile.

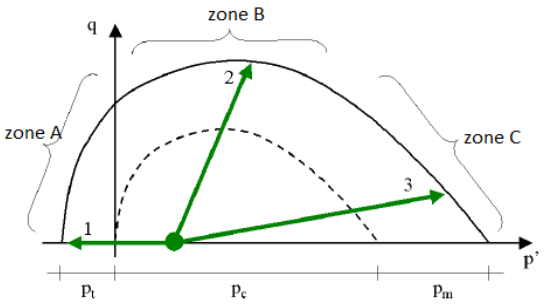

Figure 1.11: Failure surface for a cemented material in which the various areas corresponding to the different failure modes are remarked

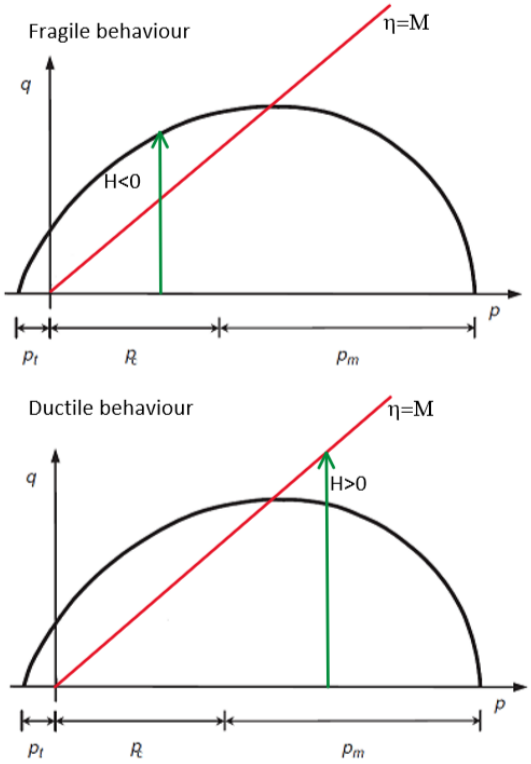

Figure 1.12: Ductile and fragile responses in terms of hardening modulus H

In zone B the shear failure is associated with the dilatancy development, this is due to the fact that this phenomenon characterizes the material behaviour on the left part of the zone B. Differently from tensile failure, shear failure is characterized by the development of a finite thickness process zone, in which the intergranular bonds are completely damaged; when this occurs, the material in this zone behaves as a granular material.
As an example of soil weathering with loading a specimen of soft rock in oedometric conditions subjected to a given constant axial stress is considered ([Castellanza et al., 2002]). Until the stress state reaches the shrinking yield surface (point A of Figure1.13) the behaviour of the material is elastic and no strain or stress changes occur; when the shrinking yield locus touches the point A, the stress state is forced to move towards an higher mean pressure and a lower deviator stress level, since the stress state cannot lie outside the yield locus. This in turn implies an increase of the radial stress. The process stops at point B in Figure1.13, when the degradation is achieved ([Ciantia and Castellanza, 2016]). As shown in Figure1.13 b), the hardening parameter p_c may increase during plastic loading, even if the size of the elastic domain is decreasing, due to the occurrence of positive plastic volume strains.

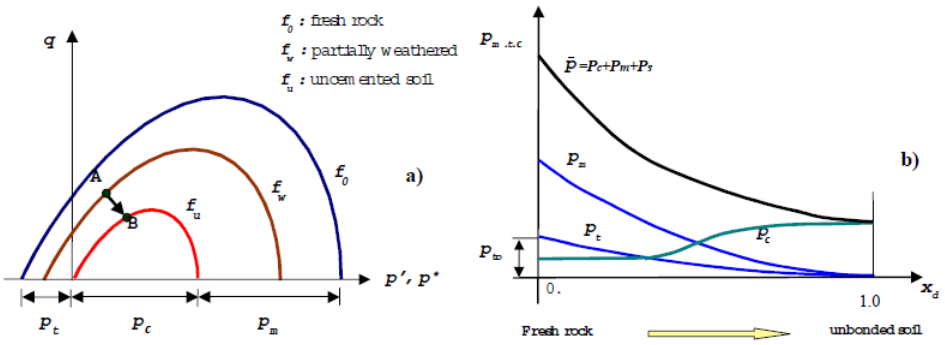

Figure 1.13: a) Evolution of the yield locus with weathering, the initial stress state begin represented by point A; b) evolution of the hardening variables with weathering

In Figure1.14 the predicted response in a displacement-controlled oedometric compression test is shown (from [Nova et al., 2003]). It can be observed that, for a certain value of the axial strain (point C in Figure1.14b), a rapid decrease of axial stress occurs. As it is clearly shown by the evolution of the internal variables illustrated in Figure1.14c, this is due to the strong destructuration, with large increase in p_m, induced by plastic strains. As this effect prevails on the increase in p_c associated with plastic volumetric compaction (at C $\dot{\varepsilon}_{ij}^{p} > 0$), a large reduction in size of the yield locus occurs after first yielding. Upon further deformation, the degradation of the material becomes less and less fast, until, at a certain state (virtually

when the original soft rock has been fully transformed to something equivalent to an unbonded non-cohesive soil), bond degeneration-induced softening vanishes and the vertical stress increases again due to volumetric hardening. From this point onwards, as the external loading is increased, the material behaves as a virgin soil with "locking" behaviour (i.e. stress increasing with stress) at a constant stress ratio.
Clearly, if the test was run under axial load control, at the peak of σ_a (point C) a sudden jump in the stress-strain response occurs and the point E in Figure1.14b is reached with a "snap through"-type of instability (actually the strain jump associated to the snap will be even larger than those shown in the figure, due to energy balance requirements).

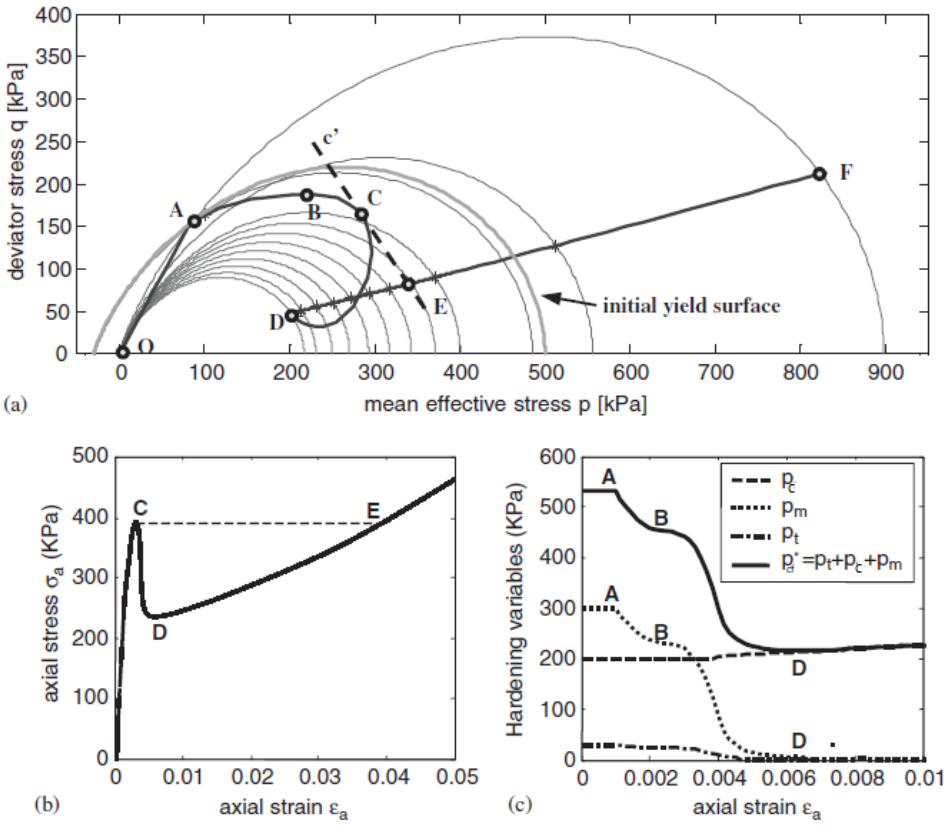

Figure 1.14: Predicted behaviour in a strain-controlled oedometric test on a bonded material from [Nova et al., 2003]: (a) stress path in the $q-p$ plane (point C corresponds to the maximum value of axial strain σ_a); (b) stress-strain response in $\sigma_a - \varepsilon_a$ plane;(c) evolution of internal variables

1.3 Creep

Cemented materials behaviour is characterized by a strong time dependence, due to the fact that their bonds can undergo damage in time if subjected to constant loading imposition.
As previously outlined, damage appears as particles debonding and crack propagation. According to fracture mechanics ([Atkinson, 1984]), under the assumption of linear elastic solid, in a medium a plane crack propagates once a critical stress is reached and it propagates at a speed approaching the one of sound.
Nevertheless, experimental evidences show that, in case of long-term loading, fissures propagate, although very slowly, at a stress level lower than the critical one: this phenomenon is called subcritical crack growth.
The fact that a level of stress bringing to failure can be reached for long-term loading is an evidence that the cemented materials behaviour is time dependent and it has to be studied in the framework of viscoplastic constitutive laws.

1.3.1 Creep: experimental evidence

To clarify the time dependent behaviour of cemented materials, a qualitative scheme of a creep test is followed ([di Prisco, 2012b]). A rock sample is subjected to a creep test along a standard triaxial compression stress path; the test is under load control conditions: the loading steps Δq are kept constant for time intervals equal to Δt (Figure1.15a); the results show that creep phenomenon can be characterized by three different phases (Figure1.15b):

1. For the first loading increments the behaviour is stable and strain accumulation reduces in time (*primary creep*):
   $\frac{\partial \varepsilon^2}{\partial^2 t} < 0$;

2. For a certain stress level a constant strain velocity for a relatively large time span is observed (*secondary creep*)
   $\frac{\partial \varepsilon^2}{\partial^2 t} = 0$;

3. The previous phase is precursory of a subsequent instability phase in which acceleration of strains occurs (*tertiary creep*):
   $\frac{\partial \varepsilon^2}{\partial^2 t} > 0$.

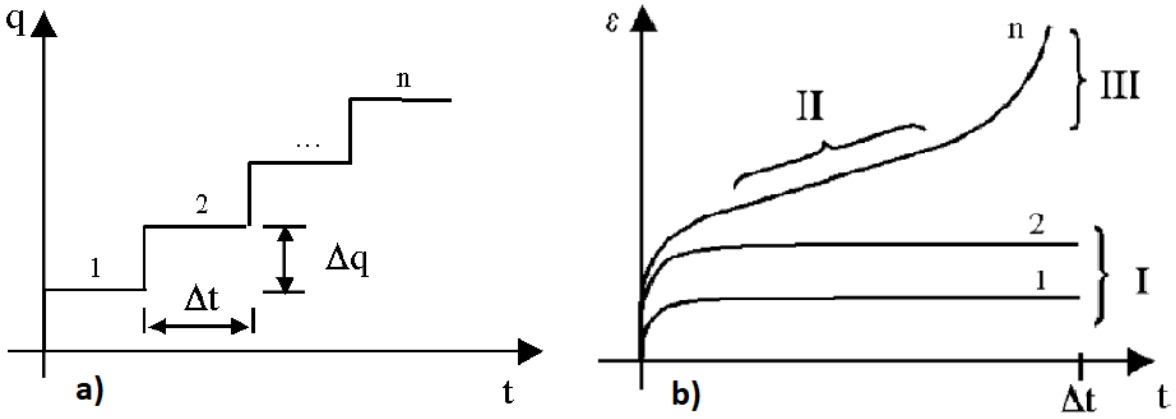

Figure 1.15: a) Loading history for a creep test b)strain-time behaviour showing the creep phases during a creep tes

In Figure1.16 the results of three creep tests on Darley Dale sandstone at different loading conditions from [Baud and Meredith, 1997] are reported.
The confining pressure (equal to $75MPa$) was applied first, and after setting the pore-fluid pressure (controlled at $45MPa$), the samples were loaded at a constant axial strain rate up to the desired level of axial stress. From that point, axial stress was maintained constant while axial strain were monitored continuously. The loading system was switched from strain-rate control to load control when the desired level of axial stress was reached. During the creep phase, fluctuations in the axial load were less than 1%.
Figure1.16 shows the three creep regimes previously described. The creep starts with a primary phase during which the strain rate is initially high but decreases with time. If the stress level is high enough (i.e. above 80% of peak stress), the primary phase is followed by the main phase of secondary (steady-state) creep. Time-dependent cracking plays the major role during this phase. Finally, all experiments end with a period of tertiary creep characterized by an exponential increase in strain rate leading to macroscopic failure.
The level of stress has a crucial effect on the creep rate and especially on the time-to-failure; from 30 minutes at 90% of the peak stress ($146MPa$), to about four hours at 85% ($138MPa$), and to almost a day at 80% ($130MPa$). In fact, the duration of all three creep phases increases with decrease in stress level. For example, the duration of the primary creep phase increases from only a few minutes for sample a), to about 30 minutes for sample b), and almost 3 hours for sample c). The primary creep rate decreases relatively rapidly to reach a stable value that marks the onset of secondary creep.

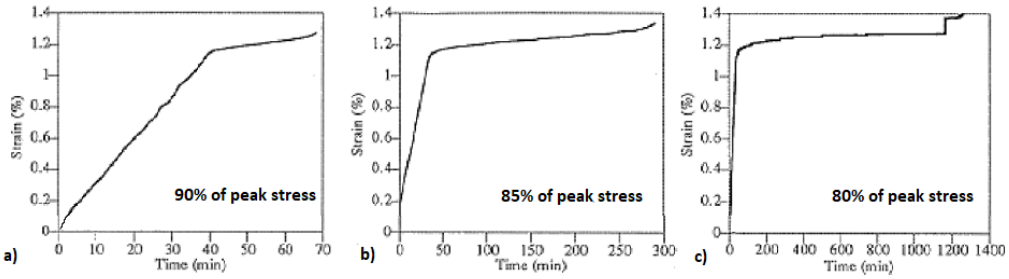

Figure 1.16: Strain against time for three experiments on Darley Dale sandstone: creep test at 90% of peak stress, creep test at 80% of peak stress, creep test at 90% of peak stress from[Baud and Meredith, 1997]

1.3.2 Constitutive modeling for creep

The elastoplastic constitutive model for cemented materials shown in the previous section is incremental: a strain variation is observed only after an effective stress state variation. Actually, the material behaviour shown in Figure1.15 cannot be reproduced with an incremental constitutive law. As a matter of facts, for time-dependent materials an increase of strains is not necessarily associated to an increase of effective stress and viceversa.
For this reason a different constitutive model has to be introduced. In literature various constitutive models have been proposed to simulate the time dependent behaviour of soils; due to its simplicity and flexibility an elastic-viscoplastic model (EVP) based on Perzyna's overstress theory will be here discussed ([Perzyna, 1963], [Freitas et al., 2013]).
The basic assumption of EVP models is that the total strain rate $\dot{\varepsilon}_{ij}$ is given by the sum of an elastic/reversible component and a viscoplastic/irreversible component:

$$\dot{\varepsilon}_{ij} = \dot{\varepsilon}^{el}_{ij} + \dot{\varepsilon}^{vp}_{ij}, \tag{1.27}$$

being the elastic stain increment $\dot{\varepsilon}^{el}_{ij}$ instantaneous and thus time/rate independent whereas the viscoplastic strain increment $\dot{\varepsilon}^{vp}_{ij}$ time dependent and irreversible.
According to the original viscoplastic theory proposed by [Perzyna, 1963], the viscoplastic strain increment can be evaluated as:

$$\dot{\varepsilon}^{vp}_{ij} = \eta \Big\langle \Phi\big(F\big) \Big\rangle \frac{\partial f_d}{\partial \sigma'_{ij}}, \tag{1.28}$$

where

$$\begin{cases} \big\langle \Phi\big(F\big) \big\rangle = \Phi\big(F\big) \ if \ F > 0 \\ \big\langle \Phi\big(F\big) \big\rangle = 0 \ if \ F \leq 0 \end{cases} \tag{1.29}$$

η is the fluidity parameter representing the time response of the system and Φ is called viscous nucleus and is a function of the overstress F, which is given by the following equation:

$$F = \frac{f_d}{f_s} - 1, \tag{1.30}$$

where f_d is the dynamic loading surface (i.e the loading surface passing through the current state of stress) and f_s is the static loading surface, that defines the region of time independent, pure elastic behaviour (i.e a a sort of yield surface), as sketched in Figure1.17.

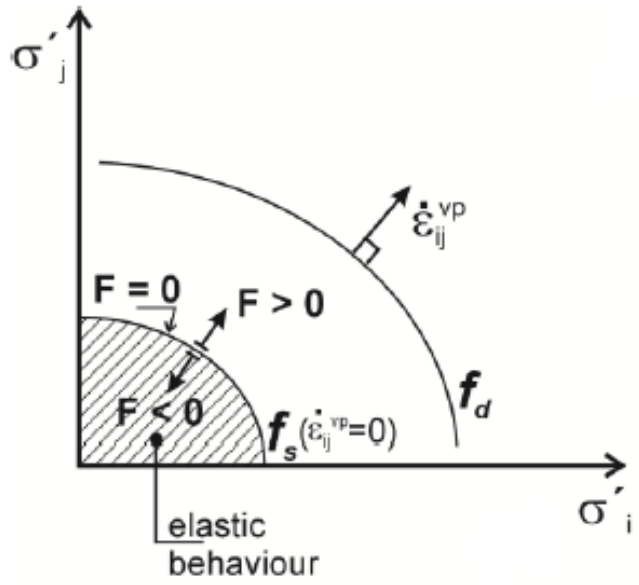

Figure 1.17: Schematic framework of EVP Perzyna's model

According to Equation1.29 and 1.30 the viscoplastic strain rate is a function of the distance between the dynamic and the static loading surface. The individual strain components are obtained from a plastic potential that is coincident with the dynamic loading surface. The size of the static loading surface is given by the hardening parameters that vary with the amount of viscoplastic strains.
The overstress theory differs from the plasticity theory as the former does not invoke the consistency rule to derive the equation that govern the strain behaviour of the soil element. Thus, differently from what happens in the elastoplastic case, the current stress state can lie on, above or below the static loading surface. When loading a soil element at a very high strain rate or if η is very small, overstress theory based models will predict that the material response is identical or very

close to pure elastic behaviour, as there is no time for delayed viscoplastic strains to occur.
The overstress theory is able to predict the creep phenomenon, provided that the stress state is outside the loading surface.
For sake of simplicity a simpler approach is used ([di Prisco, 2012a]): the overstress F is substituted with the yield function f: so f will be considered as a scalar measure of the probability of occurrence with time of irreversible strains. According to this simplified approach, Equation1.28 becomes:

$$\dot{\varepsilon}_{ij}^{vp} = \eta\Phi(f)\frac{\partial g}{\partial \sigma'_{ij}} \tag{1.31}$$

where the plastic potential g defines the direction of the visco-plastic strain rate tensor, while the yield function influences its modulus by means of the viscous nucleus Φ. As the consistency rule is abolished, the value of f may be either positive or negative, without any constraint, i.e, the stress state may be either external or internal with respect to the yield locus.
The viscous nucleus $\Phi(f)$ may take a variety of mathematical forms, for example the following simple bilinear form may be used (Figure1.18):

$$\begin{cases} \Phi(f) = f \ if \ f > 0 \\ \Phi(f) = 0 \ if \ f = 0 \end{cases} \tag{1.32}$$

The viscous nucleus is a positive function of f and, in particular, the following holds:

$$\frac{d\Phi}{df} \geq 0 \tag{1.33}$$

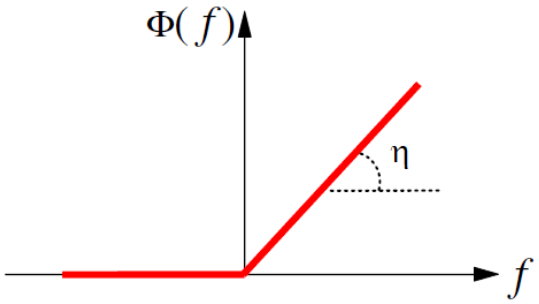

Figure 1.18: Graphic representation of the viscous nucleus $\Phi(f)$ of Equation1.32

Equations1.31 and 1.33 imply that, if the effective stress state is kept constant and, for instance, the plastic potential is assumed to be dependent only on the

effective stress state, in case of positive hardening (i.e when $H > 0$), f progressively reduces in time and strain rates continuously decrease with time and a primary creep phenomenon is expected.
To mathematically reproduce the creep behavior, as the incremental form is no more admitted, the strain acceleration tensor is defined as follows:

$$\ddot{\varepsilon}_{ij}^{vp} = \eta\dot{\Phi}\big(f\big)+\eta\Phi\big(f\big)\frac{\partial}{\partial t}\left(\frac{\partial g}{\partial \sigma'_{ij}}\right), \tag{1.34}$$

where

$$\dot{\Phi} = \frac{\partial \Phi}{\partial f}\frac{\partial f}{\partial t} = \frac{\partial \Phi}{\partial f}\left(\frac{\partial f}{\partial \sigma'_{ij}}\dot{\sigma}'_{ij} - H\Phi\big(f\big)\right) \tag{1.35}$$

and H even in the viscoplastic case is the hardening modulus defined in Equation1.12. The attainment of primary, secondary or tertiary creep basically depends on the hardening laws defining the variation of internal variables.
From Equations1.33, 1.35 and 1.12, $\dot{\sigma}'_{ij} = 0$, so the second term on the right of Equation1.34 is zero. Equally Equation1.35 becomes:

$$\dot{\Phi} = -\frac{\partial \Phi}{\partial f}H\Phi\big(f\big). \tag{1.36}$$

The strain acceleration can be written as:

$$\ddot{\varepsilon}_{ij}^{vp} = -\eta\frac{d\Phi}{df}\Phi\big(f\big)H \tag{1.37}$$

as $\Phi\big(f\big)$ is a monotonic positive function ($\Phi(f) > 0$, $\frac{d\Phi}{df} > 0$), the sign of $\ddot{\varepsilon}_{ij}^{vp}$ depends on the sign of H:

- when $H > 0$, consequently, $\ddot{\varepsilon}_{ij}^{vp} < 0$ and primary creep is reproduced;

- when $H = 0$, as a consequence, $\ddot{\varepsilon}_{ij}^{vp} = 0$ and secondary creep phenomenon (i.e. constant strain rate) can be reproduced. Secondary creep may be either a transition between primary and tertiary creep or an unstable steady state (i.e. when material evolution stopped) creep response (Figure1.19);

- when $H < 0$ tertiary creep can be reproduced, since in this case $\ddot{\varepsilon}_{ij}^{vp} > 0$.

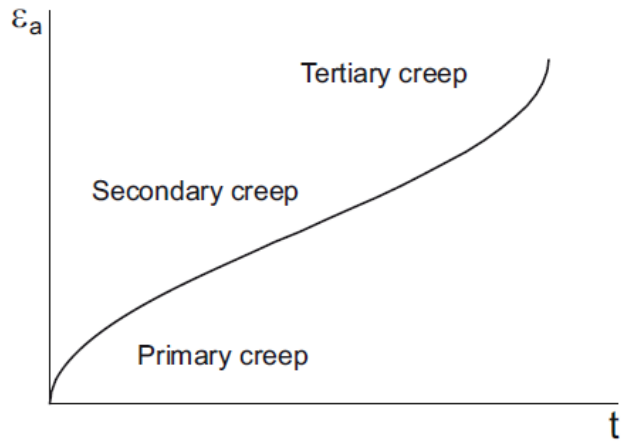

Figure 1.19: Schematic representation of the unstable mechanical response of a cemented material during a standard compression triaxal creep test (ε_a stands for axial strain)

Chapter 2

Creeping landslides

According to [Terzaghi, 1950] the term *landslide* refers to a rapid displacement of a mass of rock, residual soil or sediments adjoining a slope, in which the center of gravity of the moving mass advances in a downward and outward direction.
According to the scientific literature, there are two main classes of landslides depending on their time evolution: fast landslides and creeping landslides. The first group is related to soil movements with high velocity values occurring in a relatively small time span most of which are produced by the force of gravity, the second refers to landslides whose movement is slow, accumulating with time and with seasonal reactivations if particular triggering factors occur and they are typically due to the combined action of gravity force and various other agents. Referring to creeping landslides, the rate of deformation can be initially very slow, some mm/yr, but, in some rare unfavorable situations, as when a seasonal change of the water table level occurs, there may be a strain increase of even an order of magnitude.
In general, landslides depend on a series of parameters such as geological, geomorphological, hydraulic and hydrogeologic and also on the mechanical properties of the soils, so the transition from slow to fast movements in both inception and propagation phases depends on a series of factors:

- *geometrical* factors;
- *coupled thermo-mechanical processes* associated with volumetric expansion of water;
- *hydro-mechanical processes* associated with the effective stresses variation with water table level change, consolidation, liquefaction..;
- *strain softening*;
- *strain rate softening*;
- *viscous/rate dependent response*;

- *segregation* i.e. change in grain size distribution due to migration far from the shear zone of coarse particles;
- *grain crushing* i.e. change in particle shape occurring when large strain rates along the shear band arise.

Despite the complexity of the phenomenon implies considering a huge number of variables and physical processes, in this thesis only the strain softening, the viscous response, the geometrical factors and the water table level change influence will be considered.
For creeping landslides it is very important the displacement monitoring in time, because there are not suitable predicting models capable to give a simple and reliable information about displacement. Moreover, a careful monitoring is needed because there are specific displacement trends which are a sort of instability index. Failure often appears to occur without warning only because earlier movements have passed unnoticed.
Thus one of the main aspects to take into account is the velocity and the displacement trend of the moving mass, from which essentially depends the landslide risk, so, to better predict a possible catastrophic event, it is important to study displacement and displacement rate evolution in time.

2.1 Displacement trends for creeping landslides stability assessment

The landslide risk can be associated with the presence of three stages, characterized by specific mechanical aspects:

1. *failure stage*:it is the first failure occurring in the slope and it starts with a *pre-failure stage* in which, due to several causes, irreversible strains develop in the slope:
   - irreversible strains associated with changes in the stress field;
   - deformations related to softening and destructuring of the involved materials, due to stress changes or weathering; generally, these phenomena reduce both stiffness and strength;
   - viscous deformations;
   - strains and displacements associated with the development of progressive failure and to the corresponding distribution of stresses.

   These mechanism of strain accumulation often displays as a formation of a shear band. So the failure stage is influenced by the same factors controlling the shear band formation: softening and destructuration, viscous phenomena and progressive failure;

2. *post-failure stage*: the moment in which soil stops moving and the energy accumulated by the soil may dissipate.
   In [Leroueil, 2001] the post failure stage is seen as an energy redistrubution process: at the time of failure, some potential energy (E_p) becomes available and what happens then depends on how this energy is redistributed. Part of the potential energy will dissipate into friction (E_F), the rest will be dissipated in breaking up, disgregating and remoulding the soil (E_D) and for generating movements (kinetic energy, E_K). Over a time interval during the post-failure stage the following relationship holds:

   $$\Delta E_P + \Delta E_F + \Delta E_D + \Delta E_K = 0 \tag{2.1}$$

   The shear strength and the available potential energy at failure are closely related as can be noticed by Figure2.1. As post-failure movements progress, the potential energy decreases, the difference with that available at failure being progressively dissipated in the previously cited components.

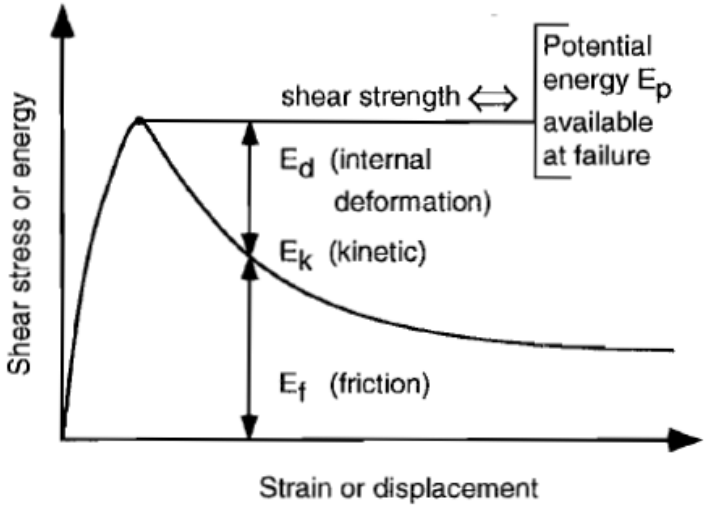

Figure 2.1: Schematic representation of the potential energy after failure from [D'Elia, B.,Picarelli, L., Leroueil, S., Vaunat, 1998]

   The dissipation of the accumulated energy depends on the type of material: in ductile materials most of the available potential energy is dissipated into friction and kinetic energy and rates of movement are small, while in fragile materials (in which a loss of strength occurs) the driving forces may become unbalances and there may be the cause of a new acceleration of the soil mass.

3. *reactivation stages*: they can be defined as failure stages occurring after the first failure of the slope. For landslides in which there is a movement along

one or several pre-existing failure slip surfaces, the mobilized shear strength corresponds to a residual condition. As the residual strength represents a lower limit, the soil does not present any strain softening and the rates of deformation are generally small.
Between the reactivations two different kinds of landslides can be distinguished:

(a) *active landslides*, in which the rate of displacement varies with the seasonal change in pore pressure. This is particularly true for translational landslides, in which the driving forces do not significantly change in time. The rates of displacement are generally very small, varying between some centimeters and some meters per year;

(b) *occasionally reactivated landslides*: may be associated with sudden and fairly rapid displacements. According to [Hutchinson, 1987] and [Morgenstern, 1990] the most common mechanisms that can produce such movements are:

- rapid pore pressure increase;
- stress change due to excavation;
- rapid change in load distribution along the shear surface;
- increase in strength along the shear surface due to cementation or chemical change that could give some brittleness to the soil at the time of failure;
- seismic forces.

In Figure2.2 the sequence of the various phases in terms of displacement rate in time is qualitatively sketched.

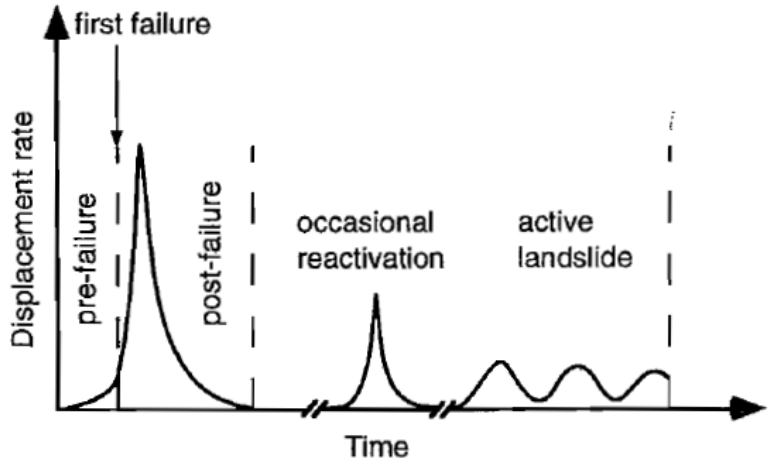

Figure 2.2: Schematic representation of the different stages of slope movements from [D'Elia, B.,Picarelli, L., Leroueil, S., Vaunat, 1998]

[Scoppettuolo et al., 2020] studied a database of eighteen different landslides to understand the typical displacement trends. In literature graphs of cumulate displacement in time can be found showing that landslides always exhibit a complex response; despite this, all the diagrams allow recognizing that data tend to place in recurrent ways: linear traits (linear behaviour) or curved profiles, that can be concave or convex, analogous to those described by [Singh, 1966] and [Emery, 1978] to introduce primary, secondary and tertiary creep movements. So it is possible to see that typical landslide evolution can be partitioned in ordered sequences as those showed in Figure2.3, where an active landslide (a), an occasional reactivation (b) and a phenomenon evolving towards a catastrophic stage (c) are qualitatively shown. Actually, the slope of the trends still depends on several factors such as the shape of shear surfaces, the materials composing the moving body and the materials among the shear surface.
The linear behaviour called, according to the nomenclature proposed in
[Cascini et al., 2014], Trend I is characterized by a "stable" condition, for which the internal and external forces acting on the landslides are balanced, given by a constant velocity and zero acceleration.
If an instantaneous and transient loss of equilibrium occurs in which the external forces overcome the internal stabilizing forces, an increase of the diagram slope (i.e. of the landslide velocity) could be observed; as time passes the system leaves this transient phase and returns to the initial equilibrium condition of Figure2.3a.This concave phase can be called Trend II and the whole process can be considered representative of an active landslides subjected to reactivations. An example could be a rapid increase of pore water pressure due to intense rainfall followed by a slow decrease of the groundwater level in time.
Also in Figure2.3b Trend II can be observed: in this case it has a different conceptual meaning as the process is characterized by data arranging on a convex curve, representing an acceleration in the landslide movement. The alternation of shapes physically indicates a perturbed state, caused by initially unbalanced force fields globally acting on the landslide, which evolves towards a new equilibrium configuration. The latter is reached if the acceleration of deformation becomes nil, provided that no other perturbations take place. It can be also noticed that the new equilibrium state reached after Trend III in Figure2.3b is different from the initial equilibrium configuration: the slope velocity is greater, due to the fact that the material has been damaged in time (for example it could have shown a softening response). The convex curve, referring to [Cascini et al., 2014], can be called Trend III. This kind of response is typical of occasional reactivation and the moderate perturbations causing them are usually called occasional triggering factors. Trend III also occurs when an increasing perturbation verifies, but in this case it is not associated with the system instability, because the increase in the slope velocity is due to the perturbation increase.
The catastrophic collapse of the system is associated to the so called Trend IV:

this is a phase characterized by data gathering along a convex curve and not likely to reach a new stable state for the subsequent instants of time. If such a trend is reached (Figure2.3c) largely unbalanced forces are present in the landslide. [Leroueil et al., 1996] call this response as failure stage and it is typical of occasionally reactivated landslides. For instance this is the case of the Vajont landslide, caused by an occasional triggering factor of a particularly high intensity which was the sudden lowering of water table level into the basin of Vajoint dam.

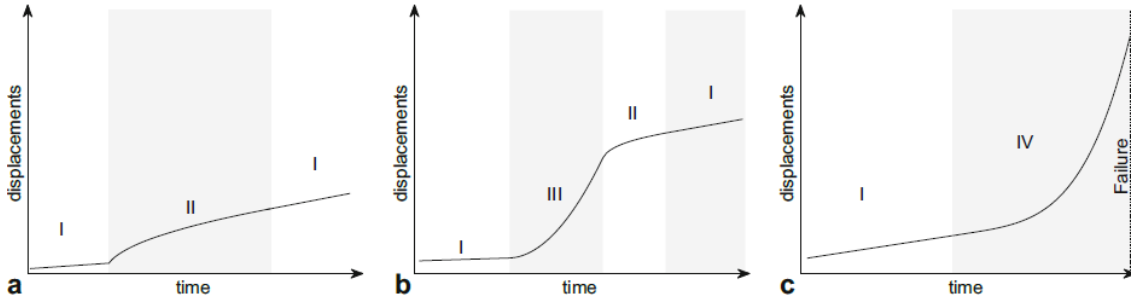

Figure 2.3: (a) Main typical sequences of displacement trends for an active landslide, systematically reactivated by recurrent triggering factors, in between two steady states;(b) a lanslide reactivated by an occasional event (e.g. earthquake) in between steady state and Trend II followed by a steady state ;(c) and evolution to failure from a steady state. Roman numbers indicate different trend types present in the sequences

For the sake of completensess, a more detailed analysis for Trend III and IV is done in th following section and with the reference to the Vajont landslide.

2.1.1 Overview on some creeping landslides cases

In this section some cases of creeping landslides are reported. The common aspect of all the following cases is that the displacements triggering factor is represented by water.

La Clapière landslide

The La Clapière landslide ([Scoppettuolo et al., 2020]), located in the southern French Alps, mobilizes a volume of approximately $55 \times 106m^3$ in a gneissic rock slope covered by a forest and shows a complicated sequence of active stages and occasional reactivations related to the river level flowing at the toe and other triggering factors ([Helmstetter et al., 2004]). It probably started to move before the

beginning of the twentieth century, although the first changes in slope geometry were highlighted only in the period 1950–1980, through an aerial photogrammetric survey. A slope displacement survey started in 1982 with the aid of topographic measurements suggested a correlation between slope displacements and river flow fluctuations and snow melting, possibly accompanied by heavy precipitation.

Figure2.4a provides a map of the landslide referring to a monitoring point whose

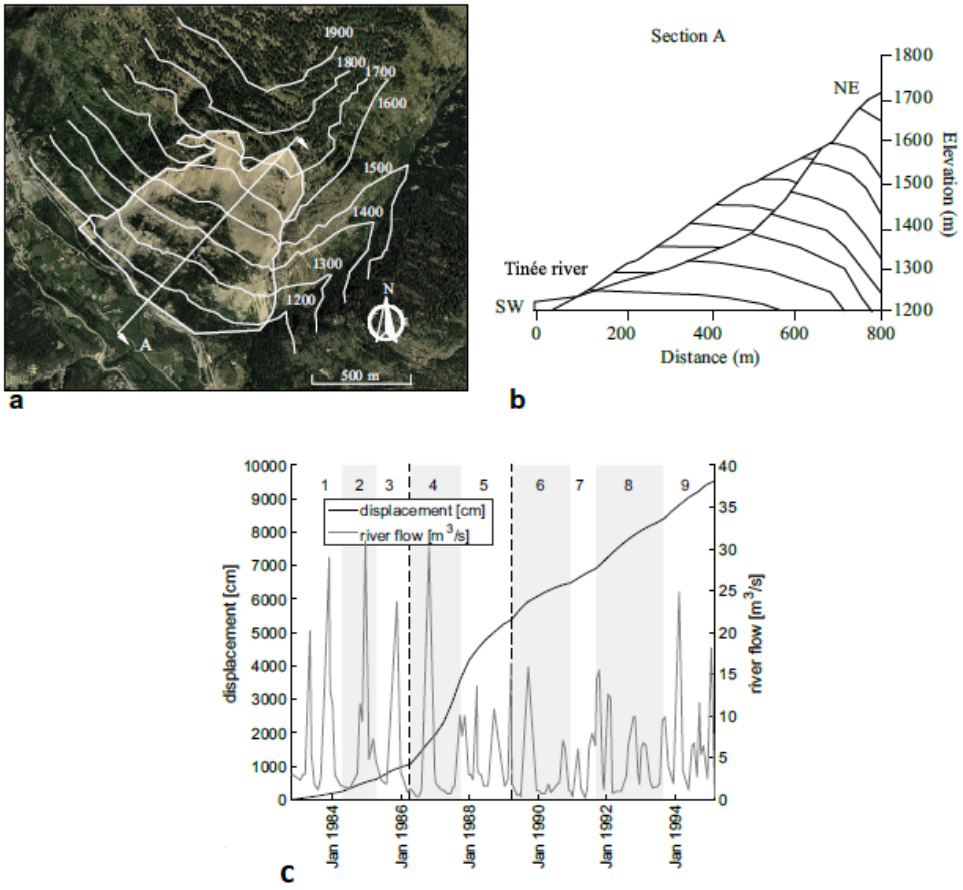

Figure 2.4: a) Satellite imagine of La Clapière landslide taken from a public repository (Google Earth, 2004) with the indication of the instability area and cross-sectional plane ([Bouissou et al., 2012], [Bigot-Cormier et al., 2005]). b) Cross section (modified from [Bouissou et al., 2012]). For further detail, e.g. qualitative indication of monitoring stations, we refer to [Helmstetter et al., 2004]. c) La Clapière landslide: monitoring data of cumulative displacements and river flow with the indication of a convex-concave sequence, in between the two vertical dashed lines.

cross section in represented in Figure2.4b.

In Figure2.4c the whole displacement data record is superimposed to the river flow record (representative of the triggering causes, not examining rainfall and snow

melting data) to identify the activity stages. The resulting nine stages are neither seasonal nor periodic and are usually longer than 1 year, in agreement with the occurrence of triggering factors.

Vajont landslide

In 1963 the Vajont disaster provoked approximately 2000 casualties and caused the total destruction of the downhill towns, in particular Longarone. Between 1950 and 1960 the Vajont stream was blocked by a concrete dam near the confluence of the Piave River in the Italian Alps. Following the first two fillings of the reservoir, the new boundary conditions at the toe of the slope caused two accelerating stages of a complex existing landslide in the reservoir level, the third fatal landslide reactivation mobilized $270 \times 10^6 m^3$ of rock that, flooding in the reservoir, generated a $220 - m-$high wave that overpassed the dam.

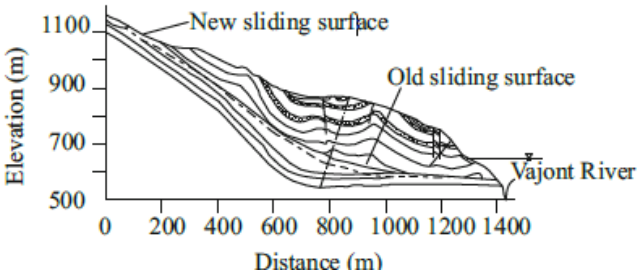

Figure 2.5: Cross section of Vajont landslide

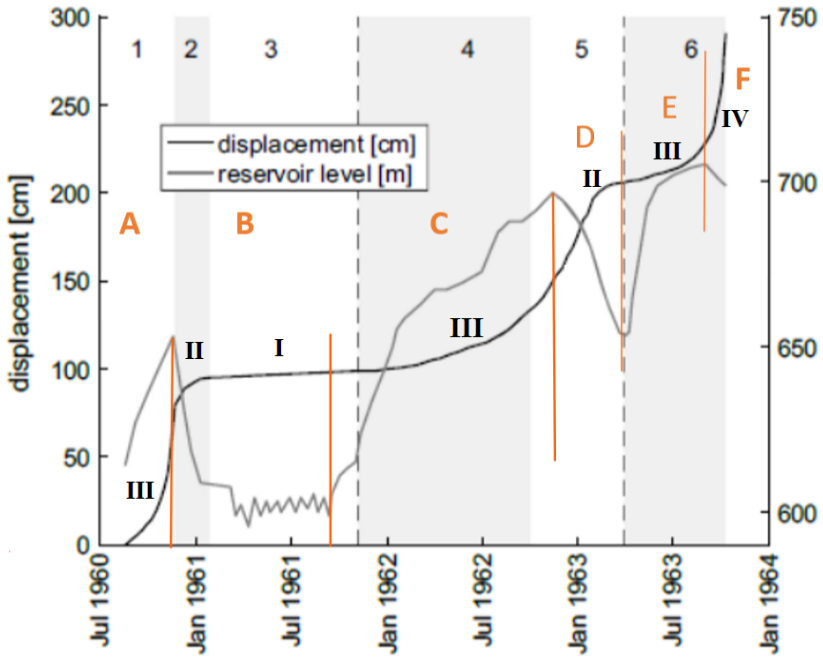

Figure 2.6: Monitoring data of cumulative displacements and reservoir level for Vajont landslide

In in Figure2.5 the Vajont landslide mechanism is sketched: it can be represented with two interacting wedges, the upper unstable and the lower resisting. In Figure2.6 the evolution of displacement in time for a certain monitoring station superimposed to the reservoir level can be seen; the available data show an alternation of linear segments and convex-concave curves until July 1963; these changes are related to the lowest and the highest values of the reservoir level, respectively, that confirm the phenomenon was an occasionally reactivated landslide.
Trend III and IV, despite being both characterized by strain acceleration, have to be distinguished; they are present in case of occasional triggering factor, so not related to seasonal events: earthquakes, anthropic activities or specific variations of boundary conditions, such as those related to the presence of a new water reservoir at the toe of the slope. The difference between Trend III and IV is that the first one is associated with occasional reactivation and the second with a first failure phase and in both the velocity clearly increases. In Trend III, as can be seen in phase number 4 and 5 of Figure2.6, a first acceleration of displacement is present because of the increase in the perturbation, but after the triggering cause has ceased, the landslide undergoes a Trend II deceleration process up to a constant value of velocity, characterizing a new stable condition for the slope.
On the other hand, a landslide developing a Trend IV response tends to naturally gain kinetic energy with increasing velocity until collapse occurs, as in phase 6 of Figure2.6. There may be rare cases in which specific external condition slow down

the landslide: this is in the case of phase 1 of the Vajont landslides that decelerated on 1960 and 1962 just after lowering of water level of the reservoir (Figure2.6). Actually, in the greatest part of cases, Trend IV is associated to the collapse of the slope because of the great increase of kinetic energy of the system.
Instead of considering the displacement trends, another analysis could be done focusing on the relationship between the change in perturbation and the system response in terms of displacements: in Figure2.6 other zones are marked with capital letters. In zone A, C and E, after an increase in perturbation, deformations tend to accelerate; when the perturbation diminishes in intensity (zone B) deformations slow down until they stop. Differently from what happens in zone B, in zone D, when perturbation reduces, displacements initially tend to accelerate: this happens because of the viscous response deriving from the previously applied load; after this phase, displacements slow down as in the previous cases and a new equilibrium configuration is reached.
When an acceleration occurs after a decrease of the perturbation is an index that the system is going to reach failure. Indeed, in zone F, after the water table level is lowered, an unstable behaviour occurs, consisting in the indefinite acceleration of deformation due to the delayed in time slope response. So, when an unstable configuration is reached, all the kinetic energy accumulated during perturbations is released causing a sudden catastrophic failure. All this considered, while the trends in terms of displacement seem to be stable, an unexpected failure may occur due to the time dependent response of the slope.
The instability phenomenon occurring in the slope is the result of a the propagation of cracks that take place locally in the material: this propagation phenomenon is called progressive failure and in the following section its main features will be outlined.

Capo Vallemaggia landslide

The Campo Vallemaggia landslide ([Bonzanigo et al., 2007]) is located in the crystalline Pennic nappes of the Canton Ticino, in the southern Swiss Alps, near the Italian border. This deep-seated, creeping landslide is characterized by an immense size. The slide mass reaches the depth of up $300m$ and incorporates approximately 800 million cubic meters of crystalline rock. The body of the slide mass is subdivided into several blocks by sub-vertical fault zones varying in thickness from several meters to tens of meters, with sub-horizontal shear–slip surfaces developed along lithological boundaries or zones of varying alteration. As a result, its movements are complex and difficult to describe.
Two small villages, Campo Vallemaggia and Cimalmotto, are situated on the slide mass where surface displacements have been geodetically measured for over 100 years. Recorded observations in the villages go back 200 years. Based on these

surveys, it could be resolved that the horizontal translation of the slide mass had advanced approximately $30m$ between 1892 and 1995. These displacements were of great concern in the two villages, as with each passing year of slope movement, the villages moved closer and closer to a steep erosional front at the toe of the slide mass (Figure2.7). Inspection of the displacement–time record showed that accelerated movements were associated with periods of intense precipitation, often provoking fear among the local population and authorities. Intervention to stabilize the landslide has repeatedly been called for and emergency plans prepared in the event evacuation was considered necessary.
Figure2.8 shows some monitoring data in terms of annual precipitation and slide velocity; it also shows that slope accelerations are not necessarily proportional to the amount of precipitation.

Figure 2.7: Areal view of the foot of the Campo Vallemaggia landslide and the two villages located on it from[Bonzanigo et al., 2007]

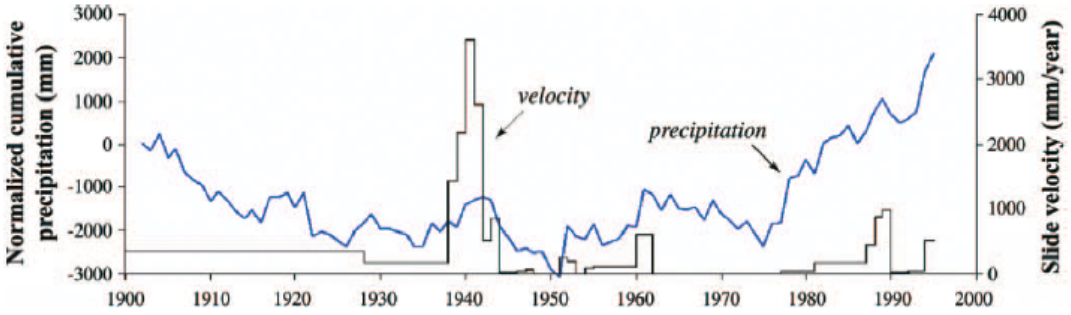

Figure 2.8: Correlation between precipitation and landslides velocity for the period 1892 to 1995. Annual cumulative precipitations normalized to yearly average of 1825 mm/year recorded for that period. Slope velocities are based on geodetic measurements.

Sunjia Landslide

The Sunjia landslide ([Xiao et al., 2020]) occurred in Wanzhou County, in an area considered one of the most landslide-prone in China.
Sunjia Town suffered a $1.5 \times 10^6 m^3$ landslide on 4 April 2013. The source slope of the landslide initiated in a low to middle elevation mountainous region with a slope inclination of 5° and a slope angle of 20° – 35°. Destabilized by abundant rainfall, the Sunjia slope experienced progressive incipient failure one day prior to the eventual landslide that slid downslope about 30 m toward the northeast with catastrophic consequences for most of the infrastructure along its trajectory. Thanks to the local government geohazard measurements and prevention, the residents on the landslide path were given an early warning and evacuated before the disaster. As a result no fatalities or injuries occurred on the slope, but the deposits on the post-slide slope remain unstable and continue to pose a threat to people's lives and public infrastructures further down the slope. In Figure2.9 some photos showing the characteristics of the landslide deformation are reported.
In Figure2.10 the monthly rainfall of the zone are reported; in Figure2.11a the investigated landslide boundary with monitoring stations is reported and in Figure2.11b the recorded displacements at the monitoring stations of the period 5 April - 31 August 2013 are reported.

Figure 2.9: Photographs showing the characteristics of landslide deformation at the 2013 Sunjia landslide site from [Xiao et al., 2020]. a) The tensile groove; b) the drum hill; c) the damaged rural road; d) the dilapidated houses. The red dashed lines and arrows indicate the direction of surface displacements and the blue lines indicate the specific microtopography.

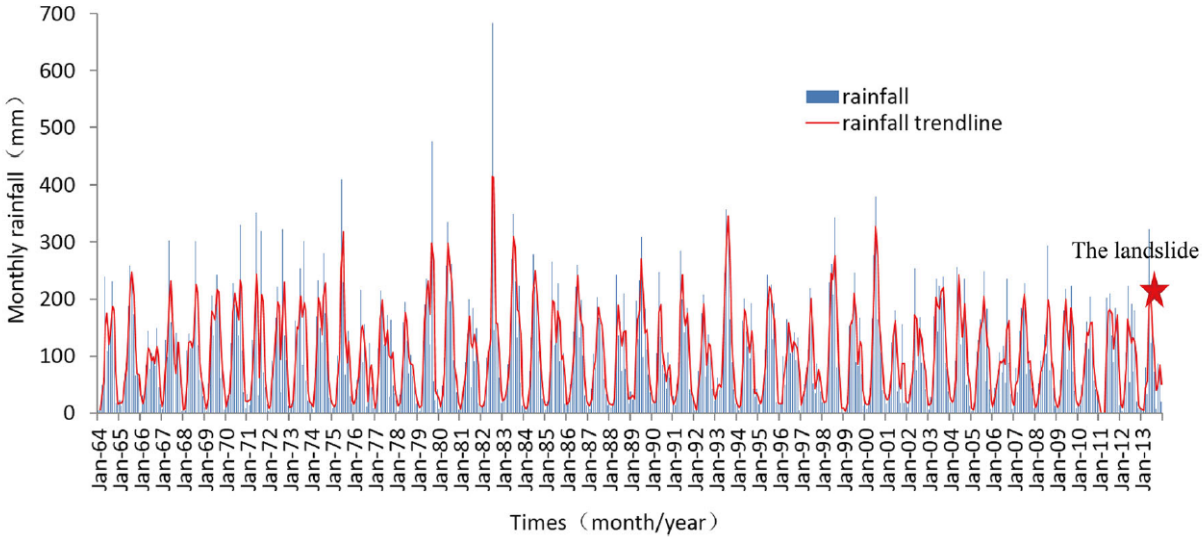

Figure 2.10: Bi-monthly rainfall in Wanzhou Country in 1964-2013, Three Georges Reservoir region (data collected from the Wanzhou Geological Environmental Monitorin Staion). The red star indicates the time when landslide occurred from [Wang, 2015]

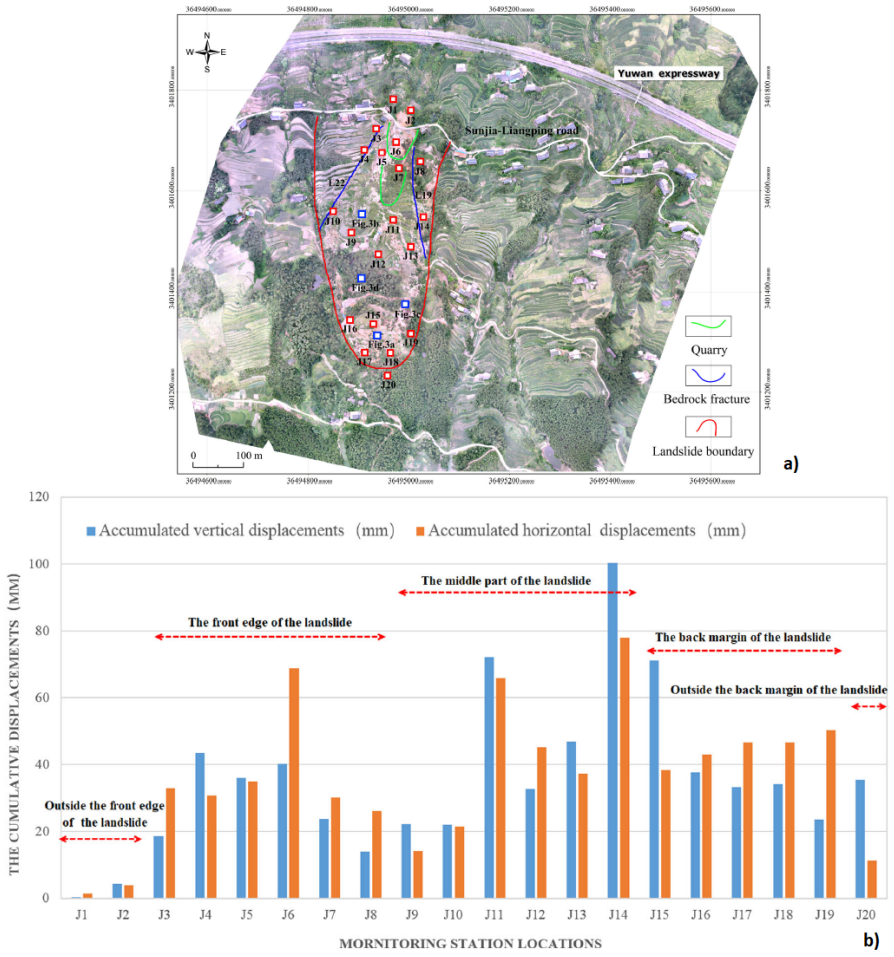

Figure 2.11: a) An aerial image of the post-slide Sunjia slope provided by the Nanjiang Hydrogeological Engineering Geological Team. The red squares point out the locations of the monitoring stations, and the blue squares indicate the sites of the photos shown in Figure2.9. b) Emergency monitoring at the surface of the 2013 Sunjia landslide in Wanzhou Contry from 5 April to 31 August 2013

2.2 Progressive failure mechanism

A possible triggering factor for creeping landslides acceleration is an increase in precipitation; indeed often the instability verifies when no precipitation increase is observed or some time after the end of the perturbation: this may derive from the progressive damage of the material.
Progressive failure mechanism is the result of crack accumulation in time: this process appears as a shear band development and spatial evolution; it is not instantaneous, but derives from (i) strain accumulation and progressive degradation

occurring in the soil, (ii) spatial stresses redistribution, associated to material failure in other parts of the domain.
According to [Leroueil, 2001] the conditions necessary to the development of progressive failure are:

- brittleness of the soil: it generally takes place in overconsolidated clayley soils, in geomaterials characterized by an high level of fragility and in structured cemented granular materials, so in all the materials that present a softening behaviour (Figure2.12). This process is related to the so called *subcritical crack growth*, which is leading to breakage of either bonds or particles ('grain crushing');
- non-uniformity in the distribution of shear stress;
- local shear stresses that exceed the peak strength of the soil;
- boundary conditions loading the slope.

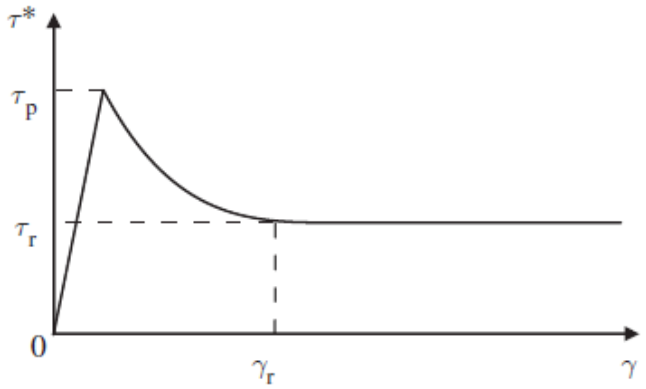

Figure 2.12: Shear beaviour of a strain softening material

Brittleness is a characteristic of most natural soils in their overconsolidated range and of weak rocks; also owing to the geometry of the problem, shear stresses are generally not uniform in the slope and, in particular, along potential failure surfaces. As a result, progressive failure plays a major role in pre-failure phenomena. The mechanism of progressive failure was recognised by [Terzaghi K., 1948] and [Taylor, 1948] but only in the following it was understood and discussed in the context of overconsolidated clays and soft rocks. In the following some aspects about the mechanism in the cited materials are reported.
If the shear stress locally reaches the peak shear strength of the material, there is local failure. If soil presents some strain softening behaviour, the failed soil elements will support a decreasing shear stress and strain increase. The part of the

shear stress that is no longer supported by the failed elements is then transferred to the neighbouring soil elements, which can fail in turn. The process continues until an equilibrium between shear stresses and strains has been reached. At that time, along a potential failure surface, part of it can exceed the peak, with possibly some elements at large deformation or residual strength, whereas another part of the potential surface has not reached the peak. If such equilibrium cannot be obtained, the process will continue until failure conditions extend along the entire failure surface.
Even if some equilibrium seems to exist at a given time, it can be modified and the process of progressive failure can resume or continue. The main factors leading to this situation are:

- a change in the geometry of the problem (e.g erosion at the toe or loading at the top of the slope);
- a decrease in normal effective stress and thus in the peak and residual strength (e.g excavation during pore pressure equilibration or pore pressure increase in general);
- a decrease in strength parameters (e.g lowering of the peak strength envelope due to creep, fatigue or weathering).

[Bjerrum, 1973] particularly emphasized the importance of bonds and weathering and of the possible release of stored energy in the process of progressive failure.
Brittleness is the major factor in the development of progressive failure and it has been characterized by [Bishop, 1970] with the brittleness index I_B:

$$I_B = \frac{\tau_p - \tau_r}{\tau_p}, \% \tag{2.2}$$

where τ_p and τ_r are the peak and residual strengths defined under the same effective normal stress. The value I_B given by Equation2.2 denotes the only difference which would be obtained in the factor of safety by making the assumption that the whole of the rupture surface had reached the residual state at the moment at which failure eventually took place, in place of the conventional assumption that the peak strength operated over the whole surface.
However, as indicated by [Vaughan and Hamza, 1977] and [Chandler, 1984], the brittleness index alone is not sufficient to characterize the susceptibility to progressive failure: the rate at which the strength decreases from peak strength to ultimate strength is also important. [D'Elia, B.,Picarelli, L., Leroueil, S., Vaunat, 1998] proposed a generalized brittleness index, I_{GB}, defined as follows:

$$I_{GB} = \frac{\tau_p - \tau_{mob}}{\tau_p}, \% \tag{2.3}$$

where τ_{mob} is the mobilized shear stress at the considered strain or displacement. I_{GB} thus varies with strain or displacement from 0 at the peak, to a value equal to I_B at large displacements (Figure2.13). Moreover, in the context of slopes, the index I_{GB} must be associated with stress paths that are representative of those followed in situ and must not be seen as a fundamental characteristic of soils.

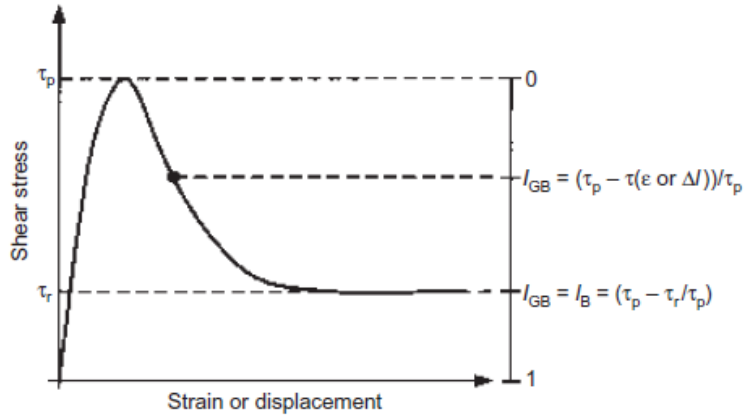

Figure 2.13: Brittleness of soils

2.2.1 Progressive failure: weakened zone, shear zone and slip surface

From what emerged from progressive failure remarks, it appears that the failure or slip surface in a slope develop within a weakened zone. Observations, however, show that there is an intermediate structure surrounding the slip surface, usually called shear zone (Figure2.14).

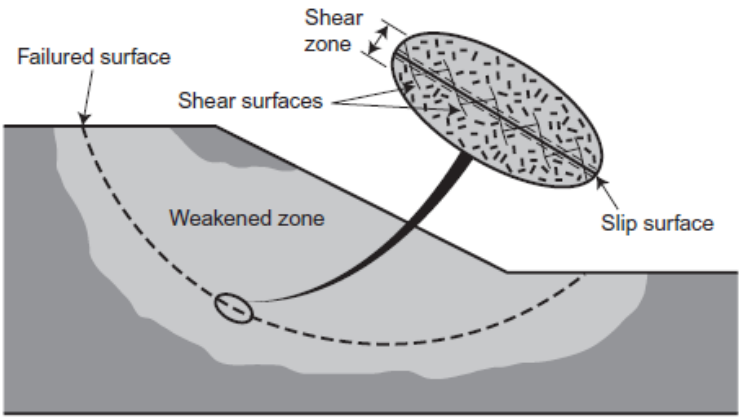

Figure 2.14: Weakened zone, shear zone and slip surface in the slope

According to Rankine theory, in case of zero dilatancy, shear surface form an inclination of $45° + \phi'/2$ to the direction of the minor principal stress. When such shear surfaces cannot develop, due to kinematic constraints, there is at first the formation of a shear zone and then the development, within the shear zone, of a slip surface that is kinematically possible. This is particularly the case in direct shear tests and in many slopes.
[Riedel, 1929] was the first to describe such a process, which was observed during a shear test on a clay specimen. According to Riedel's observations (Figure2.15b), the mechanism of rupture is characterized by initial formation of single separate shear surfaces, called Riedel shears (R), that are slightly inclined to the direction of main shear, and by some conjugate discontinuities (Figure2.15b1). The another set of discontinuities, the thrust shears (P), are formed at locations almost symmetrical to the R shears (Figure2.15b2). None of these minor shears allows for significant displacements ([Skempton et al., 1966]). Finally, the displacement discontinuities (D) are formed in the direction of the imposed shear (Figure2.15b3). In the final stage, these latter link to form a unique principal displacement discontinuity. This process was confirmed by laboratory experiments (Figure2.15a) [Morgenstern, 1967], [Wilcox et al., 1981]). The described zone of discrete thickness, including the system of minor shears and more or less disturbed lenses, is the shear zone ([Skempton et al., 1966]).
Also in situ observations confirm what already assessed: in Figure2.15c) the details of a shear zone observed by [Morgenstern, 1967] in an old landslide that occurred in London Clay can be seen.
So, as already indicated in Figure2.14, there are several "structures" associated with progressive failure in slopes:

- a weakened zone in which soil has reached local failure and should be generally destructured;

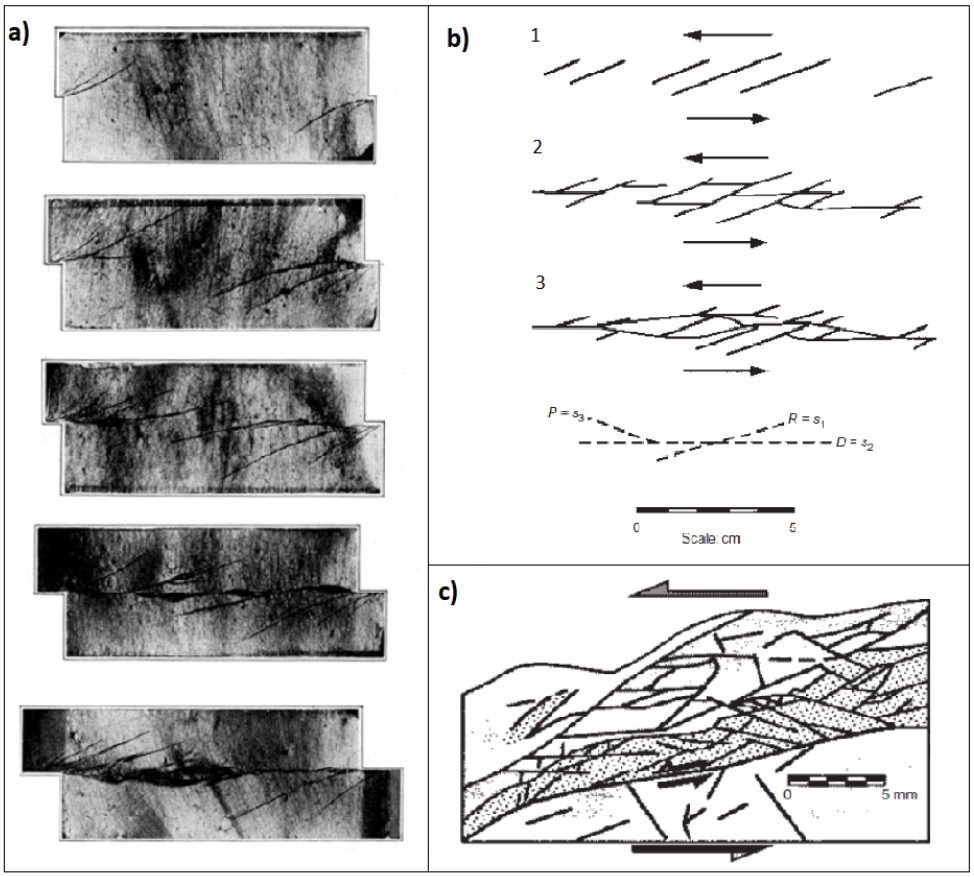

Figure 2.15: a) Sequence of structures in specimens sheared normal to original fabric ([Morgenstern, 1967]) b) Sketch showing three successive stages in the development of slip surfaces in clay subjected to shear (from [Riedel, 1929] and [Skempton et al., 1966]) c)details of shear zone in old landslide near Guildforn ([Morgenstern, 1967])

- a shear zone, surrounding the shear surface, with a thickness varying from a few centimeters to a few decimeters and including shears and lenses of soil, more or less disturbed, depending on the material and on the displacement involved;

- the failure surface, along which there is localization and possible particle orientation.

It is worth noting, however, that there is no evidence that weakened zones and shear zones develop or can be observed in all cases.

2.2.2 Puzrin interpretation of progressive failure mechanism

According to [Puzrin and Schmid, 2011] interpretation, at the microscopic scale, the propagation with time of cracks causes a progressive spatial rearrangement of the microstructure; more in detail this mechanism is based on the propagation of an intensely sheared zone, which causes earth pressure increase in the compression zone of the landslide, followed by visco plastic yielding of this soil zone (Figure2.16). Strain localization and propagation of shear bands (few millimeter thick zones of intense shearing, where shear strength decreases to residual value) take place in materials that exhibit a softening behaviour. In these materials (Figure2.12), the shear resistance τ^* on the sliding surface drops from the peak value τ_p to the residual value τ_r as the shear deformation reaches its critical value γ_r.
This progressive propagation of the shear band causes a delayed failure in cemented material slopes and helped to explain the mechanism of catastrophic landslides that sometimes can occur with no apparent signal.
When the shear strains of the landslide overcomes the critical value $\gamma_r = \delta_r/d$, where d is the sliding surface thickness, local value of shear resistance on the sliding surface drops to the residual value, which implies the formation of a shear zone. Creeping and yielding of the soil in the compression zone cause the tip of the shear zone to move along the slip surface. This leads to the progressive propagation of the shear zone and the drop of the shear strength along the slip surface to the residual value τ_r, which has to be compensated by an increase of the effective earth pressure in the compression zone. After this pressure reaches the yield stress p_y, the elastic and viscous resistances decrease significanlty causing increase in the landslide displacement rates.
This complex phenomenon is generally governed by the combination of many actions of stresses, water (both liquid and gaseous state) and chemical reactions (weathering). Despite in cemented materials weathering and hydro-mechanical coupling play an important role, the collapse of the system is here studied neglecting these aspects and only considering the mechanical perturbation given by water table level change and the strain softening behaviour will cause a cohesion degradation with time and strains.
The main limit of Puzrin model is that an infinite configuration is assumed, as a consequence all the derivatives of the static variables with respect to t direction have to be nil: actually, despite this assumption, in the model the shear stress, the shear strains and the displacement derivatives along t direction are not nil.

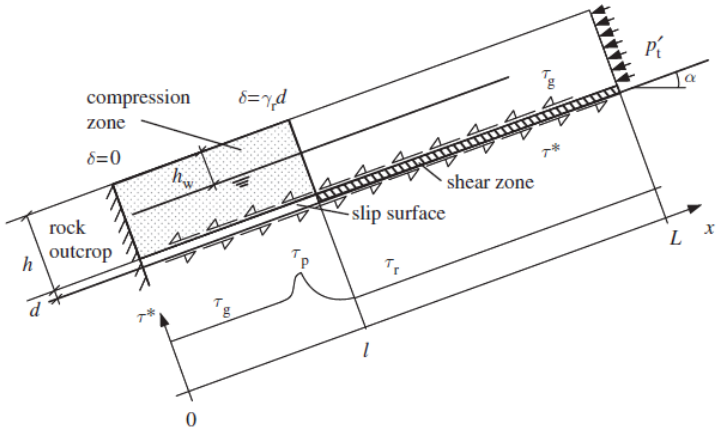

Figure 2.16: Conceptual model of shear band propagation of Puzrin model

2.2.3 Instability indicators prior to main landslides

Some indicators exists that sometimes can occur prior to a slope first-time failure. [Terzaghi, 1950], referring to Goldau landslide (1806), reported *'that took villagers by surprise, but the horses and cattle became restless several hours before the slide and the bees deserted their hives '*. [Tavenas et al., 1971] reported similar facts in relation to Saint-Jean-Vianney landslide (1971), which occurred in extremely sensitive clays. As indicated by witnesses, in the hours preceding the slide, dogs became extremely nervous as during a thunderstorm and cows, though usually docile, refused to go to their usual grazing land- which was, a few hours later, completely washed away by the slide. All these events are due to the acoustic emissions coming from the intense crack propagation, that show increasing activity as failure approaches.
It thus appears that many slope failures are preceded by prefailure phenomena and movements. As a consequence, as well indicated by [Terzaghi, 1950], *'if a landslide comes as a surprise to the eyewitnesses, it would be more accurate to say that the observers failed to detect the phenomena which preceded the slide'*. Another consequence is certainly that particular attention should be payed to precursory signs of landslides, in particular in area subjected to high risk and in which preceding remarkable movements have been registered.

2.3 1D rigid-visco-plastic model for monitoring data back analysis

As already remarked, monitoring data in time is fundamental for creeping landslide risk analysis; in this section a 1D rigid-viscoplastic model to reproduce the creeping landslide behaviour is proposed.
Very used for creeping landslides description is the 1D constitutive model developed by [Secondi et al., 2013]. It is a 1D pseudo-dynamic, visco-plasic model used, for example, to model the evolution in time of Bindo-Cortenova translational landslide formed by conglomeratic rock blocks immersed in gravely sand matrix.
To use the 1D model and to have a good understanding of this behaviour, monitoring systems were set up: inclinometric records have been used to determine the depth the thickness of the sliding zone. In particular, for the model description, only piezometric data and optical targets displacements have been adopted.

2.3.1 1D model formulation

Soils behaviour is rate dependent: the propagation of a stress due to a load increment (such as the oscillation of water table level) induces a time-dependent evolution in the soil micro-structure, strictly linked to the mechanical properties of the continuum.
Hence, the stress distribution evolves, and may carry to a new non-equilibrated stress configuration. If a new equilibrium state is reached, the time interval needed to reach this state can be interpreted as the time period during which plastic deformations occur.
In this model the limit equilibrium approach is used; it is based on the hypothesis of rigid-visco-perfectly-plastic behaviour for the interface material, so no ductility for the system is expected. The deformations start only after failure condition is reached.
Bindo-Cortenova landslide is considered as a non-deformable mass on a stable-rigid layer (Figure2.18).
The model has the aim to describe the displacement rate $\dot{x}$ of the landslide. This choice is linked to the inclinometric measures performed during the landslide ([Secondi et al., 2013]); these measures and shape of the unstable mass (Figure2.17) suggest that the landslide is a rigid block translating on a discontinuity plane. Due to the landslide translational nature, the problem is studied condensing all the non linearities at the interface between the bedrock and the rigid block, so $\dot{x}$ can be defined as:

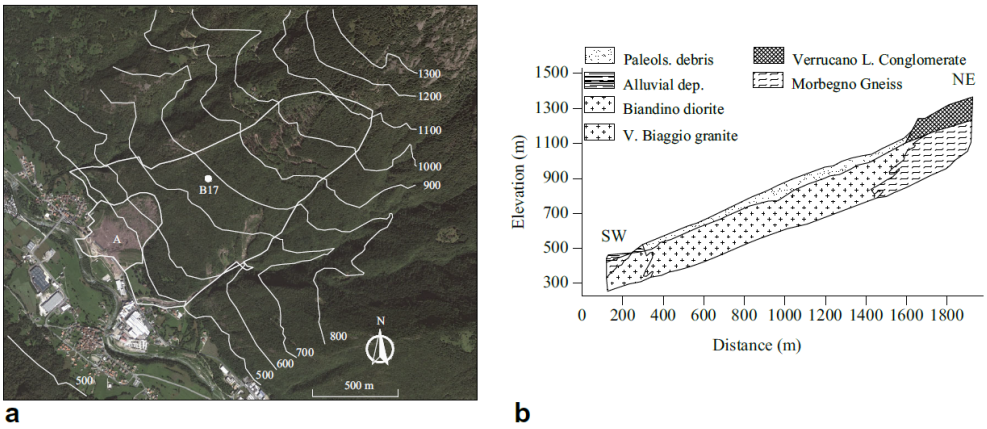

Figure 2.17: a) Satellite imagine of Bindo-Cortenova landslide with the indication of the instability area and monitoring optical target B17 (simplified from [Secondi et al., 2011]). "A" refers to slope failure occurring in November–December 2012 b) Schematic cross section (simplified from[Crosta et al., 2006]). The corresponding section plane is not reported in the satellite image due to lack of information in the analyzed literature

$$\dot{x} = \dot{\gamma}\Delta s, \tag{2.4}$$

where Δs is the shear band thickness, depending on the grain size.
The shear strain is evaluated according to Perzyna's viscoplastic theory; the total strain is supposed to be the sum of an elastic part and a viscoplastic part:

$$\dot{\varepsilon}_{ij} = \dot{\varepsilon}_{ij}^{el} + \dot{\varepsilon}_{ij}^{vp}. \tag{2.5}$$

Since (i) the elastic deformation can be neglected and (ii) a rate of angular deformation $\dot{\gamma}$ (a 1D model is considered) is assumed to be sufficient for describing the slope mechanical response, Equation2.5 can be simplified as follows:

$$\dot{\gamma} = \dot{\gamma}^{vp}. \tag{2.6}$$

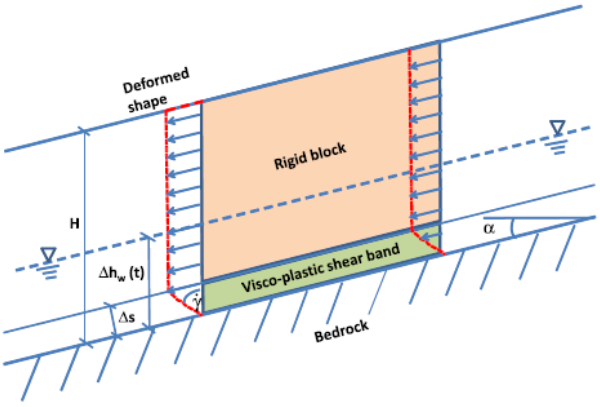

Figure 2.18: Block schematization proposed for the 1D model

According to Perzyna, viscoplastic strains can be defined as:

$$\dot{\gamma}_{ij}^{vp} = \frac{\tilde{\gamma}}{p'}\Phi(f)\frac{\partial g}{\partial \sigma'_{ij}}, \tag{2.7}$$

where f is the yield function, g the plastic potential, $\tilde{\gamma}$ a viscous constitutive parameter, p' the isotropic pressure, σ'_{ij} the effective stress tensor and $\Phi(f)$ the viscous nucleus.
It is possible to model the system in a 1D configuration because residual conditions are considered for the slope (the shear band is assumed at a steady state), consequently dilatancy is nil and no displacement normal to the sliding surface has to be taken into account. For this reason Equation2.7 becomes:

$$\dot{\gamma}_{ij}^{vp} = \frac{\tilde{\gamma}}{p'}\Phi(f) \tag{2.8}$$

In Equation2.8 material hardening or softening are neglected (the material is assumed to be at critical state). It means that the shape and the dimension of the yield surface are constant during the irreversible visco-plastic deformation.
So Equation2.4 for displacement evaluation becomes:

$$\dot{x} = \frac{\tilde{\gamma}}{p'}\Phi(f)\Delta s \tag{2.9}$$

$\tilde{\gamma}$ represents the velocity through which the system evolves and reaches the asymptotic value of deformation.
The viscous nucleus $\Phi(f)$ directly governs the modulus of $\dot{\gamma}^{vp}$, thus no consistency law is needed and the stress state can violate the condition $f \leq 0$ and irreversible deformations can accumulate for any value of f. In addition, visco-plastic deformations can occur even without any effective stress increment.
An analytic expression for the viscous nucleus is needed: a simple formulation for

the viscous nucleus is the bilinear form shown in Figure2.19: the deformative behaviour of the slope is different if the stress state lies inside or outside the plastic surface.This particular form of Φ takes into account of the possibility of accumulating viscous deformations even for $f < 0$. In particular the viscous strain rate will be lower in the case $f \leq 0$. So two parameters $\tilde{\gamma}_1(f > 0)$ and $\tilde{\gamma}_2(f \leq 0)$ must be introduced:

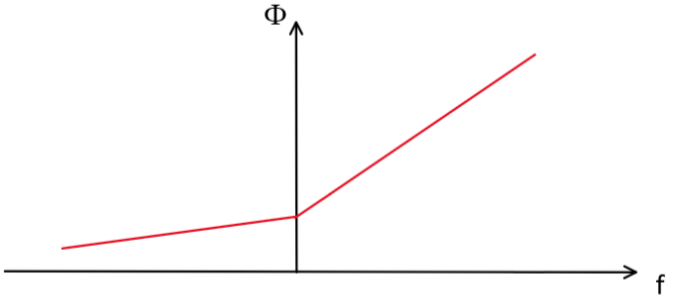

Figure 2.19: Bilinear form of the viscous nucleus

$$\begin{cases} \Phi(f) = y' + \tilde{\gamma}_1 f & if \quad f > 0 \\ \Phi(f) = y' + \tilde{\gamma}_2 f & if \quad f \leq 0 \end{cases} \tag{2.10}$$

where $\tilde{\gamma}$ is replaced with $\tilde{\gamma}_1$ $(f > 0)$ and $\tilde{\gamma}_2$ $(f < 0)$ and y' is a new constant parameter identifying the velocity value in x-direction when $f = 0$.
The 1D yield function can be written as:

$$f = \tau - \tau_{res} \tag{2.11}$$

where τ is the effective shear stress and τ_{res} is the yield threshold.
A Mohr Coulomb failure criterion is introduced. As the slope considered is characterized by slow movements inducing irreversible deformations due to post-failure conditions, a residual friction angle ϕ'_{res} is used:

$$\tau_{res} = \sigma'_n tan\phi'_{res}, \tag{2.12}$$

where σ'_n is the effective force normal to the sliding plane divided by the total contact area.
As dynamic and inertial forces effects must be taken into account, the effective shear stress can be written as:

$$\tau = \tau_{stat} - m^* \ddot{x}, \tag{2.13}$$

where τ_{stat} is the static term, given by the weight of the masses acting on the system and $m^*\ddot{x}$ is the dynamic term, depending on the acceleration in the x-direction and on the masses per unit area m^*.
The static force τ_{stat} is given by:

$$\tau_{stat} = W'\big[h_w(t)\big] sin\alpha + J, \tag{2.14}$$

where W' is the submerged weight divided by the total contact area, J the seepage force divided by the total contact area and $h_w(t)$ is the water table level varying with time.
Substituting Equation2.9, 2.11 and 2.13 into Equation2.10 and introducing the viscous parameters in the following expression:

$$\begin{cases} y = y'\Delta s \\ \eta_i = \frac{p'}{\Delta s \gamma_i} i = 1{,}2 \end{cases} \tag{2.15}$$

The following equation of motion for the slope can be obtained (where $i = 1$ means $f > 0$ and $i = 2$ means $f \leq 0$):

$$m^*\ddot{x} + \eta_i\dot{x} - \eta_i y = \big(\tau_{stat} - \tau_{res}\big) \tag{2.16}$$

Equation2.16 is formed by the sum of a dynamic term, taking into account of the slope acceleration, of a viscous term, in which the delayed strains is accounted and a forcing term, deriving from external forces acting on the system . Substituting Equations2.14 and 2.12 in Equation2.16 and by means of a finite difference integration scheme, both for $f > 0$ and for $f \leq 0$, it is possible to simulate the displacement of the slope.

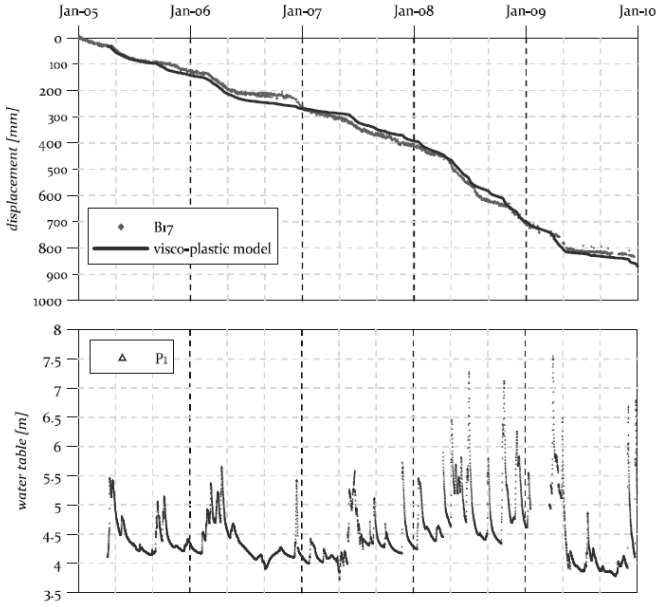

Figure 2.20: Measured and predicted displacements obtained by using the 1D rigid-visco-plastic model

In Figure2.20 a comparison between the predicted and measured displacement at a point of the landslide called B17 can be seen.
As can be noticed, the model predictions fit quite well the monitored data.
A multi-block application of this model can be found in [Crosta et al., 2014], in which La Saxe rockslide has been analyzed.
As it was previously mentioned, this simplified 1D rigid-visco-plastic model works under the hypothesis of no structural hardening or softening. Not considering these aspects implies that the plastic resources of the system have already been exploited and there is no possibility to take into account of a possible degradation of cohesion. As a consequence, this model is not able to predict the triggering of a landslide but only to foresee landslides reactivation.

Chapter 3

Elastoplastic response of infinite slopes under simple shear conditions

In this chapter the mechanical response of an infinite slope under simple shear conditions will be described, with particular attention to structural hardening phenomenon and the results of some numerical simulations will be shown.
The infinite slope configuration is sketched in Figure3.1. This configuration is analyzed under mixed controlled conditions; moreover, along n direction, the problem is incrementally uncoupled: each layer behaves as an in series system and can be studied separately.
Due to the mixed control conditions, τ_{nt} and σ'_{nt} are imposed. Two unknowns in terms of stresses are present: due to the fact that the system is infinite in t and y direction, shear stresses in y direction cannot develop. So the effective stress tensor for an infinite slope configuration is defined as:

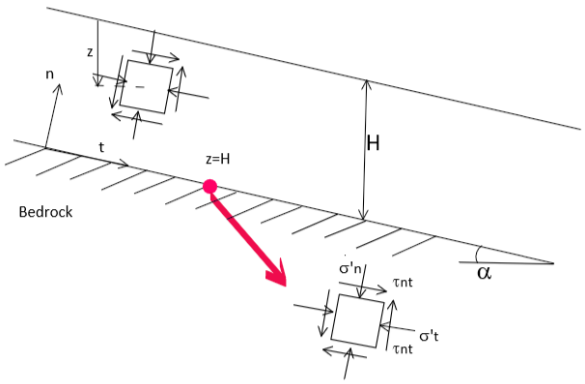

Figure 3.1: Geometrical scheme of the infinite slope

$$\sigma'_{ij} = \begin{bmatrix} \sigma'_n & \tau_{nt} & 0 \\ \tau_{nt} & \sigma'_t & 0 \\ 0 & 0 & \sigma'_y \end{bmatrix} \tag{3.1}$$

In y direction the stresses are self balanced due to symmetry. Under the hypothesis of constant material weight, the equilibrium equations under static conditions along t and n direction can be written as:

$$\begin{cases} \frac{\partial \dot{\sigma}'_n}{\partial n} + \frac{\partial \dot{\tau}_{nt}}{\partial t} + \frac{\partial \dot{\tau}_{ny}}{\partial y} = 0 \\ \frac{\partial \dot{\tau}_{tn}}{\partial n} + \frac{\partial \dot{\sigma}'_t}{\partial t} + \frac{\partial \dot{\tau}_{ty}}{\partial y} = 0 \end{cases} \tag{3.2}$$

The shear stress components τ_{ny} and τ_{ty} have to be nil and, being the geometry of an infinite extension in t direction, all the derivatives with respect to t must be zero, due to the fact that the state of stress along each vertical is identical to the one on the adjacent vertical. For these reasons, Equations3.2 become:

$$\begin{cases} \frac{\partial \dot{\sigma}'_n}{\partial n} = 0 \\ \frac{\partial \dot{\tau}_{nt}}{\partial n} = 0 \end{cases} \tag{3.3}$$

Only two unknowns in terms of strains are present. For the compatibility condition, all the strain components in y direction and the strain ε_t are nil. So the strain tensor is defined as:

$$\varepsilon_{ij} = \begin{bmatrix} \varepsilon_n & \varepsilon_{nt} & 0 \\ \varepsilon_{nt} & 0 & 0 \\ 0 & 0 & 0 \end{bmatrix} \tag{3.4}$$

Owing to the symmetry of the problem, the displacement component along y direction u_y is nil, so the displacement vector is defined as:

$$u_i = \begin{bmatrix} u_n \\ u_t \\ 0 \end{bmatrix} \tag{3.5}$$

The stress, strain and displacement show that the slope loading conditions are the so called simple shear conditions (SSC). In the static case, only the equilibrium equations are enough to determine the stresses along n direction, while a redundancy still exists in t and y direction.
In this chapter some simulations with a numerical model integrating the constitutive equations under SSC will be performed (§3.3). To study the problem a strain softening elastic plastic constitutive relationship is adopted. The constitutive law is characterized by the following ingredients:

- An isotropic linear elastic law;

$$\dot{\varepsilon}^{el}_{ij} = C^{el}_{ijhk}\dot{\sigma'}_{hk}, \tag{3.6}$$

where C^{el}_{ijhk} is the elastic compliance matrix and σ'_{ij} is the effective stresses tensor.
The elastic properties, the Young modulus and the Poisson's ratio are hereafter named E and ν, respectively.

- a yield function defined according to the Mohr Coulomb failure criterion:

$$f = \frac{1}{2}\Big[\sqrt{4\tau^2_{nt} + \big(\sigma'_n - \sigma'_t\big)^2} - \big(\sigma'_n + \sigma'_t\big)sin\phi' - 2c'cos\phi'\Big], \tag{3.7}$$

where ϕ' is the material friction angle, whereas c' is the cohesion, which is also the hardening variable

- a plastic potential defined as follows:

$$g = \frac{1}{2}\Big[\sqrt{4\tau^2_{nt} + \big(\sigma'_n - \sigma'_t\big)^2} - \big(\sigma'_n + \sigma'_t\big)sin\psi - 2\bar{c}cos\psi\Big], \tag{3.8}$$

where ψ is the soil dilatancy angle assumed to be constant for the sake of simplicity and $\bar{c}$ is a dummy variable.

- an hardening law defined as:

$$\dot{c}' = -c'm\big(|\dot{\varepsilon}^{irr}_n| + |\dot{\varepsilon}^{irr}_t| + |\dot{\gamma}^{irr}_{tn}|\big), \tag{3.9}$$

where the non dimensional parameter m defines the brittleness of the material response.

As simple shear conditions have to be studied the presence of a "volumetric cap" for the yield function was not taken into account.

3.1 Structural hardening under simple shear conditions

In this chapter an elastic perfectly plastic constitutive model will be considered: this implies that the parameter m of Equation3.9 is set equal zero.
The assumption of "virgin slope" is considered: it implies that the unique loading process experienced by the stratum is just fresh deposition (i.e. gravity loading).

A deposition process on a plane inclined of an angle α is considered: during this phase on that plane this static condition holds:

$$\tau_{nt} = \sigma'_n tan\alpha. \tag{3.10}$$

Writing a linear elastic isotropic law and the compatibility law:

$$\dot{\varepsilon}_t = \dot{\varepsilon}_n = 0 \longrightarrow -\nu\frac{\dot{\sigma}'_n}{E} + \frac{\dot{\sigma}'_t}{E} - \nu\frac{\dot{\sigma}'_y}{E} = -\nu\frac{\dot{\sigma}'_n}{E} - \nu\frac{\dot{\sigma}'_t}{E} + \frac{\dot{\sigma}'_y}{E} = 0 \tag{3.11}$$

the following is obtained

$$\dot{\sigma}'_t = \dot{\sigma}'_y = \frac{\nu}{1-\nu}\dot{\sigma}'_n. \tag{3.12}$$

With the hypothesis that no plastic phenomenon occurred during the deposition process, Equation3.12 can be integrated as follows:

$$\sigma'_t = \frac{\nu}{1-\nu}\sigma'_n. \tag{3.13}$$

The yielding shear stress can be found imposing $f = 0$ and solving the following equation with respect to τ_{nt}

$$f = \frac{1}{2}\Big[\sqrt{4\tau_{nt}^2 + \big(\sigma'_n - \sigma'_t\big)^2} - \big(\sigma'_n + \sigma'_t\big)sin\phi' - 2c'cos\phi'\Big] = 0 \tag{3.14}$$

Equation3.13 can be rewritten as:

$$\frac{\sqrt{\big(\sigma'_n - \sigma'_t\big) + 4\tau_{nt}^2} - 2c'cos\phi}{\sigma'_n + \sigma'_t} = sin\phi' \tag{3.15}$$

subsitutiting Equation3.15 in Equation3.13 and taking into account of the balance of momentum the following can be written:

$$\frac{\sqrt{\left(\sigma'_n - \frac{\nu}{1-\nu}\sigma'_n\right)^2 + 4\sigma'^2_n tan^2\alpha} - 2c'cos\phi'}{\sigma'_n + \frac{\nu}{1-\nu}\sigma'_n} = \frac{\sqrt{\left(1 - \frac{\nu}{1-\nu}\right)^2 + 4tan^2\alpha} - 2c'cos\phi'}{1 + \frac{\nu}{1-\nu}} = sin\phi', \tag{3.16}$$

so the angle for which the system yields can be found.

$$tan\alpha_y = \frac{1}{2}\frac{\sqrt{4\nu\big(1-\nu\big) - cos^2\phi'}}{1-\nu} + \sqrt{c'cos\phi\left[c'cos\phi\big(1-\nu\big)^2 + sin\phi\right]}. \tag{3.17}$$

If the slope angle is equal to α_y the system yielding occurs, but, due to the system redundancy, the failure is not reached. In case of not statically redundant system and associated flow rule α_y would be equal to the material friction angle ϕ'. In case of non associated flow rule $\alpha_y = \phi'_{SSC}$.
For angles of deposition higher than α_y the effective stress σ'_t will not satisfy anymore Equation3.15.
To study the structural hardening phenomenon a simple shear stress path (SS) is taken in exam, starting from an initial condition in terms of stresses which is elastic, but with $\alpha = \alpha_y$: this implies that the loading path is elastic-plastic since its very beginning.
For sake of simplicity a stress path characterized by $\dot{\sigma'}_n = 0$ will be considered; later on (§3.2) a more generic case will be discussed.
In an elastic percfectly plastic case it is possible to write the consistency condition, according to which plastic strain develop when $f = \dot{f} = 0$:

$$\dot{f} = \frac{\partial f}{\partial \sigma'_{ij}} \dot{\sigma}'_{ij} = 0 \tag{3.18}$$

in this particular case it becomes:

$$\frac{\partial f}{\partial \sigma'_n} \dot{\sigma}'_n + \frac{\partial f}{\partial \sigma'_t} \dot{\sigma}'_t + \frac{\partial f}{\partial \sigma'_y} \dot{\sigma}'_y + 2 \frac{\partial f}{\partial \tau_{nt}} \dot{\tau}_{nt} = 0 \tag{3.19}$$

a non associate flow rule is assumed and plastic deformation are written as:

$$\varepsilon^p_{ij} = \dot{\Lambda} \frac{\partial g}{\partial \sigma'_{ij}}; \tag{3.20}$$

combining compatibility equations with the flow rule the following is obtained.

$$\begin{cases} \dot{\varepsilon}_t = -\nu \frac{\dot{\sigma}'_n}{E} + \frac{\dot{\sigma}'_t}{E} - \nu \frac{\dot{\sigma}'_y}{E} + \dot{\Lambda} \frac{\partial g}{\partial \sigma'_t} = 0 \\ \dot{\varepsilon}_y = -\nu \frac{\dot{\sigma}'_n}{E} - \nu \frac{\dot{\sigma}'_t}{E} + \frac{\dot{\sigma}'_y}{E} = 0 \end{cases} \tag{3.21}$$

In Equation3.21 the plastic strains along y direction are not present: this is due to the fact that σ'_y is the average effective stress and the Mohr Coulomb failure criterion has the hypothesis of no influence of the intermediate stress, so the plastic potential does not depend on σ'_y (Equation3.8).
As previously assumed $\dot{\sigma}'_n = 0$, so Equation3.21 becomes:

$$\dot{\sigma}'_y = \nu \dot{\sigma}'_t, \tag{3.22}$$

while from Equation3.18 and 3.21:

$$df = \frac{\partial f}{\partial \sigma'_t} \dot{\sigma}'_t + 2 \frac{\partial f}{\partial \tau} \dot{\tau} = 0 \rightarrow \dot{\sigma}'_t = -\frac{2 \frac{\partial f}{\partial \tau}}{\frac{\partial f}{\partial \sigma'_t}} \dot{\tau}, \tag{3.23}$$

$$\dot{\Lambda} = \frac{\nu\dot{\sigma}'_y - \dot{\sigma}'_t}{E\frac{\partial g}{\partial \sigma'_t}} \longrightarrow \dot{\Lambda} = \frac{2\left(1-\nu^2\right)\frac{\partial f}{\partial \tau_{nt}}}{E\frac{\partial g}{\partial \sigma'_t}\frac{\partial f}{\partial \sigma'_t}}\dot{\tau}_{nt}. \tag{3.24}$$

Substituting the denominator with the controllability modulus H_χ, whose meaning will be better clarified in Appendix B, Equation3.24 can be rewritten as:

$$\dot{\Lambda} = \frac{2\frac{\partial f}{\partial \tau_{nt}}}{H_\chi}\dot{\tau}_{nt}. \tag{3.25}$$

The shear strain increment for this case can be written as:

$$\dot{\gamma}_{nt} = \frac{\dot{\tau}_{nt}}{G} - \dot{\Lambda}\frac{\partial g}{\partial \tau_{nt}} = \frac{\dot{\tau}_{nt}}{G} - \frac{2\frac{\partial f}{\partial \tau_{nt}}}{H_\chi}\dot{\tau}_{nt}\frac{\partial g}{\partial \tau_{nt}}. \tag{3.26}$$

From integration of Equation3.26 the red curve of Figure3.2 is obtained. From point A plastic strains start to develop and, despite the perfect elastoplasticity assumption, the curve is characterized by a pseudo-hardening branch: this effect is basically due to the static redundancy of the constrained soil element and it is thus called "structural". This structural hardening is due to the increase in σ'_t.

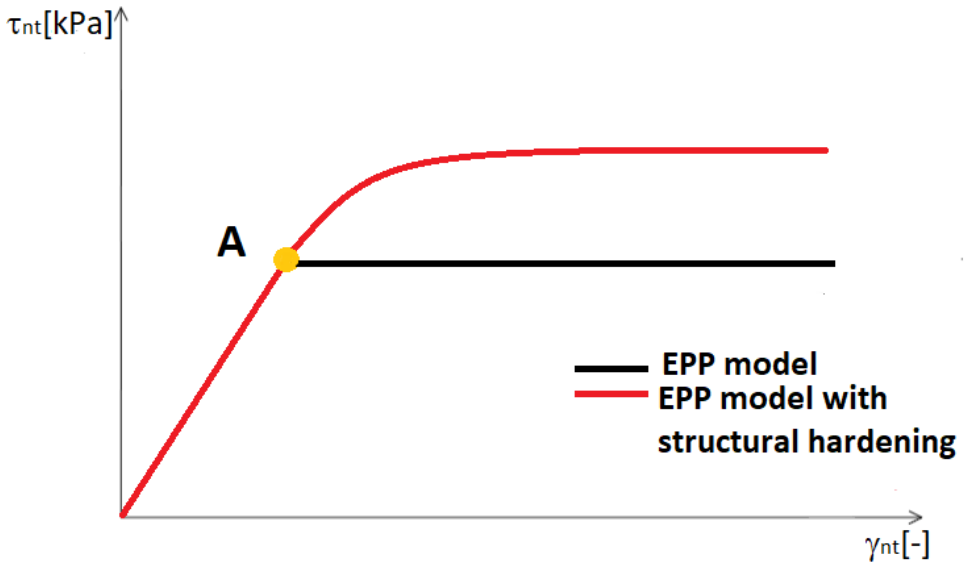

Figure 3.2: τ_{nt}-γ_{nt} curves showing the difference between the elastic perfectly plastic constitutive law in the presence of structural hardening and the law without it

Equation3.26 with Equation3.23 completely describe the system response. In particular, Equation3.26 could be interpreted as a 1D constitutive model relating γ_{nt} and τ_{nt}, in which σ'_t can be seen as an internal variable, whose evolution law is

defined by Equation3.23.
From Equation3.26 it is possible to notice that the system failure (loss of controllability) coincides with the nullification of the denominator:

$$H_\chi = 0. \tag{3.27}$$

If Equation3.27 is satisfied, the plastic multiplier is no longer defined and infinite irreversible strains will develop. This aspect is better described in AppendixB.
For this particular loading path, Equation3.27 implies that loss of controllability is reached if one of the following conditions holds:

$$\frac{\partial g}{\partial \sigma'_t} = 0, \tag{3.28}$$

$$\frac{\partial f}{\partial \sigma'_t} = 0. \tag{3.29}$$

In particular, to find the maximum values of the shear stress and hyperstatic variable $\tau_{nt,max}$ and $\sigma'_{t,max}$, the following system of equations has to be solved:

$$\begin{cases} f = 0 \\ \frac{\partial g}{\partial \sigma'_t} = 0 \end{cases} \tag{3.30}$$

The following expressions for $\sigma'_{t,max}$ and $\tau_{nt,max}$ are obtained:

$$\tau_{nt,max} = \frac{\left(c' cos\phi' + \sigma'_n sin\phi'\right) cos\psi}{1 - sin\psi \ sin\phi'}, \tag{3.31}$$

$$\sigma'_{t,max} = \sigma'_n + 2tan\psi\tau_{nt,max}. \tag{3.32}$$

The presence of this structural hardening regime generates a difference between the yielding shear stress and the maximum shear stress, that according to the standard elastic-perfectly plastic law should coincide (black curve of Figure3.2).

3.2 Stress path dependence

As already outlined in the previous section, the $\gamma_{nt} - \tau_{nt}$ relationship described by Equation3.26 can be interpreted as a 1D lumped model, whose internal variable is the hyperstatic variable σ'_t. In general, the evolution of γ_{nt} is expected to depend on the imposed stress path.
In this section a more generic stress path, characterized by $\dot{\tau}_{nt} \neq 0$ and $\dot{\sigma'}_n \neq 0$ is discussed.

Following the same steps of the previous section, writing the linear elastic isotropic law and compatibility law the following is obtained:

$$\dot{\varepsilon}_y^{el} = 0 = \frac{\dot{\sigma'}_y}{E} - \nu\frac{\dot{\sigma'}_n}{E} - \nu\frac{\dot{\sigma'}_t}{E}, \tag{3.33}$$

$$\dot{\sigma'}_y = \nu\big(\dot{\sigma'}_n + \dot{\sigma'}_y\big). \tag{3.34}$$

Imposing $\dot{\varepsilon}_t = 0$ and substituting Equation3.34:

$$\dot{\varepsilon}_t^{el} = \frac{\dot{\sigma'}_t}{E} - \nu\frac{\dot{\sigma'}_n}{E} - \frac{\nu^2}{E}\big(\dot{\sigma'}_n + \dot{\sigma'}_y\big), \tag{3.35}$$

$$\dot{\varepsilon}_t = 0 \longrightarrow \dot{\varepsilon}_t^{el} = -\dot{\varepsilon}_t^{p} \longrightarrow \frac{\dot{\sigma'}_t}{E}\big(1-\nu^2\big) - \nu\big(1+\nu\big)\frac{\dot{\sigma'}_n}{E} = -\dot{\Lambda}\frac{\partial g}{\partial \sigma'_t} \tag{3.36}$$

the increment of the hyperstatic variable σ'_t can be obtained:

$$\dot{\sigma'}_t = -\dot{\Lambda}\frac{\partial g}{\partial \sigma'_t}\frac{E}{\big(1-\nu^2\big)} + \frac{\nu}{\big(1-\nu\big)}\dot{\sigma'}_n. \tag{3.37}$$

Writing the consistency law, substituting the increment of σ'_t in Equation3.36 and dividing the terms multiplied by the stresses from those multiplied by the plastic multiplier increment, the following expression is obtained:

$$\left(\frac{\partial f}{\partial \sigma'_n} + \frac{\partial f}{\partial \sigma'_t}\frac{\nu}{\big(1-\nu\big)}\right)\dot{\sigma}_n + \frac{\partial f}{\partial \tau_{nt}}\dot{\tau}_{nt} = \dot{\Lambda}\left(\frac{\partial g}{\partial \sigma'_t}\frac{\partial f}{\partial \sigma'_t}\frac{E}{\big(1-\nu^2\big)}\right). \tag{3.38}$$

It is thus possible to find an expression for the plastic multiplier:

$$\dot{\Lambda} = \frac{\left(\frac{\partial f}{\partial \sigma'_n} + \frac{\partial f}{\partial \sigma'_t}\frac{\nu}{\big(1-\nu\big)}\right)\dot{\sigma'}_n + \frac{\partial f}{\partial \tau_{nt}}\dot{\tau}_{nt}}{H_\chi}, \tag{3.39}$$

so the complete costitutive law can be written as:

$$\dot{\gamma}_{nt} = \frac{\dot{\tau}_{nt}}{G} + \frac{\left(\frac{\partial f}{\partial \sigma'_n} + \frac{\partial f}{\partial \sigma'_t}\frac{\nu}{\big(1-\nu\big)}\right)\dot{\sigma'}_n + \frac{\partial f}{\partial \tau_{nt}}\dot{\tau}_{nt}}{H_\chi}\frac{\partial g}{\partial \tau_{nt}}. \tag{3.40}$$

As can be noticed from Equation3.40 and 3.37, both the total strain increment and the internal variable increment depend on $\dot{\tau}_{nt}$ and $\dot{\sigma'}_n$. The ratio $\frac{\tau_{nt}}{\sigma'_n}$ (i.e. the stress path), governs the evolution of both γ_{nt} (Equation3.40) and σ'_t (Equation3.37): different stress paths (Figure3.3) imply different evolution of γ_{nt} and σ'_t
Calling β the ratio $\frac{\sigma'_n}{\tau_{nt}}$ Equation3.40 can be rewritten as:

$$\dot{\gamma}_{nt} = \frac{\dot{\tau}_{nt}}{G} + \frac{\left(\frac{\partial f}{\partial \sigma'_n} + \frac{\partial f}{\partial \sigma'_t}\frac{\nu}{\big(1-\nu\big)}\right)\beta\dot{\tau}_{nt} + \frac{\partial f}{\partial \tau_{nt}}\dot{\tau}_{nt}}{H_\chi}\frac{\partial g}{\partial \tau_{nt}}. \tag{3.41}$$

The constitutive law is thus dependent on the τ_{nt} and on the constant β representing the stress path ("incrementally non-linear").
From Equation3.40 it is possible to see that integrating this constitutive law taking into account of σ'_t is not very straightforward. So, even if it is possible to take into account the structural hardening phenomenon through the hyperstatic variable σ'_t, an alternative, more feasible procedure has been chosen to simplify the model, which is the introduction a 1D elastic plastic constitutive relationship. In this relationship the role of static redundancy (evolution of σ'_t) is introduced with an hardening rule. This hardening rule is expected to depend on the stress path.

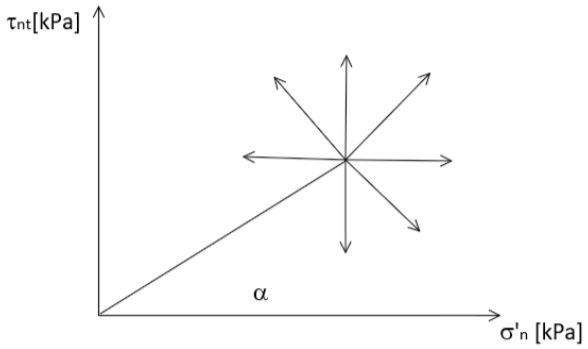

Figure 3.3: Some of all the possibile stress paths that could be studied

For sake of brevity, the only stress path discussed in this thesis is the evolution of $\tau_{nt} - \sigma'_n$ related to the water table level change, that can be due to intense rainfall or to anthropic activity and it is the main triggering factor for landslide development; it is characterized by a reduction in σ'_n and an increase in τ_{nt} (Figure3.4). The hydromechanical coupling is neglected: it is assumed that permeability is sufficiently high in order not to have excess pore pressure development.
The stress path can be written as follows:

$$\begin{cases} \dot{\sigma'}_n = -\left(\gamma_d - \gamma'\right) cos^2 \alpha \dot{h}_w \\ \dot{\tau}_{nt} = \left(\gamma_{sat} - \gamma_d\right) cos \alpha sin \alpha \dot{h}_w \end{cases} \tag{3.42}$$

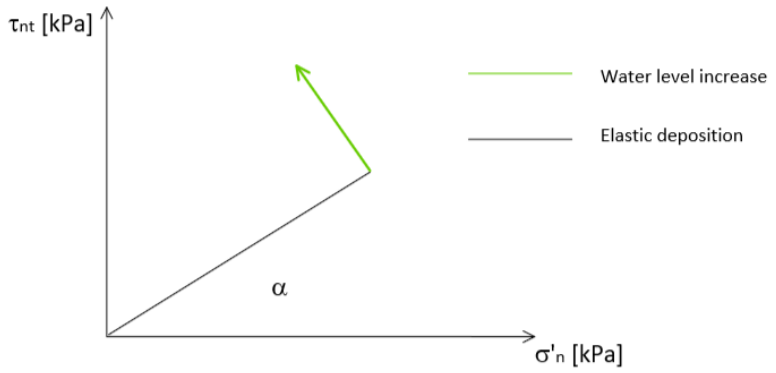

Figure 3.4: Stress path representing the water table level increase after an elastic deposition process

From Equations3.42 a relationship between the increment of σ'_n and τ_{nt} can be found:

$$\begin{cases} \dot{\sigma'}_n = -\dfrac{\left(\gamma_d - \gamma'\right)}{\left(\gamma_{sat} - \gamma_d\right) tan\alpha} \dot{\tau}_{nt} \\ \beta = \frac{\dot{\sigma'}_{nt}}{\dot{\tau}_{nt}} \end{cases} \tag{3.43}$$

The increment of σ'_t is obtained substituting Equation3.43 in Equation3.37 and writing the consistency law:

$$\dot{\sigma'}_t = -\frac{\left[\frac{\partial f}{\partial \sigma'_n} + \frac{\partial f}{\partial \sigma'_t}\frac{\nu}{1-\nu}\right]\frac{\gamma' - \gamma_d}{\gamma_{sat}-\gamma_d}\frac{1}{tan\alpha} + \frac{\partial f}{\partial \tau_{nt}}}{H_\chi} \frac{\partial g}{\partial \sigma'_t} \frac{E}{1-\nu^2} \beta \dot{\sigma'}_n + \frac{\nu}{1-\nu}\frac{\gamma' - \gamma_d}{\gamma_{sat} - \gamma_d}\frac{\beta \dot{\sigma'}_n}{tan\alpha}. \tag{3.44}$$

Substituting Equation3.43 in the constitutive law given by Equation3.40 the constitutive model is obtained. The direct relationship between $\dot{\tau}_{nt}$ and $\dot{\gamma}_{nt}$ can be written as follows:

$$\dot{\gamma}_{nt} = \frac{\beta \dot{\sigma'}_n}{G} + \frac{\left[\frac{\partial f}{\partial \sigma'_n} + \frac{\partial f}{\partial \sigma'_t}\frac{\nu}{1-\nu}\right]\frac{\gamma' - \gamma_d}{\gamma_{sat}-\gamma_d}\frac{1}{tan\alpha} + \frac{\partial f}{\partial \tau_{nt}}}{H_\chi} \frac{\partial g}{\partial \tau_{nt}} \beta \dot{\sigma'}_n. \tag{3.45}$$

3.3 Numerical simulation

The introduction of softening is important to reproduce the phenomenon of material damage typical of cemented materials. This particular material behaviour cannot be analyzed through the elastoplastic constitutive model, due to the fact

that in mixed control conditions, if consistency law is valid, it is not possible to proceed with loading after the peak. So this phenomenon will be analyzed only in the framework of viscoplasticity (Chapter4): the removal of consistency law lets the system to reach every load level, because the state of stress can lie also outside the yield surface.
Despite this, for sake of simplicity, in this section the numerical solution under simple shear conditions completely integrating the constitutive law equations (hereafter called SSC solution) will be analyzed: as a first step, an elastoplastic constitutive law (Equation3.45) will be used to study the influence of structural hardening on the system response, so the parameter m, governing the fragility of the material is set equal to zero. The model equations that are integrated are those reported in the previous section.
The study is focused on a reference case of a material element at a depth $z = H$.
The attention is focused on the case of water level change from 0 to H (Figure3.4), implying the increase of τ_{nt} and a decrease in σ'_n. As it was previously mentioned, this stress path can be described by Equations3.42.
Where $\gamma_d = 16kN/m^3$ is the dry unit weight of the material, $\gamma' = \gamma_{sat} - \gamma_w$ is the effective unit weight, with $\gamma_{sat} = 20kN/m^3$ the saturated unit weight and $\gamma_w = 10kN/m^3$ water unit weight.
In the table below the parameters used for a SSC simulation are shown.

H	α	E	ν	ϕ'	ψ	c'
$[m]$	$[°]$	$[MPa]$	$[-]$	$[°]$	$[°]$	$[kPa]$
5	15	130	0.3	30	30	24

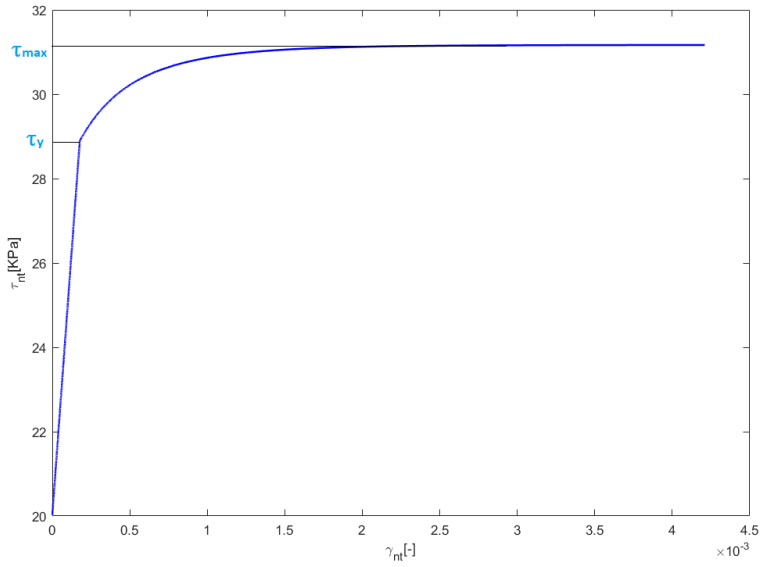

Figure 3.5: $\tau_{nt} - \gamma_{nt}$ curve resulting from the SSC simulation

In Figure3.5 the result of SSC simulation are reported in the $\tau_{nt} - \gamma_{nt}$ plane. The $\tau_{nt} - \gamma_{nt}$ is characterized by an initial elastic branch, whose slope is the shear modulus G and only elastic/reversible strains are accumulated; at a certain stress level, identified with the yield shear stress τ_y, irreversible strains start to develop and the material behaviour becomes irreversible, so during an unloading process, only the elastic part of deformation would be recovered. Due to the system static redundancy, after τ_y is reached, the system accumulates irreversible strains without collapsing,: in this range of stresses the structural hardening phenomenon takes place. When the hyperstatic variable σ'_t has reached its maximum value, the maximum shear stress τ_{max} is reached and the loss of controllability of the system is obtained.

Yielding stress τ_y evaluation

The yielding stress is the value of shear stress for which the yield function f is equal to zero and corresponds to the starting of plastic deformation and of structural hardening. To calculate it, it is necessary to solve a system of three equations and

three unknowns (i.e τ_y, $\sigma'_{n,y}$, $h_{w,y}$).

$$\begin{cases} f = \frac{1}{2}\left[\sqrt{4\tau_{nt}^2 + (\sigma'_n - \sigma'_t)^2} - (\sigma'_n + \sigma'_t)sin\phi' - 2c'cos\phi'\right] = 0 \\ \sigma'_n = -\big(\gamma_d - \gamma'\big)cos\alpha^2 h_w + \gamma_d cos\alpha^2 H \\ \tau_{nt} = \big(\gamma_{sat} - \gamma_d\big)cos\alpha sin\alpha h_w + \gamma_d cos\alpha sin\alpha H \end{cases} \tag{3.46}$$

The first equation represents the yielding condition, which corresponds to the annulment of the yield function f and the other two equations represent the stress path which is characterized by the dependency of stresses on the water table level: $\sigma'_n = \sigma'_n(h_w)$ $\tau_{nt} = \tau_{nt}(h_w)$.
Through the solution of this system it is possible to find: $\tau_{nt,y}$, $\sigma'_{n,y}$ and h_{w_y} representing the variables for which the elastic regime is abandoned.
Solving the system of Equations3.46 the following expression for $\tau_{nt,y}$ is obtained:

$$\tau_{nt,y} = \frac{-\big[-\frac{2be}{d^2} + \frac{2bsin^2\phi'}{d^2h^2} + \frac{4c'sin\phi'cos\phi'}{dh}\big] + \sqrt{\big[-\frac{2be}{d^2} + \frac{2bsin^2\phi'}{d^2h^2} + \frac{4c'sin\phi'cos\phi'}{dh}\big]^2 - 4\big[4 + \frac{e}{d^2} - \frac{sin^2\phi'}{d^2h^2}\big]C^*}}{2\big[4 + \frac{e}{d^2} - \frac{sin^2\phi'}{d^2h^2}\big]} \tag{3.47}$$

where

$$C^* = \frac{b^2 e}{d^2} - \frac{b^2}{d^2}\frac{sin^2\phi'}{h^2} - 4c^2cos^2\phi' - \frac{4b}{dh}csin\phi'cos\phi' \tag{3.48}$$

$$d = atan\alpha \tag{3.49}$$

$$e = \frac{\big(1-2\nu\big)^2}{\big(1-\nu\big)^2} \tag{3.50}$$

$$h = 1 - \nu \tag{3.51}$$

$$a = \frac{\gamma_{sat} - \gamma_d}{\gamma_d - \gamma'} \tag{3.52}$$

$$b = Hcos\alpha sin\alpha\gamma_d\Big[\frac{\big(\gamma_{sat} - \gamma_d\big)}{\big(\gamma_d - \gamma'\big)} + 1\Big] \tag{3.53}$$

Maximum allowable shear stress τ_{max} evaluation

The maximum allowable shear stress is the maximum value of the stress that the system is able to sustain; due to the redundancy of the system, this value is reached after structural hardening has completely developed.

This limit value is evaluated solving a system of four equations with four unknowns (i.e τ_{max}, $\sigma'_{n,max}$,$\sigma'_{t,max}$, $h_{w,max}$).

$$\begin{cases} f = \frac{1}{2}\left[\sqrt{4\tau_{nt}^2 + (\sigma'_n - \sigma'_t)^2} - (\sigma'_n + \sigma'_t)sin\phi' - 2c'cos\phi'\right] = 0 \\ \frac{\partial g}{\partial \sigma'_t} = -\frac{\left(\sigma'_n - \sigma'_t\right)}{\sqrt{4\tau_{nt}^2 + \left(\sigma'_n - \sigma'_t\right)^2}} - \frac{sin\psi}{2} = 0 \\ \sigma'_n = -\left(\gamma_d - \gamma'\right)cos\alpha^2 h_w + \gamma_d cos\alpha^2 H \\ \tau_{nt} = \left(\gamma_{sat} - \gamma_d\right)cos\alpha sin\alpha h_w + \gamma_d cos\alpha sin\alpha H \end{cases} \tag{3.54}$$

The first equation corresponds to the annulment of the yield function, the second equation represents the instability condition and the last two equations represent the followed stress path. Setting the derivative of the plastic potential with respect of σ'_t equal zero means imposing the end of the evolution of the hyperstatic variable σ'_t, which corresponds to the end of the structural hardening and, consequently, to the collapse of the system.
Solving the system of Equations3.54 the following expression for $\tau_{nt,max}$ is obtained:

$$\tau_{nt,max} = \frac{-B'^* + \sqrt{B'^{*2} - 4A'^*C'^*}}{2A'^*} \tag{3.55}$$

Where

$$A'^* = 4 + \left(-\frac{1}{d} - m\right)^2 - \left(-\frac{1}{d} + m\right)^2 sin^2\phi' \tag{3.56}$$

$$B'^* = -\frac{4b}{d}\left(-\frac{1}{d} + m\right)sin^2\phi' - 4c'cos\phi' sin\phi'\left(-\frac{1}{d} + m\right) \tag{3.57}$$

$$C'^* = -\frac{4b^2}{d^2}sin^2\phi' - 4c'^2 cos\phi' sin\phi'\frac{2b}{d} \tag{3.58}$$

$$m = -\frac{1}{d} + \frac{2sin\psi}{\sqrt{4 - sin^2\psi}} \tag{3.59}$$

3.3.1 Parametric study

Some simulations have been performed to show the influence of various parameters on the system response.
All the parameters are kept fixed and only one is changed, so that to study each aspect separately. The first parameter which has been changed is the slope angle α.
In the table below the fixed parameters used for the numerical simulation are shown.

H	E	ν	ϕ'	ψ	c'
$[m]$	$[MPa]$	$[-]$	$[°]$	$[°]$	$[kPa]$
5	130	0.3	35	35	24

As can be seen in Figure3.6 increasing α an increase of the maximum stress allowable for the system and of the stress value at which yielding takes place occurs. Another interesting result regards the structural hardening: decreasing α, $\tau_{nt} - \gamma_{nt}$ response is closer to the elastic-perfectly plastic behaviour without structural hardening; if such tendency is observed, the yielding stress and the maximum shear stress are nearly equal.

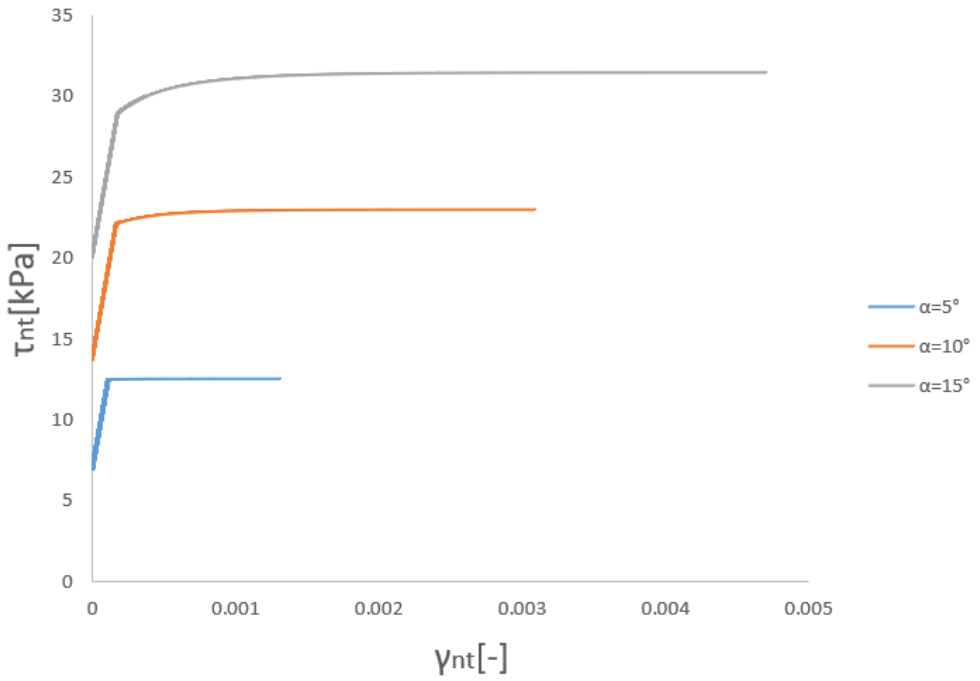

Figure 3.6: τ_{nt}-γ_{nt} curves changing the value of the slope angle α

Then the friction angle is changed keeping fixed all other parameters, which are shown in the table below ($\alpha = 15°$). An example of associative flow rule is analyzed, so $\psi = \phi'$ and the dilatancy angle is varying together with the friction angle. The reference parameters are the same of the previous table.
As can be seen in Figure3.7 both the value of yielding shear stresses and maximum shear stress donot vary a lot. This means that, if an associated flow rule has been chosen, there is no significant change τ_y and τ_{max} and also the structural hardening regime is not influenced and this is due to the fact that the value of cohesion is high.

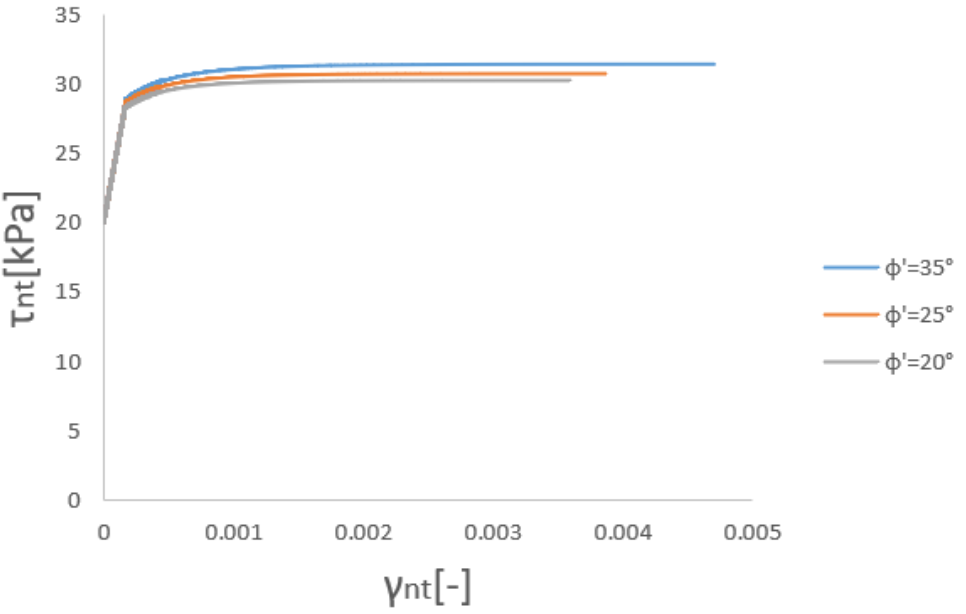

Figure 3.7: $\tau_{nt} - \gamma_{nt}$ curves changing the value of the friction angle ϕ

Then the dilatancy angle is varied keeping fixed all the other parameters (the parameters are the same of the table above with $\alpha = 15°$).
As can be seen in Figure3.8, the increase in dilatancy angle causes a slight increase of the maximum allowable shear stress, while the yielding stress remains the same. This happens because dilatancy starts to influence the system response only after the yielding stress is reached because the flow rule, and so the irreversible strain accumulation, depends on this parameter. So, a less marked structural hardening branch can be seen decreasing ψ.

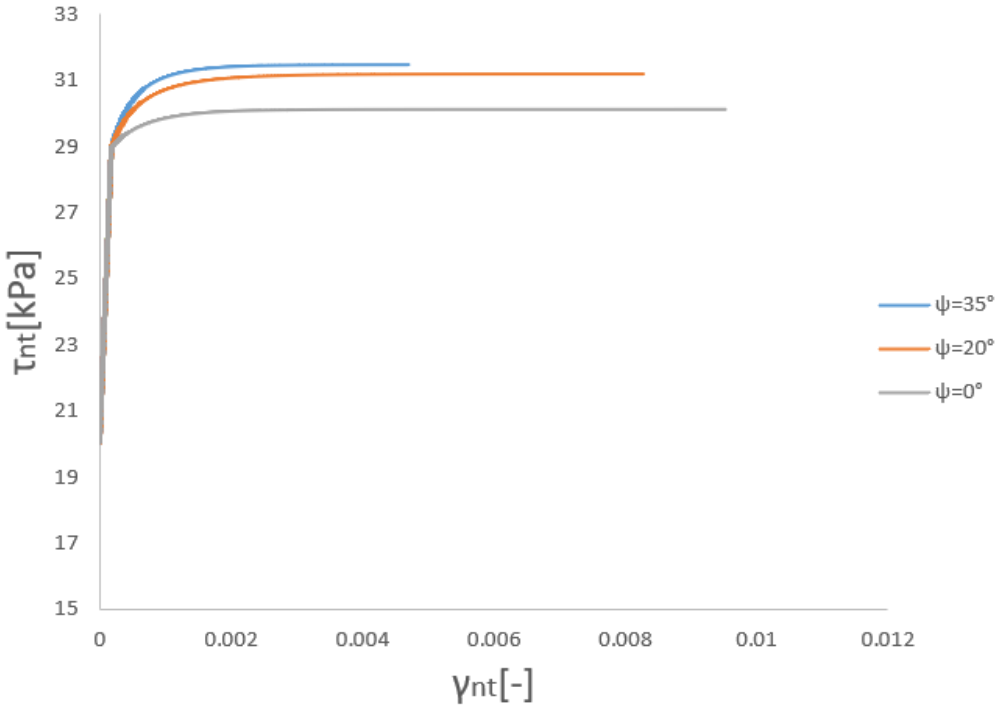

Figure 3.8: $\tau_{nt} - \gamma_{nt}$ curves changing the value of the dilatancy angle ψ

Then the height of the layer is changed. In these simulations $\alpha = 20°, c' = 8kPa$ In Figure3.9 the comparison of τ_{nt}-γ_{nt} curves obtained with different values of H can be seen. Similarly to what happens increasing the slope angle α, as H increases the values of τ_y and τ_{max} are higher. The structural hardening is not particularly influenced because, as can be noticed, the initial slope of the elastoplastic branch in the plane $\tau_{nt} - \gamma_{nt}$ is practically the same for each value of H.

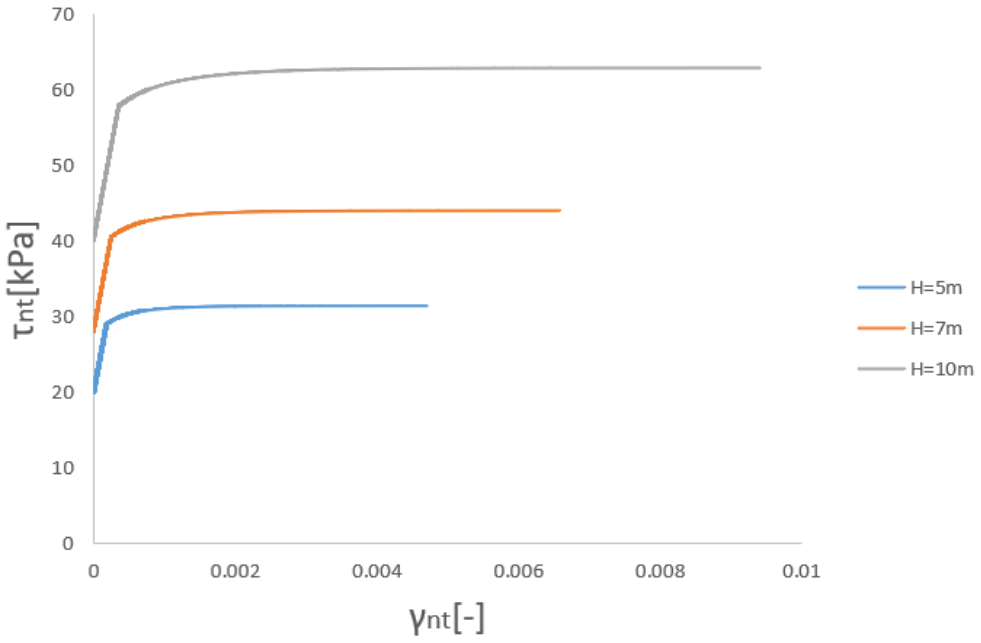

Figure 3.9: $\tau_{nt} - \gamma_{nt}$ curves changing the value of the height H

Then cohesion is changed maintaining constant all the other parameters. In these simulations $\alpha = 20°$.
As shown in Figure3.10 increasing the cohesion the yielding stress and the maximum shear stress increase. The higher c' the lower is the initial slope of the elastoplastic branch, so the less structural hardening is present. This aspect considered, for high values of cohesion, the system shows a trend closer to elastic-perfectly-plastic case without structural hardening.

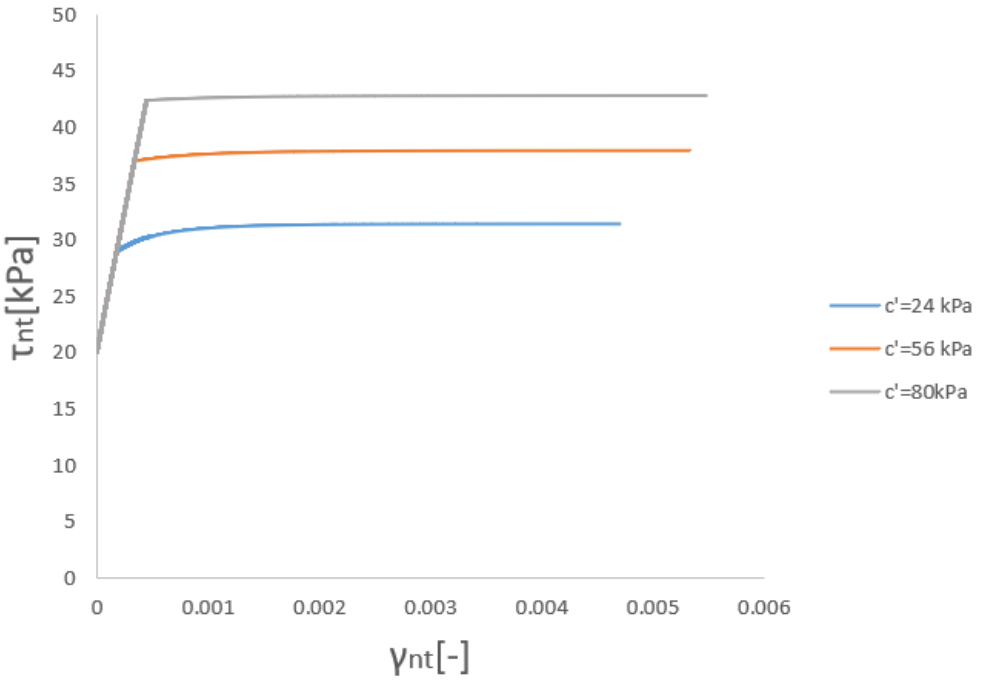

Figure 3.10: $\tau_{nt} - \gamma_{nt}$ curves changing the value of cohesion

Then the Young Modulus E is changed. In these simulations $\alpha = 10°$.
As can be seen in Figure3.11, increasing E the slope of the elastic branch increases, despite this there is no change in the yielding shear stress and maximum shear stress. The structural hardening phenomenon is influenced by the material stiffness as increasing E, the initial elastoplastic stiffness is higher and the maximum shear stress is reached after a minor strain accumulation. In addition can be noticed that the curves are omothetic.

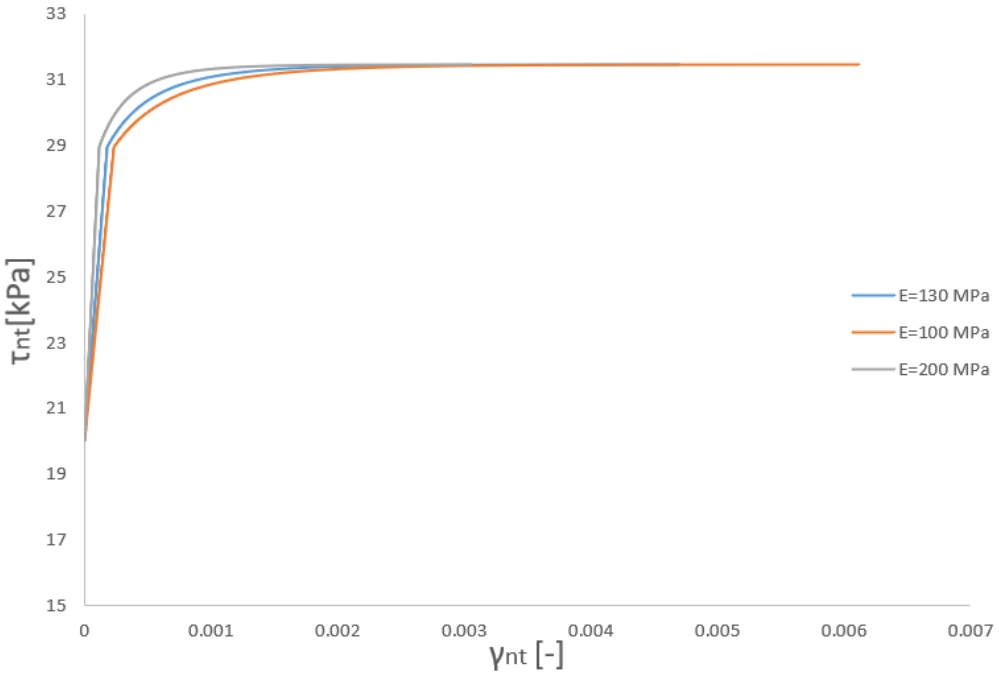

Figure 3.11: $\tau_{nt} - \gamma_{nt}$ curves changing the value of the Young modulus

Finally the poisson ration ν is changed. In these simulations $\alpha = 10°$.

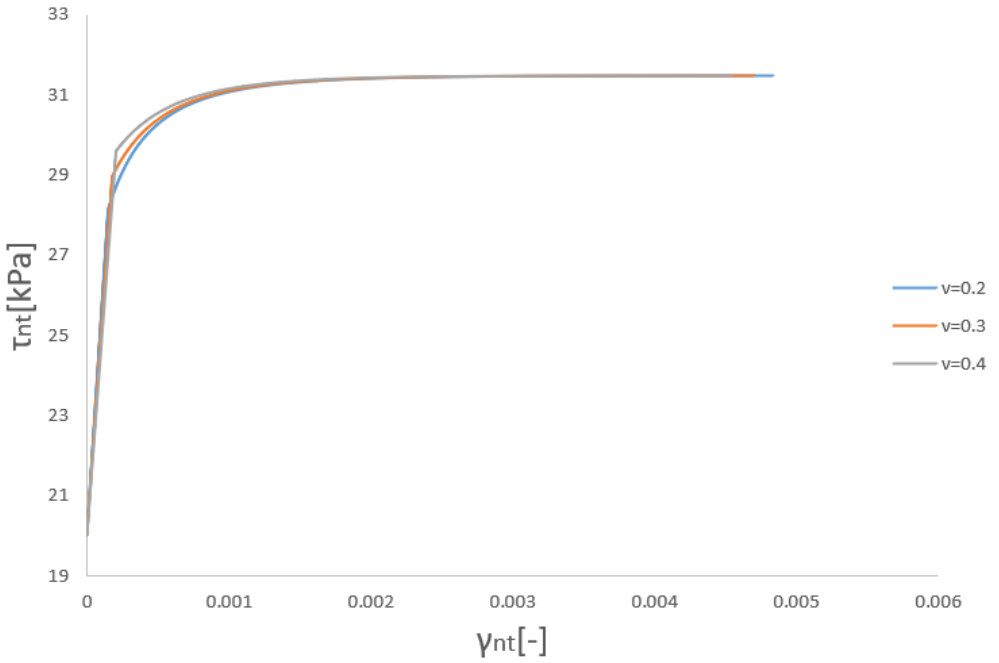

Figure 3.12: $\tau_{nt} - \gamma_{nt}$ curves changing the value of the Poisson ratio

As can be seen in Figure3.12 ν does not influence the maximum shear stress, but influences the yielding shear stress: increasing the Poisson ratio, the yielding shear stress increases and the gap between τ_y and τ_{max} decreases. So increasing ν a minor range of stresses for structural hardening development is expected. The chosen values for ν are upper and lower bounds values for the parameter, but its variability is very low.

3.4 Lumped approach for changing water table levels

In this section a 1D equivalent model aimed at reproducing the system response in terms of $\tau_{nt} - \gamma_{nt}$ curves like those reported in the previous section will be described. The objective of the 1D elastoplastic model is to reduce the number of unknowns of the system and, consequently, to decrease the computational costs. The simplification on the basis of this approach is that all the constitutive equations donot have to be integrated.
Another important objective of the elastoplastic model is to reproduce the structural hardening phenomenon occurring in the infinite slope configuration with simple parameters. This aspect is really fundamental, because structural hardening is related to the static redundancy of the system and taking into account of this phenomenon means taking into account of all the plastic resources of the system.

3.4.1 Model governing equations

In this section the simple equations on the basis of the equivalent-1D model will be discussed. The constitutive model is strain hardening elastic-plastic.
The additivity of deformations holds, so the total deformation is given by the sum of an elastic part and a plastic part:

$$\dot{\gamma}_{nt} = \dot{\gamma}_{nt}^{el} + \dot{\gamma}_{nt}^{pl}, \tag{3.60}$$

where, according to standard elasticity theory:

$$\dot{\gamma}_{nt}^{el} = \frac{\dot{\tau}_{nt}}{G}, \tag{3.61}$$

where G is the constant shear modulus of the material.
As the shear stress overcomes the yielding shear stress τ_y, plastic strains start to develop; this happens when the value of yield function f is equal zero; the 1D yield function can be written as:

$$f^* = \tau_{nt} - \tau_c. \tag{3.62}$$

τ_c is the yielding variable and describes the size of the yield surface when plastic deformation occurs and it evolves until structural hardening is present. At the beginning it is equal to the yielding shear stress τ_y and then increases with plastic strains.
A hardening law has to be introduced to take into account the structural hardening phenomenon:

$$\dot{\tau}_c = R_p\Big(1 - \frac{\tau_c}{\tau_{max}}\Big)\dot{\gamma}_{nt}^{pl}, \tag{3.63}$$

where R_p is the initial plastic stiffness.
As is evident from Equation3.63 and Equation3.62, this model is characterized by two parameters:

- the maximum allowable shear stress τ_{max};
- the plastic stiffness R_p.

As was previously mentioned (§3.1), under simple shear conditions, even if the material is characterized by an elastic-perfectly plastic behaviour, the system response in characterized by a structural hardening, which cannot be captured by an elastic-perfectly plastic 1D model. For this reason a strain hardening constitutive relationship is adopted. Information about σ_t' evolution (structural hardening) are condensed in the model parameters R_p and τ_{max}. The structural hardening is thus taken into account in both the numerical model and 1D model, but there is substantial a difference in terms of the way it is considered. In the model integrating the equations in SSC the structural hardening is given by the evolution of the hyperstatic variable σ_t' and the constitutive model is elastic-perfectly plastic; in the 1D equivalent model, as σ_t' is not considered and the model is very simplified, the hypothesis of EPP constitutive model has to be removed and the only way to take into account of structural hardening is the use of an hardening model.
As an elastoplastic consititutive model is employed, the consistency law is valid and it can be written as:

$$\frac{\partial f}{\partial \tau_{nt}}\dot{\tau}_{nt} + \frac{\partial f}{\partial \tau_c}\dot{\tau}_c = 0 \longrightarrow \dot{\tau}_{nt} = \dot{\tau}_c, \tag{3.64}$$

substituting the value of $\dot{\tau}_c$ in the consistency law the relationship between the loading variable τ_{nt} and the plastic strain is obtained:

$$\dot{\tau}_{nt} = R_p\Big(1 - \frac{\tau_{nt}}{\tau_{max}}\Big)\dot{\gamma}_{nt}^{pl}. \tag{3.65}$$

Rewriting Equation3.60 the following is obtained:

$$\dot{\gamma}_{nt} = \frac{\dot{\tau}_{nt}}{G} + \dot{\tau}_{nt}\Big(\frac{\tau_{max}}{\tau_{max} - \tau_{nt}}\Big)\frac{1}{R_p}. \tag{3.66}$$

Rearranging Equation3.66, 1D constitutive law is obtained

$$\dot{\gamma}_{nt} = \frac{R_p\big(\tau_{max} - \tau_{nt}\big) + G\tau_{max}}{GR_p\big(\tau_{max} - \tau_{nt}\big)}\dot{\tau}_{nt}. \tag{3.67}$$

3.4.2 Parameter calibration

As already outlined the parameters of the model are the maximum shear stress τ_{max} and the plastic stiffness R_p.
τ_{max} is analytically evaluated with Equation3.55, while for the plastic stiffness a different procedure has to be used.

Hardening parameter R_p

Given the $\tau_{nt} - \gamma_{nt}$ curve, the stress strain behaviour is characterized by a linear-elastic branch, whose slope is given by the shear modulus and by an elastoplastic branch, whose initial slope depends on the plastic stiffness R_p.
Due to the fact that an analytical evaluation of this variable is not possible, it has been found through a direct calibration procedure by calibrating the 1D curves on the SSC solution curves.
R_p depends on geometry, cohesion, friction angle, dilatancy angle and depth, thus it is not represented by a constant value, but by a function:

$$R_p = R_p\big(\alpha, \phi', c', \psi, H, G\big) \tag{3.68}$$

the aim of this section is the evaluation of an expression able to reproduce the variation of R_p with the cited parameters. To do so the influence of them on the variable R_p has been studied.
To study the variation of R_p the parametric study reported above, by integrating the constitutive model under simple shear conditions was performed. From this analysis emerged that R_p:

- increases with G;
- is constant with H and ϕ' (Figure3.9, 3.7);
- decreases with c';
- increases with α;
- increases with dilatancy.

As was previously mentioned, the curves of Figure3.11 are omothetic, therefore, R_p linearly depends on G.
The variation of R_p with $c^{**} = c'/(\gamma_d H cos\alpha sin\alpha)$ is reported in Figure3.13: the results are nearly superimposed, so a unique interpolation curve is assumed.
The variation of R_p with $tan\psi$ is reported in Figure3.14.

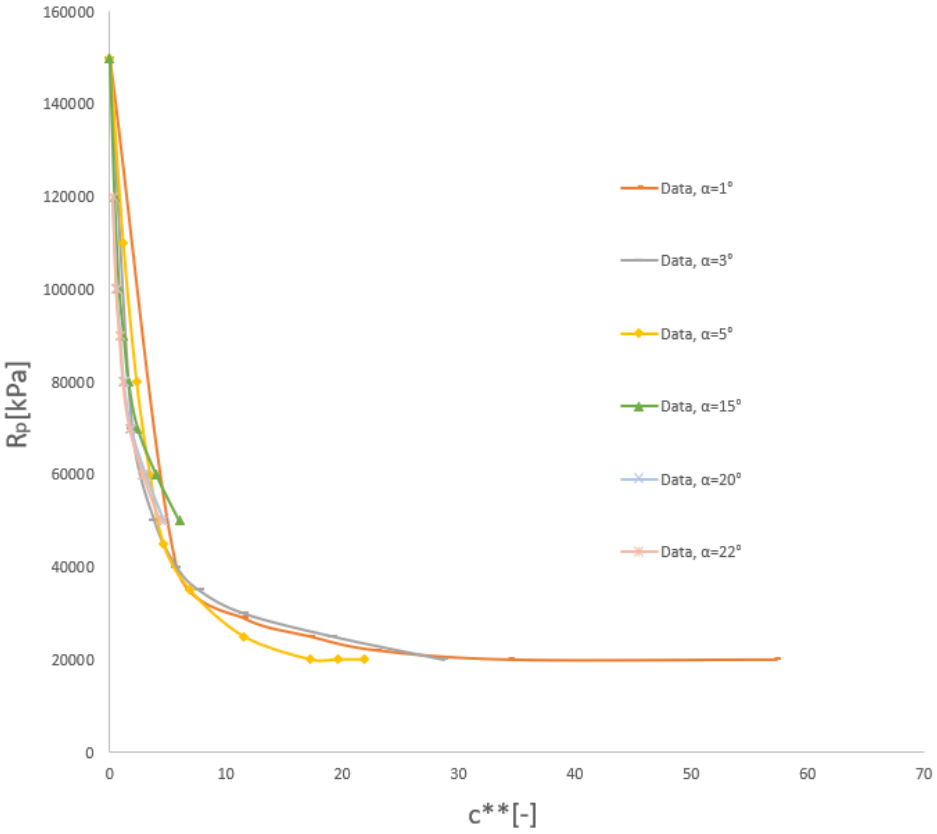

Figure 3.13: Evolution of parameter R_p varying the non-dimensional cohesion c^{**}

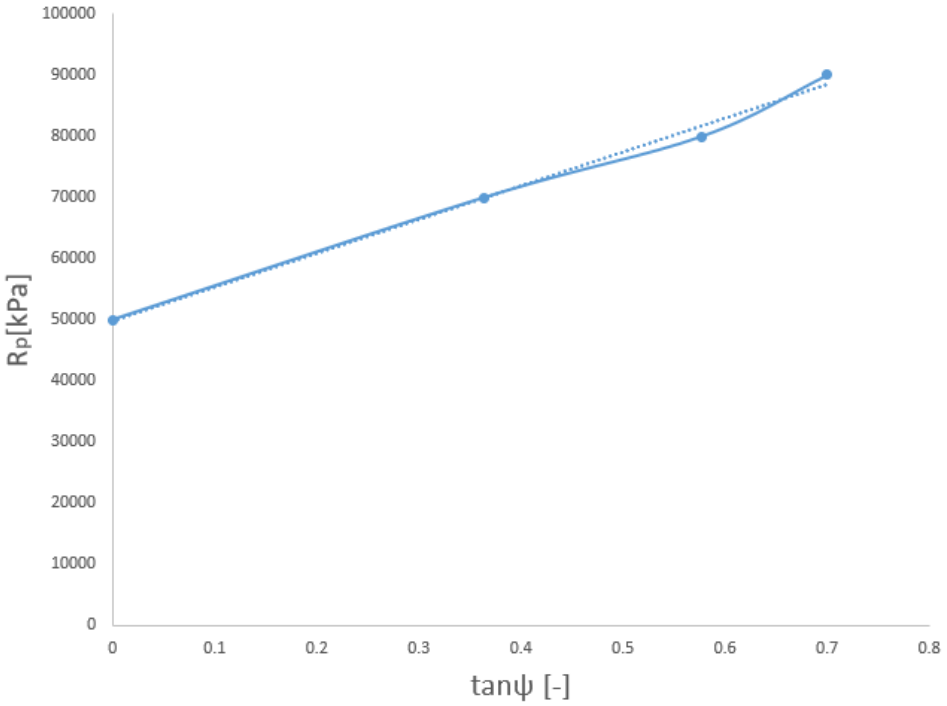

Figure 3.14: Evolution of parameter R_p varying the dilatancy angle ψ

To reproduce this variation, the following expression is proposed:

$$R_p = G\left[a_1 e^{-\frac{c^{**}a_2}{a_1}} + a_3\right]\left(b_1 + b_2 tan(\psi)\right) \tag{3.69}$$

Where the interpolating parameter values are reported in the table below.
The interpolating curve is shown in Figure3.15.

a_1	a_2	a_3	b_1	b_2
1.46	0.9	0.22	0.9945	1.1099

Table 3.4.2

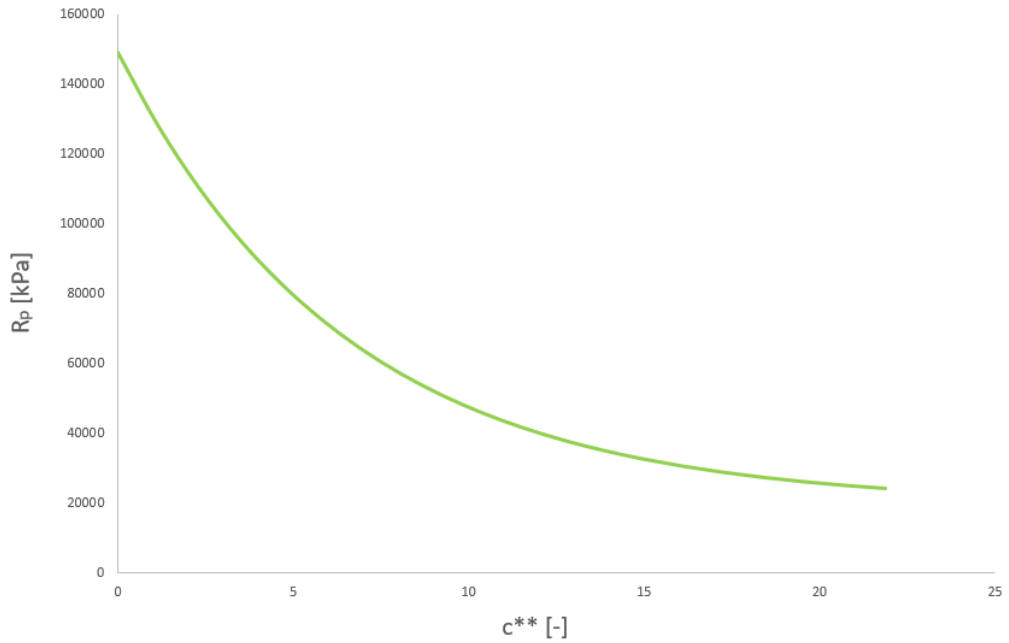

Figure 3.15: Iterpolation curve desribing R_p evolution with non-dimensional cohesion

By summarizing, the 1D equivalent model depends on a series of "micro" parameters, i.e parameters describing geometry, mechanical properties of the material and "macro" parameters, which are $\tau_y, \tau_{max}, a_1, a_2, a_3, b_1, b_2$ that describe the system response at a macro scale. The initial value or yielding variable and the maximum shear stress are evaluated with Equations3.47,3.55 and the other 5 parameters are calibrated once for all and are reported Table3.4.2.
As the "micro" parameters are concerned, in general they are expected to be very heterogeneous along the slope: for sake of simplicity only their mean values have been considered, but in Chapter6 their spatial variability will be analyzed, in order to understand its influence on the slope response.

3.4.3 1D equivalent model validation

In this section the Simple Shear Condition solution results are compared with the 1D code results.
Hereafter some examples of such comparisons are proposed.
In the table below the elastic parameters kept constant during all the simulations are shown.

E	ν
$[MPa]$	$[-]$
130	0.3

From the following figures can be noticed that for all the case considered the 1D model well fits the SSC numerical solution.

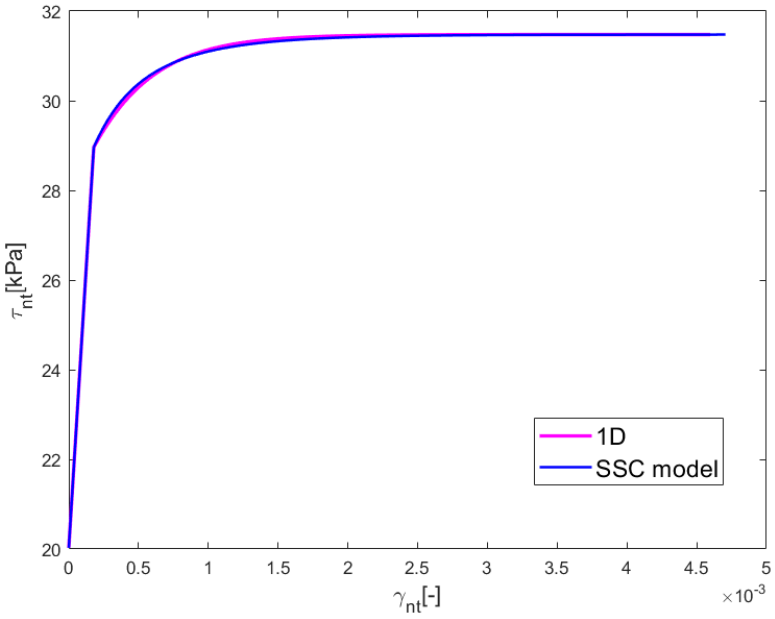

Figure 3.16: Comparison of $\tau_{nt} - \gamma_{nt}$ curves for $\phi' = \psi = 35°$,$H = 5m$, $\alpha = 15°$, $c' = 24kPa$

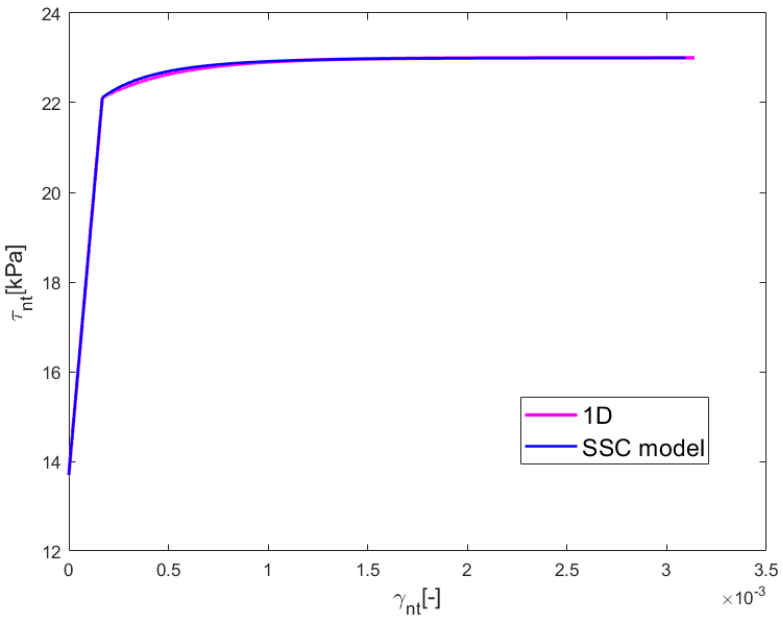

Figure 3.17: Comparison of $\tau_{nt} - \gamma_{nt}$ curves for $\phi' = \psi = 35°$,$H = 5m$, $\alpha = 10°$, $c' = 24kPa$

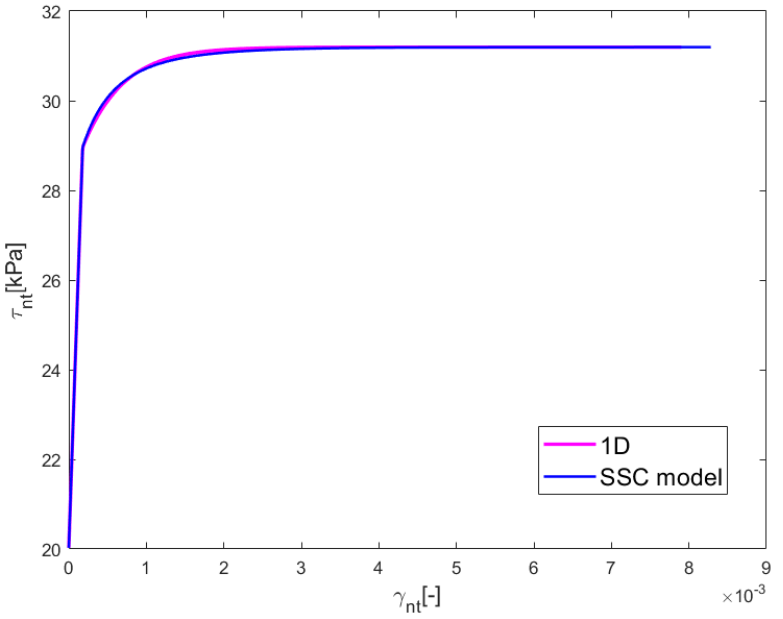

Figure 3.18: Comparison of $\tau_{nt} - \gamma_{nt}$ curves for $\phi' = 35°, \psi = 20°$,$H = 5m$, $\alpha = 15°$, $c' = 24kPa$

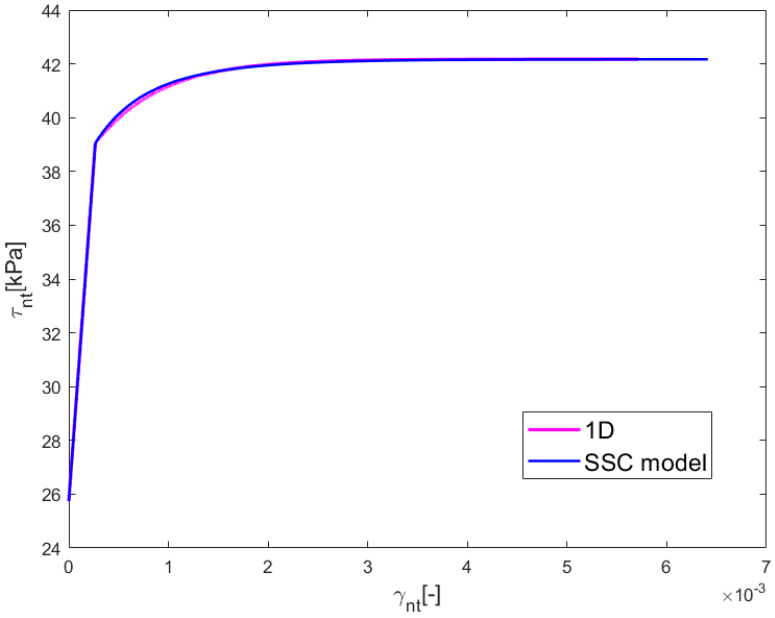

Figure 3.19: Comparison of $\tau_{nt} - \gamma_{nt}$ curves for $\phi' = \psi = 35°$,$H = 5m$, $\alpha = 20°$, $c' = 40kPa$

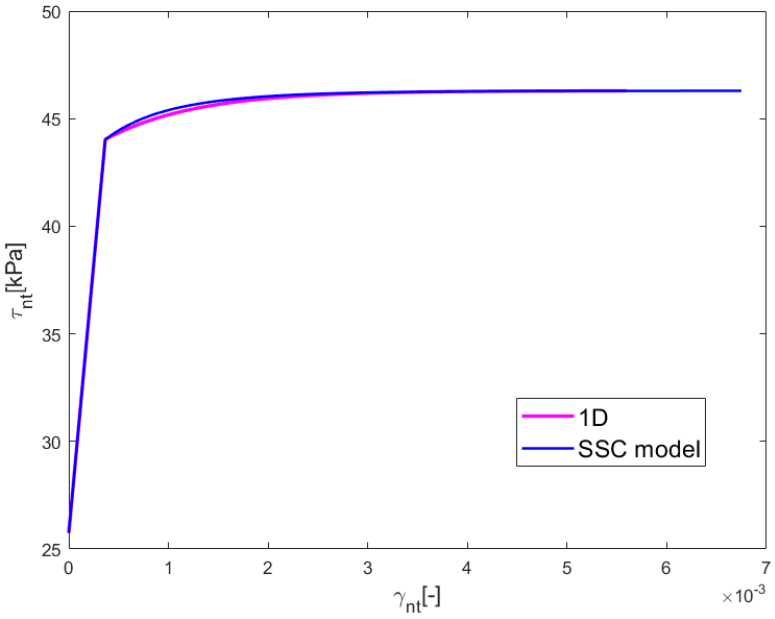

Figure 3.20: Comparison of $\tau_{nt} - \gamma_{nt}$ curves for $\phi' = \psi = 35°$,$H = 5m$, $\alpha = 20°$, $c' = 56kPa$

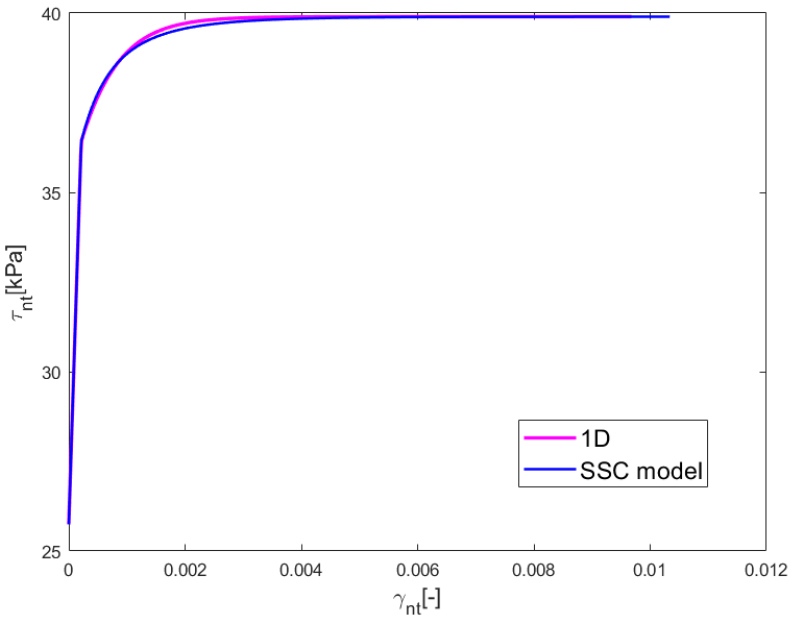

Figure 3.21: Comparison of $\tau_{nt} - \gamma_{nt}$ curves for $\phi' = 35°\psi = 25°$,$H = 5m$, $\alpha = 20°$, $c' = 32kPa$

Chapter 4

Viscoplastic constitutive model

As was previously mentioned, the cemented materials behaviour is essentially time dependent and an elastic plastic model cannot reproduce this. For these reasons viscoplastic 1D constitutive model has been introduced. Indeed, in the viscoplastic case, the consistency rule is abandoned and the current stress state can lie on, above or below the yield surface. For this reason also the description of cemented materials strain-softening behaviour will be possible.
According to viscoplasticity the total strain is give by an elastic reversible component and a viscoplastic irreversible time dependent component:

$$\dot{\varepsilon}_{ij} = \dot{\varepsilon}^{el}_{ij} + \dot{\varepsilon}^{vp}_{ij} \tag{4.1}$$

Viscous strains are defined according to Perzyna's theory:

$$\dot{\varepsilon}^{vp}_{ij} = \eta < \Phi(f) > \frac{\partial g}{\partial \sigma'_{ij}} \tag{4.2}$$

The yield function and the plastic potential and the hardening rule are the same considered in the elastic plastic (Equation3.7,3.8, 3.62,3.67).
In this case a bilinear viscous nucleus has been chosen:

$$\begin{cases} \Phi(f) = f & f \geq 0 \\ \Phi(f) = 0 & f < 0 \end{cases} \tag{4.3}$$

For the sake of clarity, firstly (§4.1) the case relative to an elastic-perfectly viscoplastic (i.e. without softening) is considered and then (§4.2) also the case of a strain softening material is discussed.
Analogously to what was done for the elastic-plastic case, before introducing the new 1D model, the results obtained by integrating the constitutive relationships are reported (§4.1).

4.1 Viscoplastic constitutive model in ductile regime

In this chapter an elastic-viscoplastic constitutive model in ductile regime will be analyzed, so no degradation of cohesion will be present.
Firstly the numerical simulations performed with the SSC code will be shown, then the equivalent 1D model will be illustrated.

4.1.1 Creep-Numerical simulation

In the table below the parameters used for the numerical simulation in which the constitutive relationship is integrated under simple shear conditions are listed. For the sake of simplicity, in this section only the case with $m = 0$ is discussed..

α	H	E	ν	ϕ'	ψ	c'	η
$[°]$	$[m]$	$[MPa]$	$[-]$	$[°]$	$[°]$	$[kPa]$	$[1/(daykPa)]$
25	5	130	0.3	35	35	24	$4 \cdot 10^{-4}$

The loading history which is adopted is an elastic deposition in a time span $\Delta t_1 = 0.005 days$ (since the deposition is elastic, the value of Δt_1 does not influences the results), followed by an istantaneous water table level increase from 0 to H_{slope}; this value is maintained constant for a time span Δt_2 (Figure4.1). This way the system undergoes a pure creep phenomenon because irreversible strains increase at constant effective stress (consolidation effects are disregarded, i.e. the system consolidation rate is significantly larger with respect to the perturbation rate).

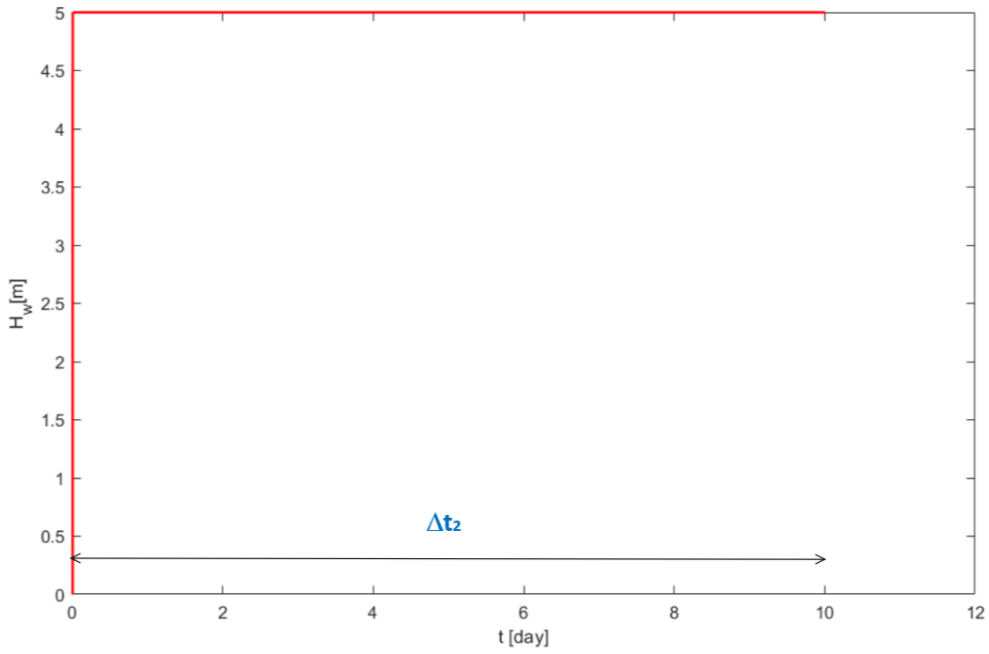

Figure 4.1: Water table path for creep simulation

Instability phenomenon under creep conditions occurs when the system does not undergo a deceleration process, i.e when $\dot{\varepsilon}_{ij}^{vp} \geq 0$: this is the case of secondary and tertiary creep. According to what demonstrated in Section 1.2.2, in case of no softening response (i.e with $H \geq 0$), tertiary creep phenomenon cannot be reproduced, so in this section instability characterized only by secondary creep is expected.
In Figure4.2 the stress path and the complete strain-time response for the stable case (a) and unstable case(b) can be seen.
In Figure4.3 can be seen a simulation characterized by a stable behaviour, appearing as an horizontal plateau of strains. In In Figure4.4 is shown an unstable creep example, characterized by a constant strain rate. This response is the so called secondary creep regime. The parameters of the unstable case are the same of the table above, except for the cohesion, which is imposed to be equal to $c' = 8kPa$.
In both cases a primary creep response verifies (that in the unstable case is just an initial response), which is associated to structural hardening.

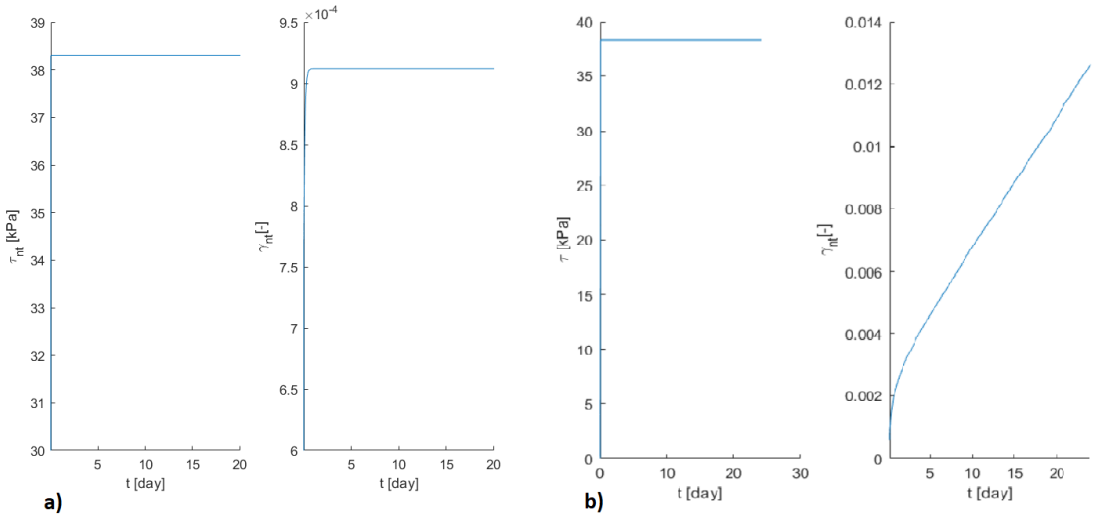

Figure 4.2: a) Stress path imposed and strain accumulation in case of stable creep b) stress path imposed and strain accumulation in case of unstable creep

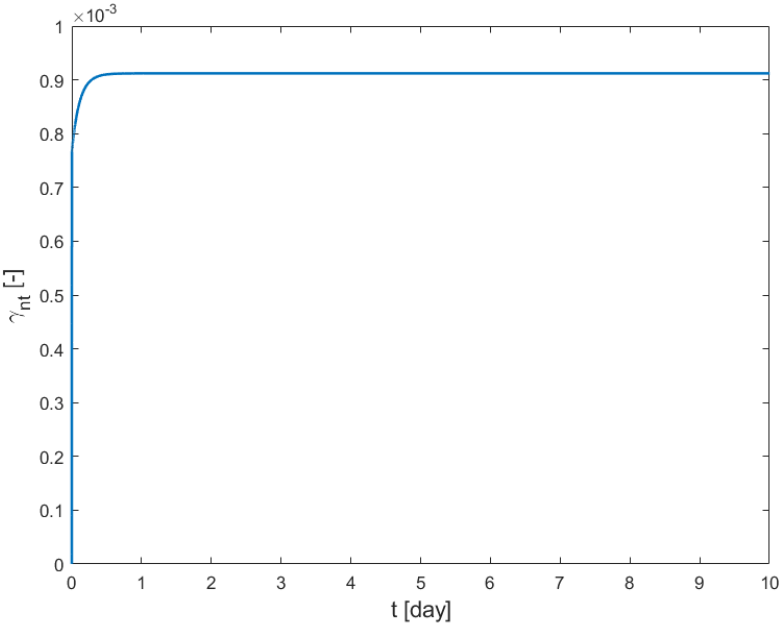

Figure 4.3: Shear strains in time in case of stable creep at a different time scale to remark the initial strain accumulation

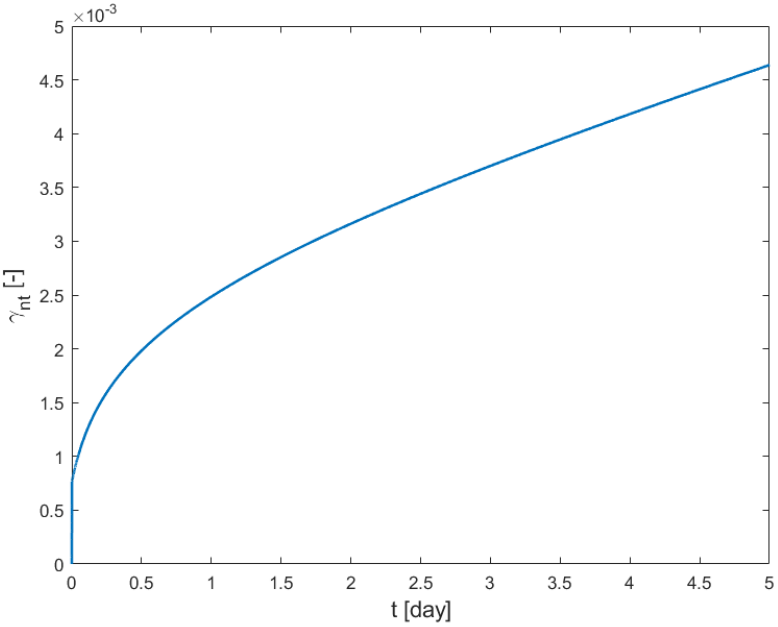

Figure 4.4: Shear strains in time in case of unstable creep at a different time scale to remark the initial strain accumulation

4.1.2 Lumped viscoplastic model: ductile response - Governing equations under creep conditions

In this section the time dependence of cemented materials will be introduced, so the development of the 1D elastic-viscoplastic model in ductile regime will be shown.
The parameters of the model are the maximum allowable shear stress τ_{max}, the elastoplastic stiffness R_p (evaluated from Equation3.69) and the value of the viscous parameter η .
As concerns the ductile regime the parameters τ_{max} and R_p and the initial value of hardening variable τ_y are the same as the elastoplastic case and a different law is used for the definition of the irreversible deformation.
As additivity holds, the total stain is given by the sum of an elastic component and a viscoplastic component (4.4):

$$\dot{\gamma}_{nt} = \dot{\gamma}_{nt}^{el} + \dot{\gamma}_{nt}^{vp}. \tag{4.4}$$

The yield function is again defined as:

$$f^* = \tau_{nt} - \tau_c, \tag{4.5}$$

where τ_c is the yieldind variable previously defined.
In the viscoplastic case the parameter R_p alone cannot correctly describe the system

behaviour: to take into account of the time dependence the introduction of non-constant parameter η would be necessary. As this procedure is not straightforward, the dependence on σ'_t, interpreted as an internal variable, is introduced in the model. The viscoplastic strains are defined as follows:

$$\dot{\gamma}^{vp}_{nt} = \eta \frac{f}{f^*} \frac{\partial g}{\partial \tau_{nt}} < f^* > dt. \tag{4.6}$$

where f and g are the previously defined yield function and plastic potential (Equations 3.7, 3.8). As their expression depends on σ'_t, f and $dg/d\tau_{nt}$ introduce in the model the dependency on the internal variable.
The internal variable evolution rule is evaluated starting from the additivity of strains and the compatibility:

$$\dot{\varepsilon}_t = 0 = \dot{\varepsilon}^{el}_t + \dot{\varepsilon}^{vp}_t \tag{4.7}$$

$$\dot{\varepsilon}_t = \dot{\varepsilon}^{el}_t + \dot{\varepsilon}^{vp}_t. \tag{4.8}$$

As an infinite slope configuration is assumed, the strains along t direction must to be nil; so imposing the compatibility condition:

$$\dot{\varepsilon}_t = \dot{\varepsilon}^{el}_t + \dot{\varepsilon}^{vp}_t = 0 \rightarrow \dot{\varepsilon}^{vp}_t = -\dot{\varepsilon}^{el}_t, \tag{4.9}$$

considering the 1D geometry of the problem, the following is obtained:

$$\dot{\varepsilon}_y = 0, \dot{\varepsilon}^{el}_y = 0, \dot{\varepsilon}^{vp}_y = 0. \tag{4.10}$$

From elasticity theory can be derived that

$$\dot{\varepsilon}^{vp}_t = -\frac{\dot{\sigma'}_t}{E} + \nu \frac{\dot{\sigma'}_y}{E}. \tag{4.11}$$

As in creep conditions $\dot{\sigma'}_n = 0$, the following holds:

$$\dot{\sigma'}_y = \nu \dot{\sigma'}_t, \tag{4.12}$$

combining Equation4.11 and 4.12 viscoplastic strains in t direction can be retrieved:

$$\dot{\varepsilon}^{vp}_t = \frac{-\left(1-\nu^2\right)\dot{\sigma}_t}{E}, \tag{4.13}$$

writing the definition of viscoplastic deformation in t direction and combining it with Equation 4.13, the increment of the internal variable σ'_t can be obtained

$$\dot{\varepsilon}^{vp}_t = \Phi(f) \frac{\partial g}{\partial \sigma'_t} = \frac{-\left(1-\nu^2\right)\dot{\sigma'}_t}{E}. \tag{4.14}$$

By solving Equation4.14 with respect to σ'_t the evolution of the internal variable is obtained

$$\dot{\sigma'}_t = -\Phi(f)\frac{\partial g}{\partial \sigma'_t}\frac{E}{\left(1-\nu^2\right)}. \tag{4.15}$$

This increment permits to update the internal variable σ'_t, that is used to calculate the expressions of f and of $\frac{\partial g}{\partial \tau_{nt}}$.
$\frac{\partial g}{\partial \tau_{nt}}$ is the derivative of the plastic potential (Equation3.8) with respect to the shear stress τ_{nt}:

$$\frac{\partial g}{\partial \tau_{nt}} = \frac{2\tau_{nt}}{\sqrt{4\tau_{nt}^2 + (\sigma'_n - \sigma'_t)^2}}. \tag{4.16}$$

The yielding variable increment is depending on viscoplastic deformations and on R_p as follows:

$$\dot{\tau}_c = R_p\left(1 - \frac{\tau_c}{\tau_{max}}\right)\dot{\gamma}^{vp}_{nt}. \tag{4.17}$$

4.1.3 1D equivalent model validation

In case of ductile regime, the viscous response is like an elastoplastic response in which the characteristic time of the material tends to zero, so the only difference is the delayed in time strain accumulation.
In this section some comparisons between the 1D equivalent model and the numerical model will be shown.
With respect to the elastoplastic case only an additional micro parameter, η, is present and, as regards the macro parameters Equations 3.69, 3.47 and 3.55 are used.
The parameters used for the stable case are shown in the table below.

α	H	E	ν	ϕ'	ψ	c'	η
$[°]$	$[m]$	$[MPa]$	$[-]$	$[°]$	$[°]$	$[kPa]$	$[1/(daykPa)]$
20	5	130	0.3	35	35	16	$4 \cdot 10^{-4}$

For the unstable case the same parameters are adopted except for $\phi' = \psi = 30°$ and $\alpha = 30°$.
As is shown in Figures4.5 and 4.6 the new model can reproduce the results obtained by integrating the constitutive relationship.

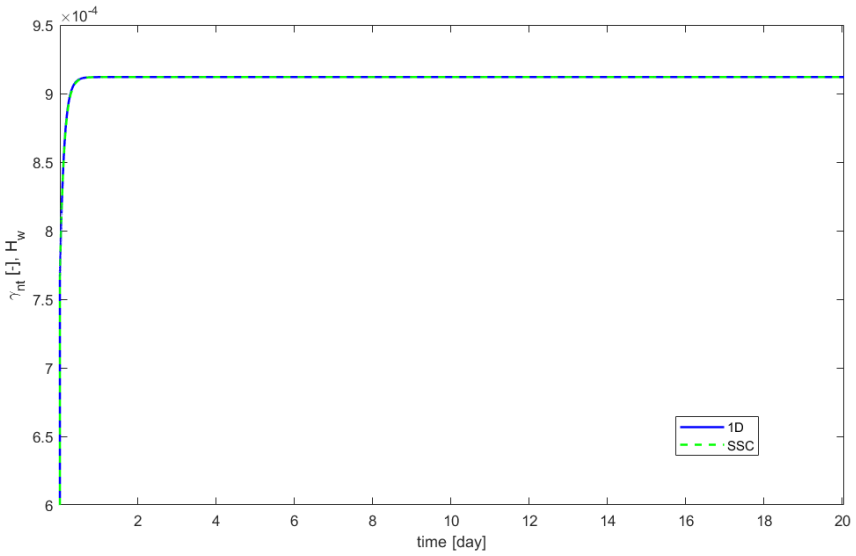

Figure 4.5: Comparison between 1D and SSC solution in the stable case

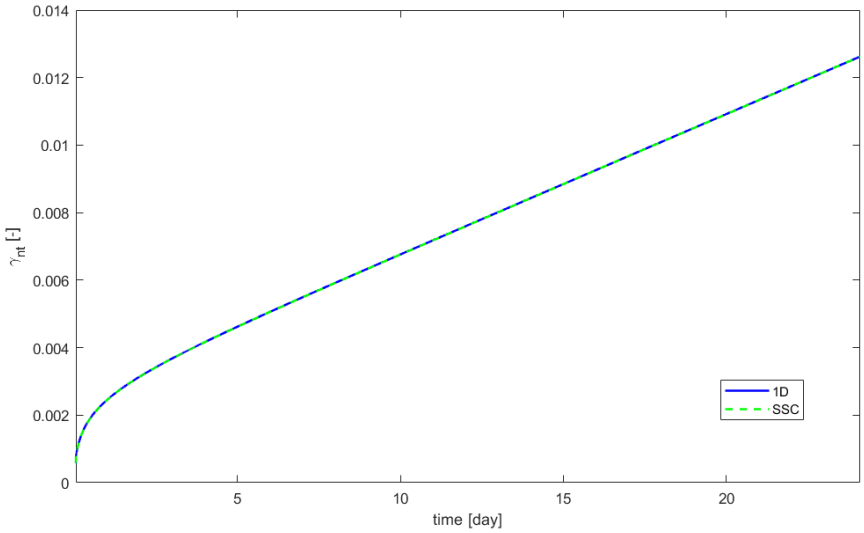

Figure 4.6: Comparison between 1D and SSC solution for the unstable case

4.1.4 From viscoplastic to elastoplastic response

As already remarked, the viscoplastic constitutive law is the limit case of elastoplastic law when the material characteristic time tends to zero, i.e. when the material response is slower with respect to perturbation time. In this section the analogy

between the elastoplastic case and the viscous case in case of ductile regime will be demonstrated.
Assuming that the viscoplastic strain increase only when the state of stress is outside the yield function (i.e. when $f > 0$), it is possible to demonstrate that ([Prisco and Imposimato, 1996]):

$$\int_0^{+\infty} d\varepsilon_{ij}^{vp}(t, dt) = \delta\varepsilon_{ij}^{pl} \tag{4.18}$$

Where $\delta\varepsilon_{ij}^{pl}$ is the plastic strain increment tensor corresponding to the limit viscous strain increment.
The parameter η influences the strain rate and consequently the rapidity with which the asymptotic strain value is reached. For instance if $\eta \to \infty$ the limit value $\delta\varepsilon_{pl}^{ij}$ is reached.
All these aspects considered, a second type of loading path can be be imposed to recover the elastic perfectly plastic case; instead of an instantaneous increase of the water table level from 0 to H, a progressive increase in a time span Δt_2 can be imposed.
In the strain-time curve a different trend characterized by a convex shape can be seen (Figure4.7).
Following this new loading path the elastoplastic $\tau_{nt}-\gamma_{nt}$ curve is retrieved (Figure4.8).

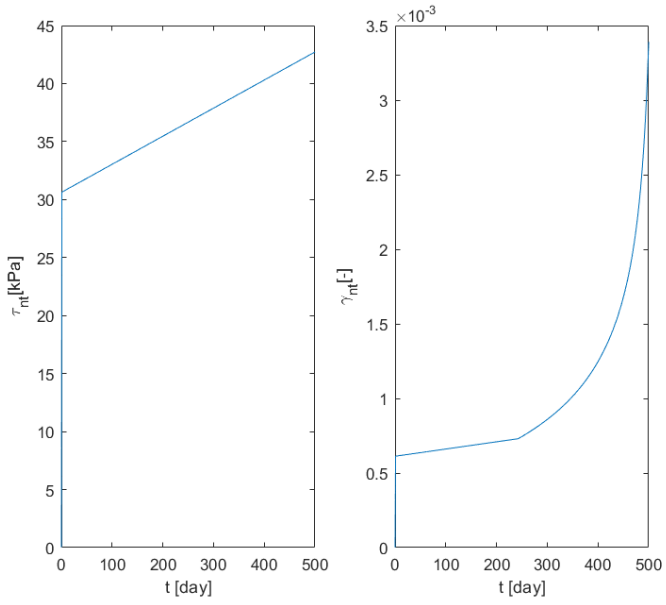

Figure 4.7: Stress path imposed and strain accumulation in case gradual load imposition

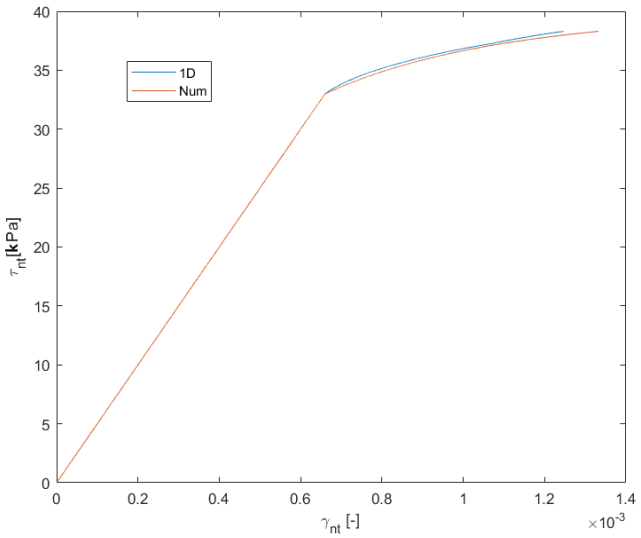

Figure 4.8: Comparison between 1D creep solution and elastic perfectly plastic solution for $\alpha = 25°$, $\phi' = \psi = 35°$,$H = 5m$ and $c' = 16kPa$

4.1.5 Water table level change - Numerical simulation

Despite being explicative for the creep phenomenon, the loading history of the previous section is not complete as regards the landslide inception phase. Strain rate increase bringing to failure in creeping landslides usually takes place after seasonal perturbations, as water table oscillations. In order to better catch the landslide inception phase, a different water table level fluctuation has been studied.
In this section a numerical simulation showing the response of the system after water table change will be shown. The water table is linearly increased up to a maximum level and then linearly decreased to zero. Typically the increase in water table level is a quick process with respect to the water table decrease, so an asymmetric water table level path has been used (Figure4.9).
The loading history in terms of water table (w.t.) level can be seen in Figure4.9; the water table-time history is characterized by the following time instants:

- t_0 is the time after deposition at which the perturbation starts;
- t_p is the time span between the beginning of w.t. increase and the peak of w.t.;
- t_{pf} is the time span from the peak to the nullification of w.t.; as already outlined $t_{pf} >> t_p$ has been chosen;
- t_f is the final time $t_f = t_0 + t_p + t_{pf} + t_{0f}$, where t_{0f} is the final time span in which the water table level is equal zero.

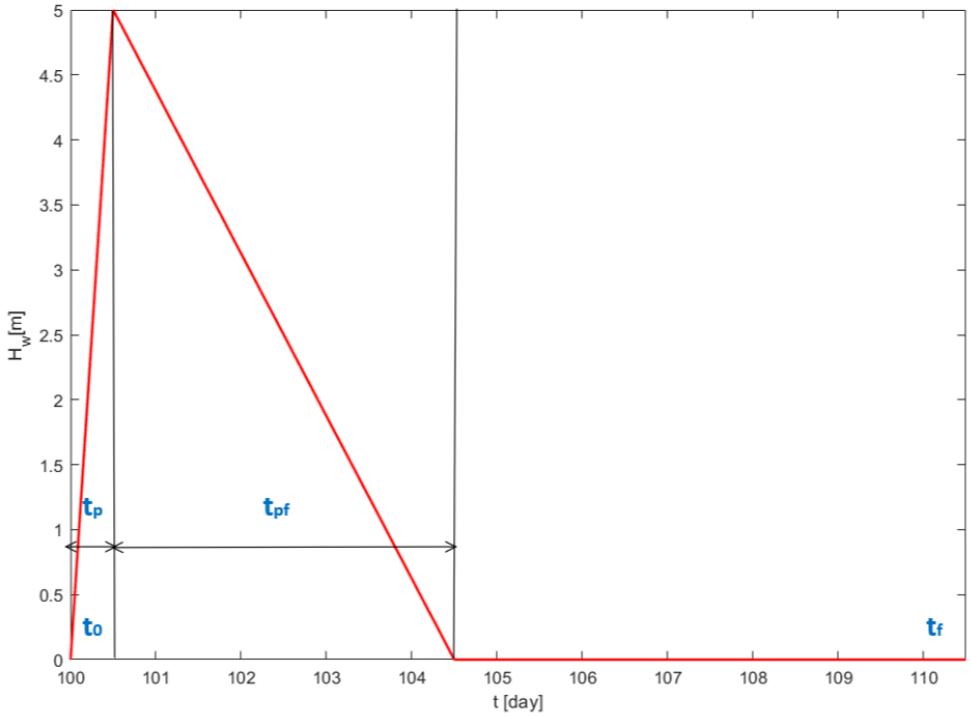

Figure 4.9: Water table level path

In this section some numerical simulations in ductile regime for the case of water table level change will be shown.
For the stable case the following parameters are used

α	H	E	ν	ϕ'	ψ	c'	η
$[°]$	$[m]$	$[MPa]$	$[-]$	$[°]$	$[°]$	$[kPa]$	$[1/day\,kPa]$
30	5	130	0.3	35	35	24	$8 \cdot 10^{-4}$

In Figure4.10 the numerical results for the stable case can be seen: In this case the response is dominated by the elastic material behaviour. When the perturbation decreases, the accumulated irreversible strains decrease until the end of the perturbation, when the strains remain on a constant value.

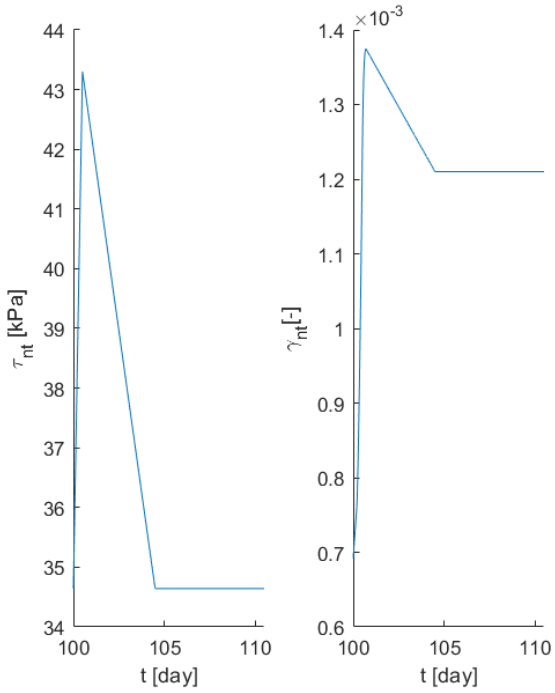

Figure 4.10: Stress path and strain accumulation in case of stable response

In absence of softening, an unstable response can not be reproduced. The only way to reproduce instability in case of water table level change without mechanical properties degradation is to start the simulation from a slope angle equal to $\alpha = \alpha_{lim}$, for which the system is already unstable without the imposition of a perturbation. For this reason, no unstable analysis for this case will be reported.

4.1.6 Lumped viscoplastic model: ductile response - Governing equations for water table level change

For the case of water table level change the yield function and the viscous strains are again defined according to Equation4.5 and 4.6 respectively. In the same way, the yielding variable evolution is defined according to Equation4.17. On the contrary, a change in the evolution law of the internal variable σ'_t is expected as it is stress path dependent. With respect to the creep case, when change in the water table occurs, $\dot{\sigma}'_n \neq 0$.
Writing the compatibility equation along y direction and the elastic law:

$$\dot{\varepsilon}_y^{el} = 0 = \frac{\sigma'_y}{E} - \frac{\nu}{E}\left(\dot{\sigma}'_t + \dot{\sigma}'_n\right), \tag{4.19}$$

solving Equation4.19 with respect to $\dot{\sigma}'_y$:

$$\dot{\sigma}'_y = \nu\left(\dot{\sigma}'_t + \dot{\sigma}'_n\right), \tag{4.20}$$

writing the elastic strains in t direction and the compatibility:

$$\dot{\varepsilon}^{el}_t = -\dot{\varepsilon}^{vp}_t = -\frac{\dot{\sigma}'_t}{E} - \frac{\nu}{E}\left(\dot{\sigma}'_y + \dot{\sigma}'_n\right) = \Phi(f)\frac{\partial g}{\partial \sigma'_t} \tag{4.21}$$

substituting Equation4.20 and solving with respect to $\dot{\sigma}'_t$, the increment of the internal variable is obtained:

$$\dot{\sigma}'_t = -\Phi(f)\frac{\partial g}{\partial \sigma'_t}\frac{E}{\left(1-\nu^2\right)} + \frac{\dot{\sigma}'_n}{\left(1-\nu\right)}. \tag{4.22}$$

4.1.7 1D equivalent model validation

In this section the 1D equivalent model validation in ductile regime for the case of water table level change will be shown. The parameters used for the stable case are the same of the numerical simulation of the previous section.
As can be seen from Figure4.11, the 1D equivalent model is able to reproduce the numerical results.

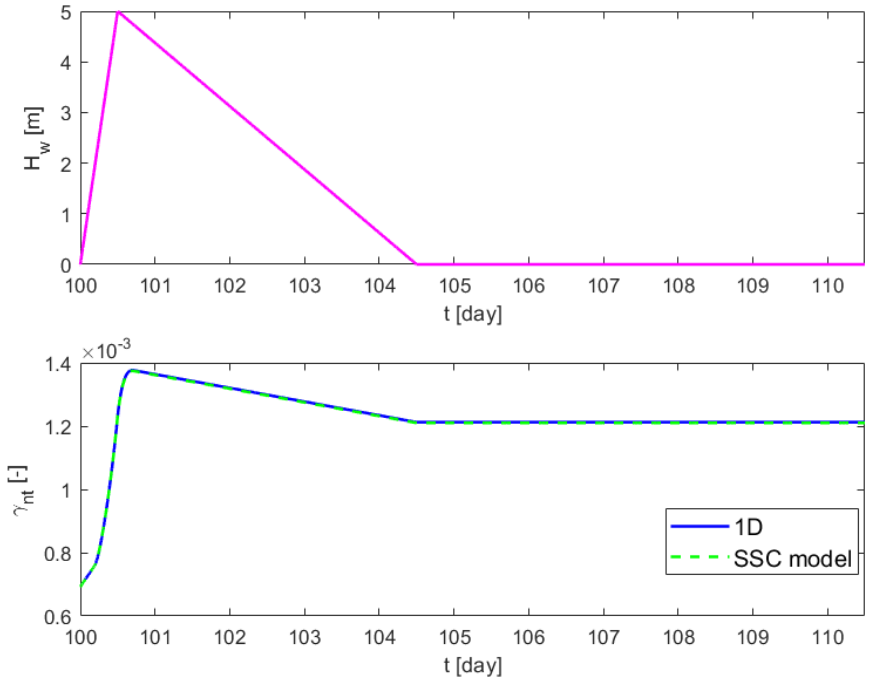

Figure 4.11: 1D equivalent model and SSC model comparison in case of stable response

4.2 Viscoplastic constitutive model with softening behaviour

Cemented materials are characterized by a strain softening response because of the fragile nature of their chemical bonds. In order to reproduce this behaviour a viscoplastic constitutive law with softening regime has to be discussed.
Cohesion will be considered constant along the slope, but governed by the following hardening law:

$$\dot{c}' = -c' m\left(|\dot{\varepsilon}_n^{irr}| + |\dot{\varepsilon}_t^{irr}| + |\dot{\gamma}_{nt}^{irr}|\right) \tag{4.23}$$

So c' will decrease as irreversible strains increase.
m is a non dimensional parameter governing the decrease of cohesion, it indicates how fast softening will occur: the greater is m the more the softening will be quick and pronounced. In Figure4.12 the cohesion degradation curve from two creep simulations can be seen; in case $m = 100$ a less marked reduction in cohesion is observed.

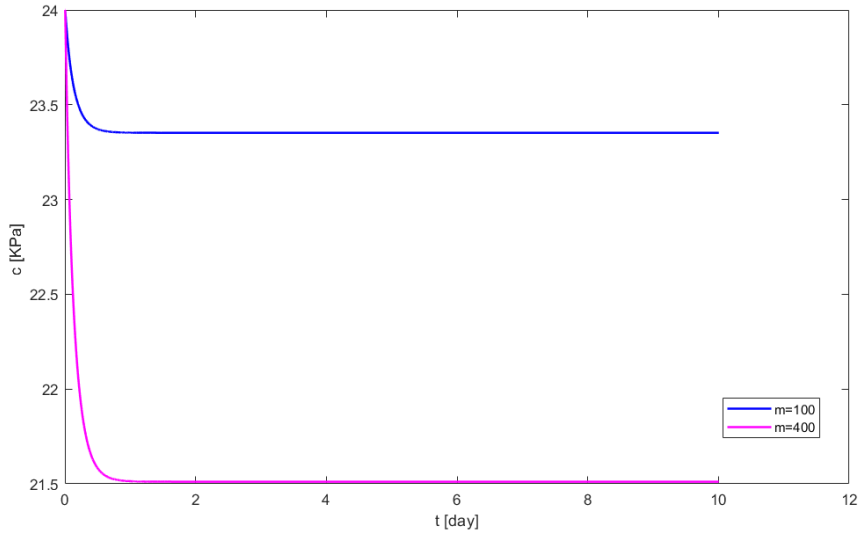

Figure 4.12: Cohesion degradation curves for two different values of m for two creep simulations in which $\alpha = 25°, \phi = \psi = 35°, H = 5m, \eta = 4 \cdot 10^{-4} 1/(day\, kPa), c' = 24kPa$

What is expected from softening analyses is the attainment of instability of the system during the perturbation decrease and so the achievement of tertiary creep phenomenon due to progressive failure, that can be interpreted as the a fast landslide inception phase.

4.2.1 Creep - Numerical simulation

In this section some numerical simulations have been performed under creep conditions with a strain softening response.
In Figure4.13 the stress path an the strains in time for the stable(a) and unstable (b) case can be seen. The parameters used for the stable simulation, whose results are shown in Figure4.14, are exactly the same used for creep simulation in ductile regime in Section4.1.1 and the parameter m is set equal to 100. This choice has been done in order to remark the influence of softening. Indeed, what can be seen in the comparison between the case in which $m = 0$ and the case $m = 100$ of Figure4.15 is that in case of softening response, due to cohesion reduction, the accumulated irreversible strain is higher.

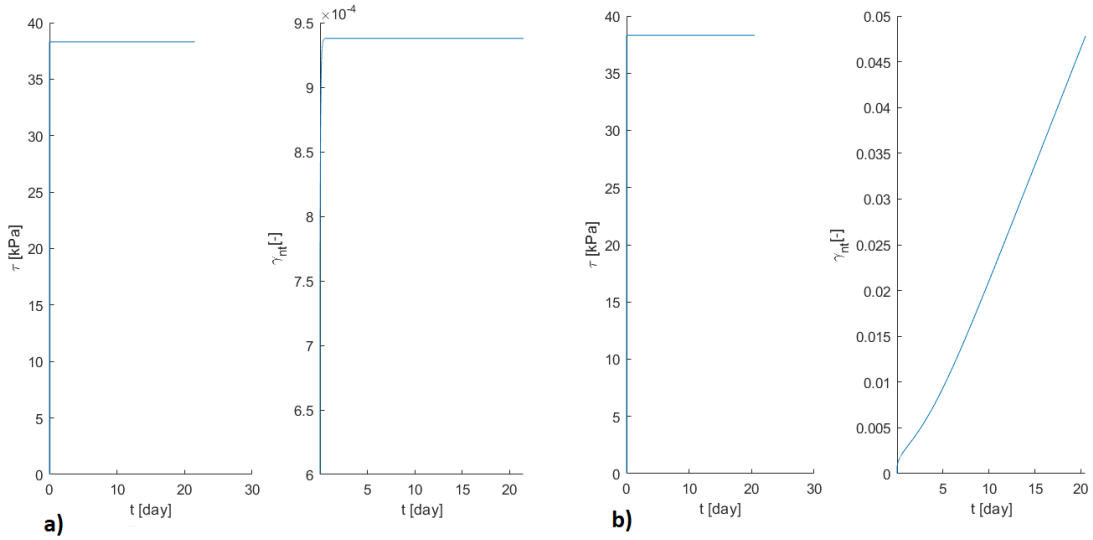

Figure 4.13: a)Stress path and strain accumulation in case of stable response b)Stress path and strain accumulation in case of unstable response

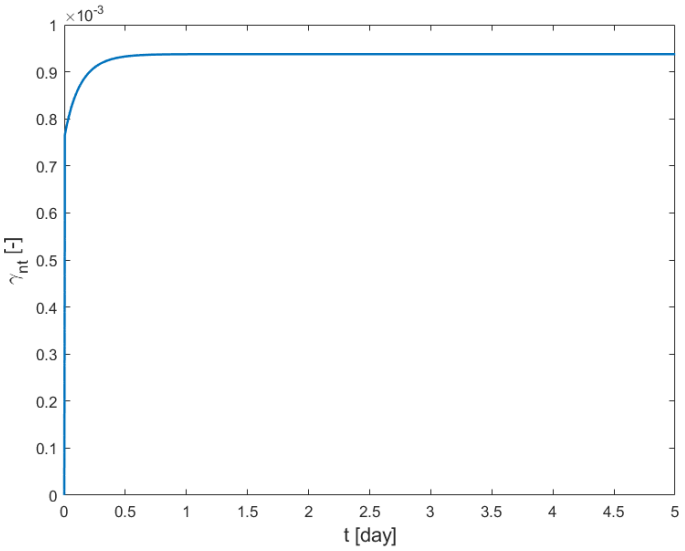

Figure 4.14: Shear strains in time in case of stable creep at a different time scale to remark the initial strain accumulation

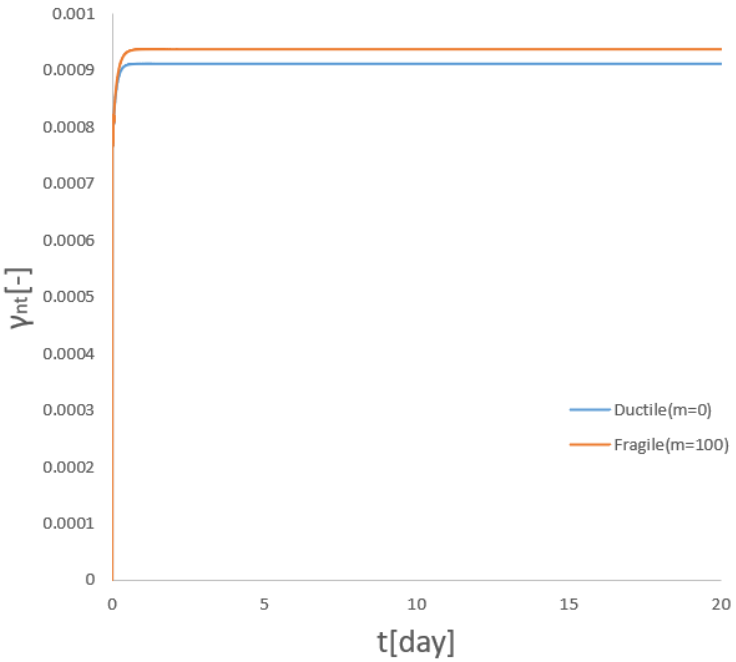

Figure 4.15: Comparison between the $\gamma_{nt} - t$ curves in case of $m = 0$ and $m = 100$

For the unstable case the same parameters of the simulation performed in Section 4.1.1 are used, the parameter m is again equal to 100.

In Figure4.16 the results of the simulation can be seen and they are plotted in order to magnify the tertiary creep phenomenon. Comparing it with Figure4.4 a different kind of instability can be observed: as remarked in Section 1.2.2, for a strain softening behaviour (i.e for $H < 0$) it is possible for the system to reach a tertiary creep response, according to which $\ddot{\varepsilon}_{nt}^{vp} > 0$. Taking into account of cohesion reduction in time it is thus possible to simulate the slope acceleration, differently from what was obtained in the ductule regime, in which only a constant strain rate could be observed.

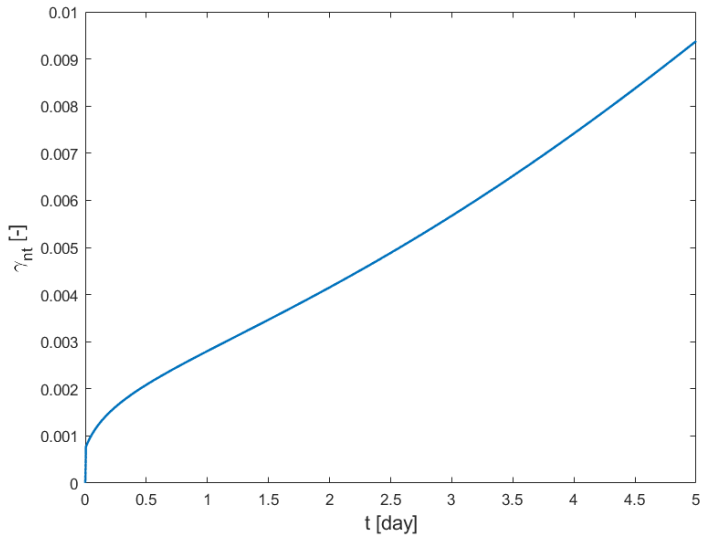

Figure 4.16: Shear strains in time in case of unstable creep at a different time scale to remark the initial strain accumulation

4.2.2 Lumped viscoplastic model: fragile response - Governing equations for creep regime

The governing equations are the same described in the previous section for the creep regime, with the addition of the cohesion evolution law: if the material exhibits a softening behaviour, cohesion is no more constant and that there is a progressive damage of the material.
The cohesion evolution law can be written as:

$$\dot{c}' = -mc'\big(|\dot{\gamma}_{nt}^{vp}| + |\dot{\varepsilon}_{n}^{vp}| + |\dot{\varepsilon}_{t}^{vp}|\big), \tag{4.24}$$

where $\dot{\gamma}_{nt}^{vp}$ are the viscoplastic shear strains given by Equation4.6, $\dot{\varepsilon}_{t}^{vp}$ is given by Equation4.13 and $\dot{\varepsilon}_{n}^{vp}$ is the increment of strains in the normal direction and it can be written as:

$$\dot{\varepsilon}_{n}^{vp} = \eta \frac{f}{f^*} < f^* > \frac{\partial g}{\partial \sigma_n'} dt \tag{4.25}$$

the increment of strains in the tangential direction $\dot{\varepsilon}_t^{vp}$ is defined as:

$$\dot{\varepsilon}_t^{vp} = \eta \frac{f}{f^*} < f^* > \frac{\partial g}{\partial \sigma_t'} dt. \tag{4.26}$$

The yield shear stress used in the model τ_y is the one previously defined by Equation3.46, while the maximum shear stress τ_{max} is obtained solving a system similar to Equation3.54 but with cohesion equal zero: it is the maximum allowable stress for the system accounting for a total degradation of cohesion. Thus in this case only an additional micro parameter is present (i.e. cohesion).

4.2.3 Equivalent model validation

In this section the 1D equivalent model validation in creep conditions for softening regime will be shown. The parameters used for both the stable and unstable case are the same used in the numerical simulation of the previous section.
As can be seen from Figure4.17 and 4.18 the model is able to reproduce the numerical results and the tertiary creep condition.

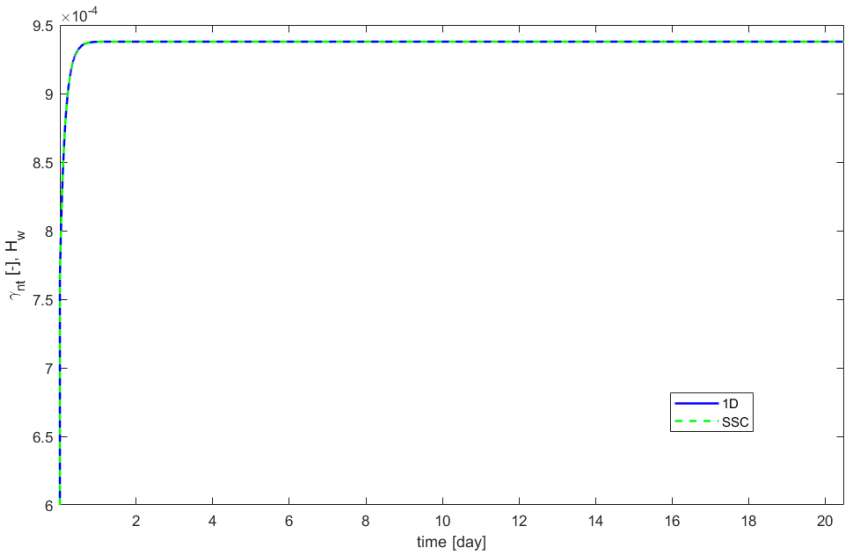

Figure 4.17: 1D equivalent model and SSC model comparison in case of stable response

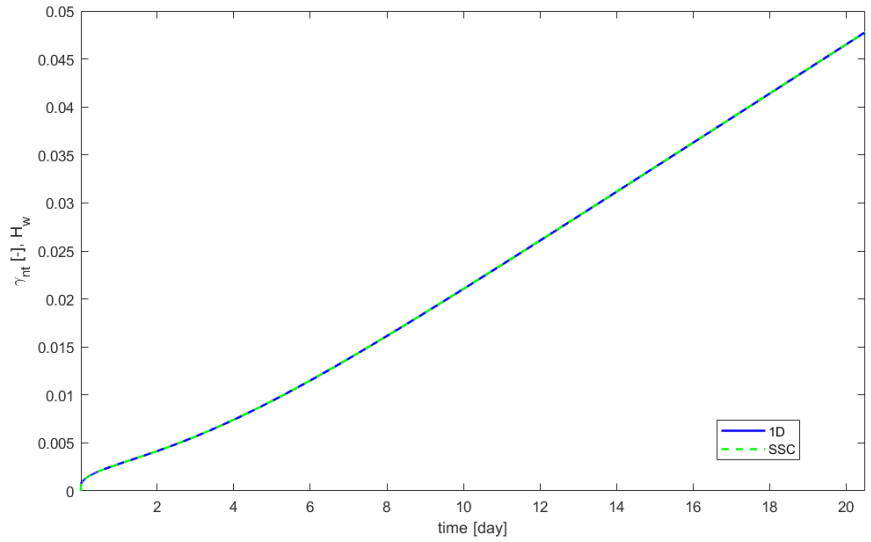

Figure 4.18: 1D equivalent model and SSC model comparison in case of unstable response

4.3 Model Employment

In this section the 1D equivalent model will be employed to simulate a water table level change with a strain softening-viscoplastic constitutive model. In addition its results are compared with those coming from the 1D rigid-viscoplastic model (analogous to the one proposed in [Secondi et al., 2013]).

4.3.1 Water table level change-Numerical simulation

In this section some numerical simulations for water table level change in strain softening conditions will be shown.
The parameters used in the numerical simulation in the stable case are summarized in the table below.

α	H	E	ν	ϕ'	ψ	c'	m	η
$[°]$	$[m]$	$[MPa]$	$[-]$	$[°]$	$[°]$	$[kPa]$	$[-]$	$[1/(day\,kPa)]$
25	5	130	0.3	30	30	24	100	$4 \cdot 10^{-4}$

In this section also the displacement-time curves will be analyzed.
Given the height of the slope H, the maximum value of displacement on the slope

surface has been evaluated as:

$$u_t = H \sum_{i=1,n} \gamma_{nt,i}, \tag{4.27}$$

where n is the number of steps in the simulation.
The $\gamma_{nt} - t$ numerical curve superimposed to the water table level path for the stable case are shown in Figure4.19. As can be seen in Figure4.19 viscous strains increase with the increase of water table level; this trend continues also for a part of the unloading phase, but then a decrease of strains is observed because the system has reached a new equilibrium condition. So the total strain arrives to a final plateau, which shows the stable response of the system.
In Figure4.20 can be seen the cohesion degradation curve of the stable case. The final value of cohesion is not so different from its initial value.

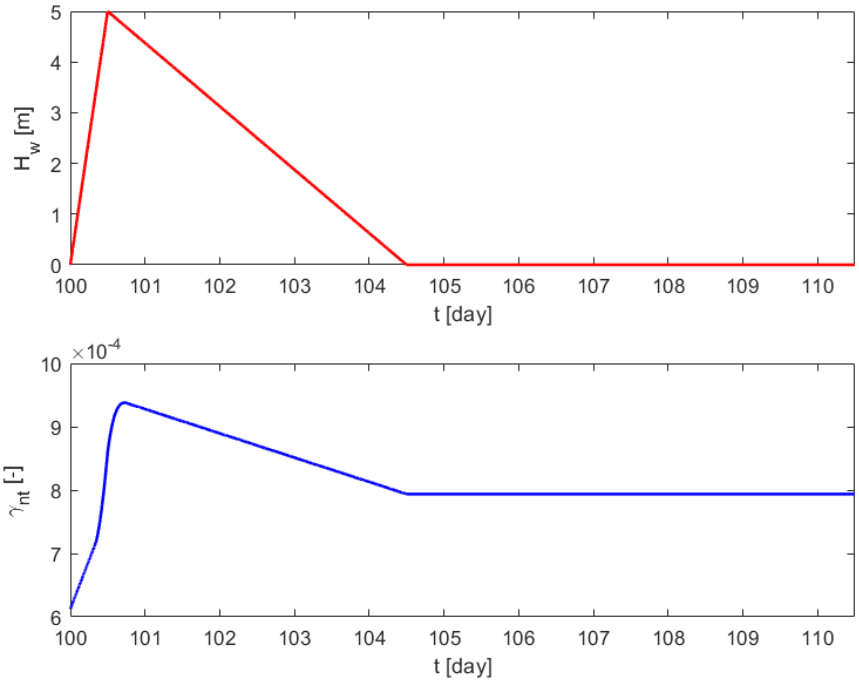

Figure 4.19: $\gamma_{nt} - t$ numerical curves for the stable case

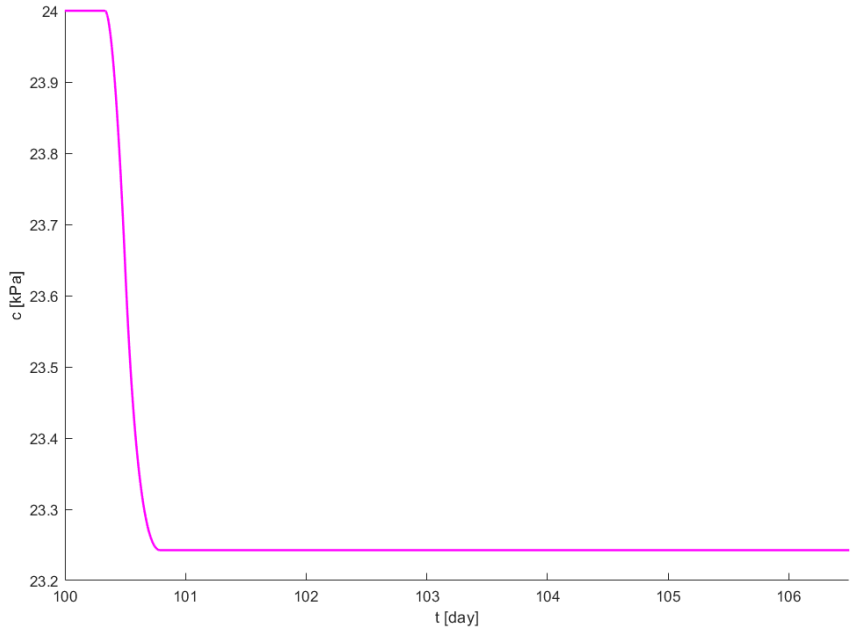

Figure 4.20: Cohesion degradation curve of stable case

In Figure4.21 the displacement trend in time and the water table path can be seen. After the water table peak, displacement tends to decrease and to stabilize.

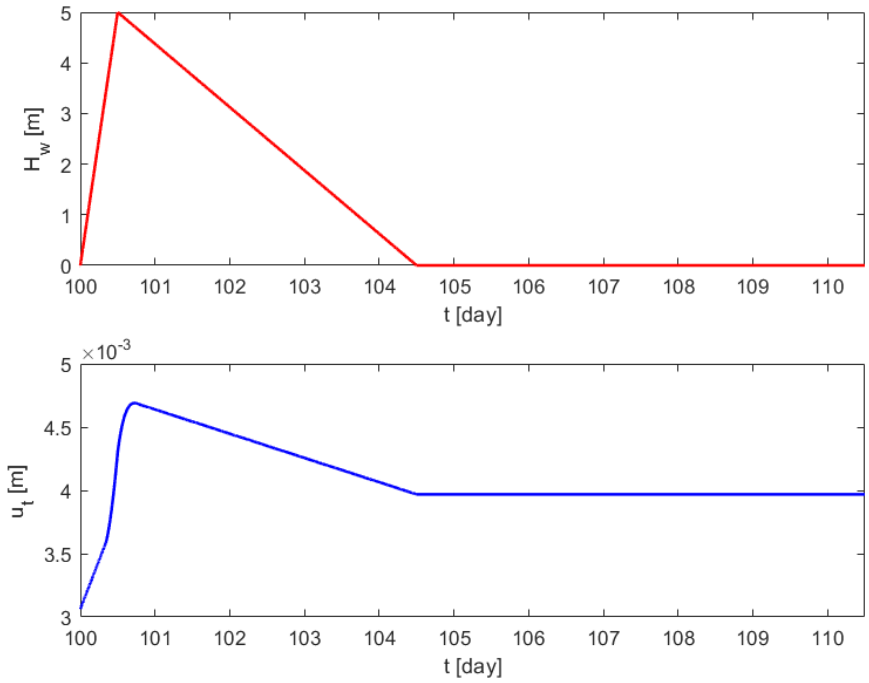

Figure 4.21: Displacement-time trend for the stable case

For the unstable case the following parameters are used:

α [°]	H $[m]$	E $[MPa]$	ν $[-]$	ϕ' [°]	ψ [°]	c' $[kPa]$	m $[-]$	η $[1/(day\,kPa)]$
30	5	130	0.3	25	25	24	80	$8 \cdot 10^{-4}$

The $H_w - t$ curve and the $\gamma_{nt} - t$ numerical curves for the unstable case are shown in Figure4.22.

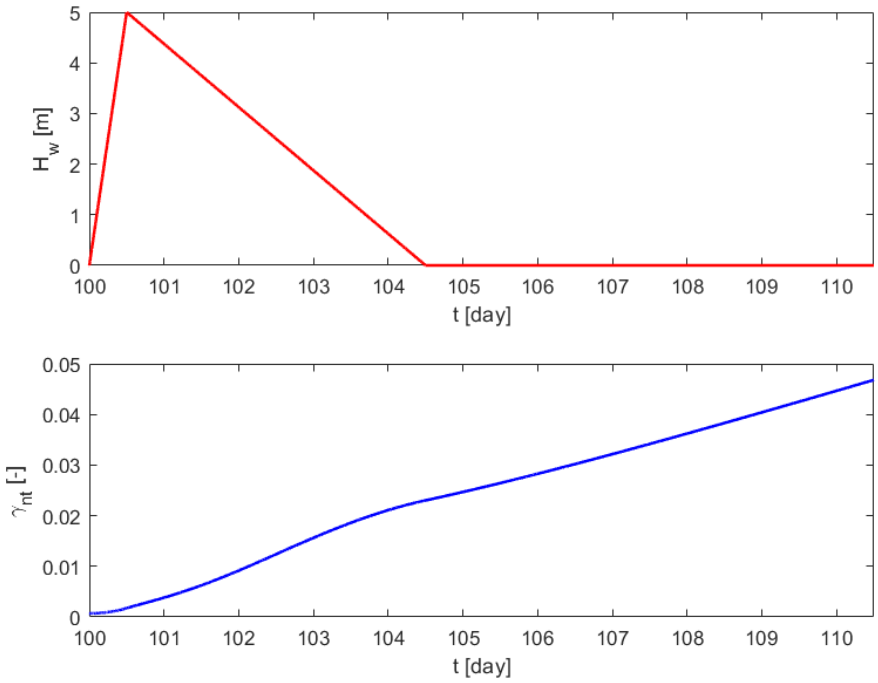

Figure 4.22: $H_w - t$ curve and the $\gamma_{nt} - t$ numerical curves for the unstable case

The water table level path is exactly the same of the previous case, but, due to the different parameters the $\gamma_{nt} - t$ behaviour is different: in particular, can be observed that the curve is associated with two accelerating phases. The first one is associated with an increase in the water table level, whereas the second one is obtained after the end of the perturbation. This second acceleration, highlighting an unstable system response, is due to the degradation of cohesion induced by the accumulation of irreversible strains (Figure4.23).
This result can be also seen in the light of [Pisanò and Prisco, 2016] approach that combines the controllability theory ([Nova, 1994]) and [Lyapunov, 1892] stability criterion. According to this approach (better described in Appendix B), for elastic-viscoplastic materials, it is possible to write a linear relationship between the variables describing the system response (hereafter called $\mathbf{X}$, being under simple shear conditions $\dot{\gamma}_{nt}, \dot{\varepsilon}_n, \dot{\sigma'}_t$ and $\dot{\sigma'}_n$) and their time derivative ($\dot{\mathbf{X}}$):

$$\dot{\mathbf{X}} = \mathbf{A}\mathbf{X} + \mathbf{F}, \tag{4.28}$$

where $\mathbf{A}$ is a matrix depending on the constitutive relationship and on controlled variables and $\mathbf{F}$ is the forcing term related to controlled variables.
In case of generalized creep tests (i.e for $\mathbf{F} = 0$), according to Lyapunov's theory, for $\mathbf{F} = 0$ a stable response is obtained (meaning that the system progressively decelerates) when all the eigenvalues of $\mathbf{A}$ are negative (so if $\mathbf{A}$ is negative defined).

In this particular case (i.e for a stress path deriving from water table level change) $\mathbf{F} \neq 0$ and therefore the same considerations are not valid. Indeed when the water table is raised the forcing term $\mathbf{F}$ is greater than zero, while when it is lowered $\mathbf{F} < 0$. As the water table level increase is a quick process, the phase in which $\mathbf{F} > 0$ can be practically neglected. Given this assumption, only the case of $\mathbf{F} \leq 0$ is considered, so the instability (i.e $\dot{\mathbf{X}} > 0$) is necessarily associated with a change in sign of (at least one) eigenvalue of $\mathbf{A}$, implying that the material response is unstable.
It is interesting to notice that, removing the hypothesis $\mathbf{F} = 0$, the system can accelerate even if the matrix $\mathbf{A}$ is negative defined: indeed, when $\mathbf{F} > 0$ an acceleration can verify, but this is not due to system instability (because $\mathbf{A} < 0$), but to the forcing term that moves the system.

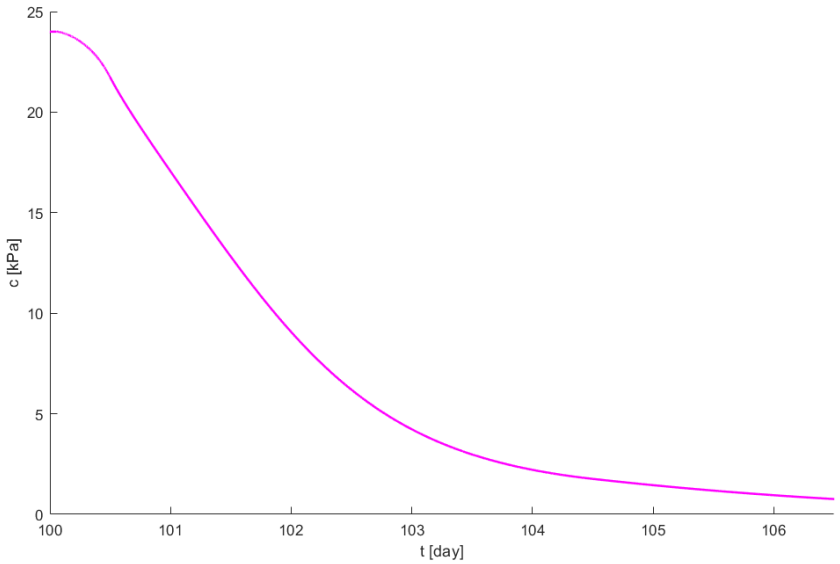

Figure 4.23: Cohesion degradation curve of unstable case

In Figure4.24 the displacement trend in time superimposed to the water table path can be seen. Differently from the stable case, after the peak the displacement shows a continuously increasing trend (the so called Trend IV of Section 2.1).

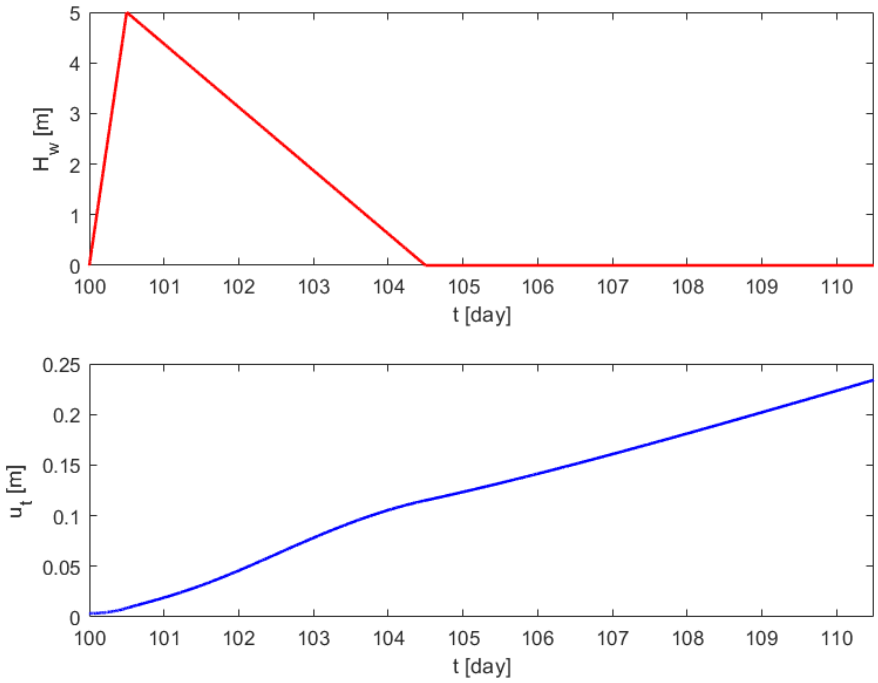

Figure 4.24: Displacement-time trend for the unstable case

4.3.2 1D equivalent model and SSC model comparison

In Figure4.25 the comparison between the two models in the stable case is shown. In Figure4.26 the comparison of the unstable case can be seen; in this case the tertiary creep phenomenon can be observed and it is remarked by the change in the $\gamma_{nt} - t$ curve concavity in correspondence of the perturbation reduction. In Figure4.26 the strain-time response superimposed to the water table path can be seen.

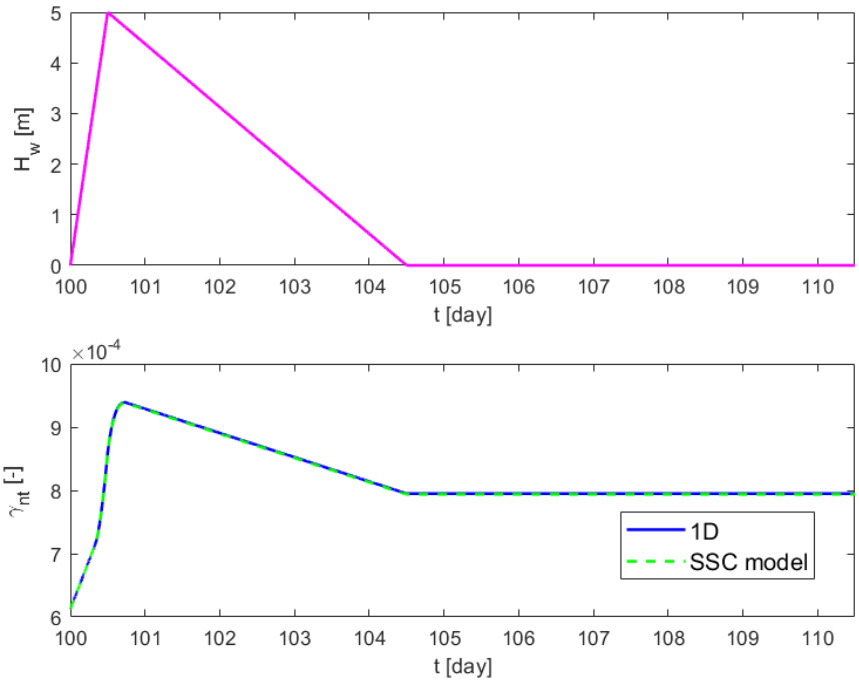

Figure 4.25: $\gamma_{nt} - t$ curves of the two models and water table level path

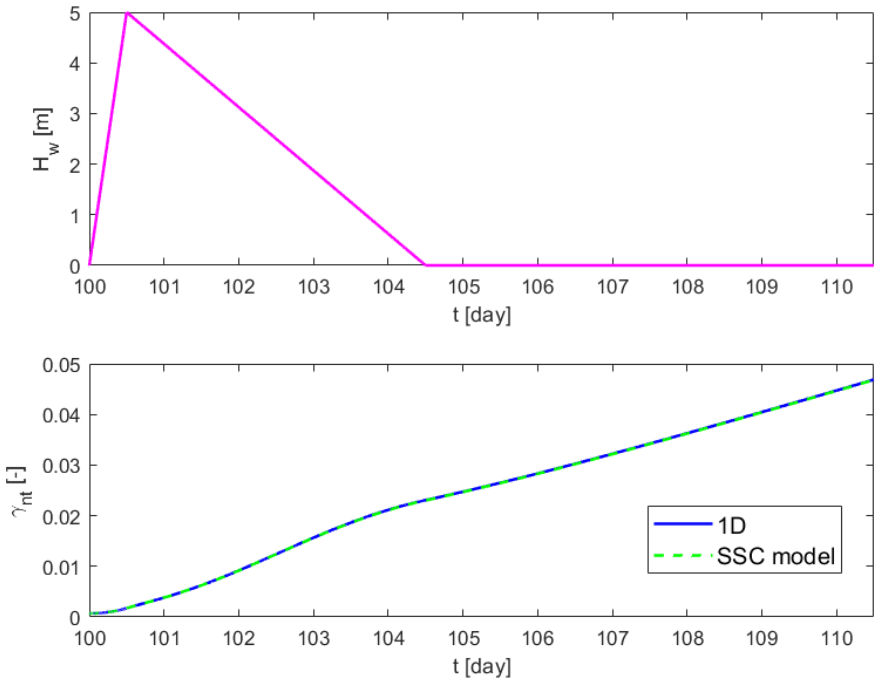

Figure 4.26: $\gamma_{nt} - t$ curves of the two models superimposed to the water table level path

4.3.3 1D viscoplastic model and 1D rigid-viscoplastic model comparison

The new 1D lumped model is capable to describe the creeping landslide inception phase, differently from the perfectly viscoplastic 1D model discussed in Section2.3. Some analyses to compare the two models have been performed in order to show the main differencies between the models.
The yield function and viscous deformation of the perfectly viscoplastic model are the same described in Section2.3:

$$f_{rvp} = \tau_{nt} - \sigma_n tan\phi' - c' \tag{4.29}$$

$$\dot{\gamma}_{rvp}^{vp} = \eta < f_{rvp} > dt = \eta \frac{\left(\tau_{nt} - \sigma_n tan\phi' - c'\right) + |\tau_{nt} - \sigma_n tan\phi' - c'|}{2} dt \tag{4.30}$$

For the 1D rigid-viscoplastic model the same bilinear viscous nucleus used for the 1D viscoplastic model is adopted.
The cohesion in the 1D rigid-viscoplastic model is set constant and equal to the initial value, while the viscoplastic model has a softening behaviour according to

which cohesion is a decreasing function of strains, moreover in the 1D viscoplastic model the evolution of σ_t is allowed, so structural hardening phenomenon is present; on the contrary, the other model completely neglects this aspect because of the implicit assumption that all the plastic resources of the system have already been exploited.
In the stable case a greater accumulation of strains during loading of the 1D viscoplastic model is observed: this comes from the fact that both structural hardening and cohesion degradation are possible for that system.
In the stable case (Figure4.27) the rigid-viscoplastic model is able to qualitatively reproduce the response, but quantitatively it underestimates the strains of about an order of magnitude. In the unstable case (Figure4.28) the rigid-viscoplastic model does not work neither from a qualitative point of view.
A more adapt use of rigid-viscoplastic model is in the field of already developed creeping landslides: once all the structural hardening of the system has developed and the cohesion has stabilized on a constant value, it is reasonable and simpler to use such a model.
The parameters for the stable case are summarized in the table below.

α	H	E	ν	ϕ'	ψ	c'	m	η
$[°]$	$[m]$	$[MPa]$	$[-]$	$[°]$	$[°]$	$[kPa]$	$[-]$	$[1/(day\,kPa)]$
27	5	130	0.3	30	30	16	100	$4 \cdot 10^{-4}$

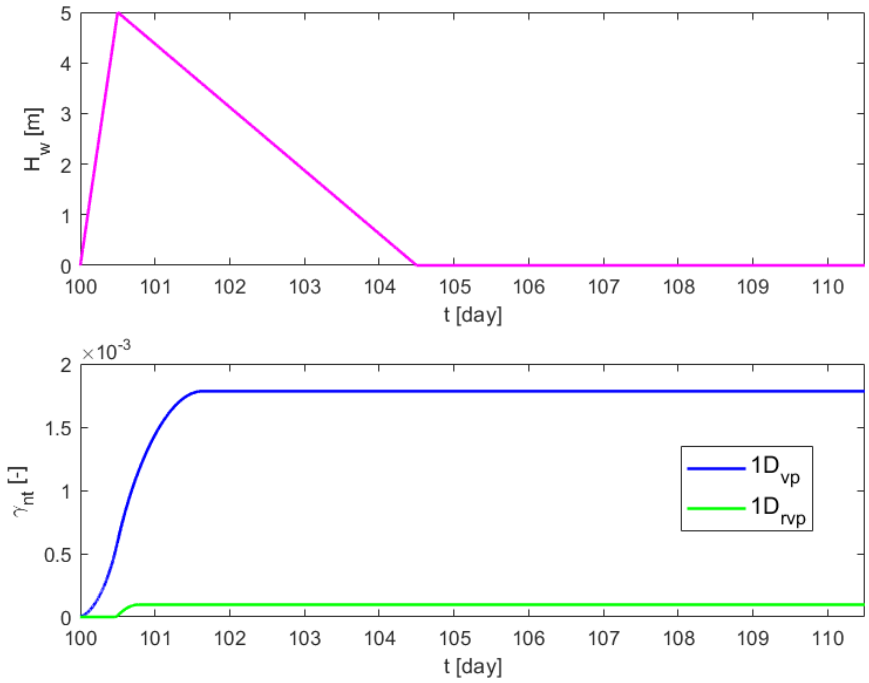

Figure 4.27: 1D viscoplastic and rigid-viscoplastic model comparison in the case of stable system

The parameters for the unstable case are summarized in the table below.

α [°]	H $[m]$	E $[MPa]$	ν $[-]$	ϕ' [°]	ψ [°]	c' $[kPa]$	m $[-]$	η $[1/(day\,kPa)]$
30	5	130	0.3	25	25	16	80	$4 \cdot 10^{-4}$

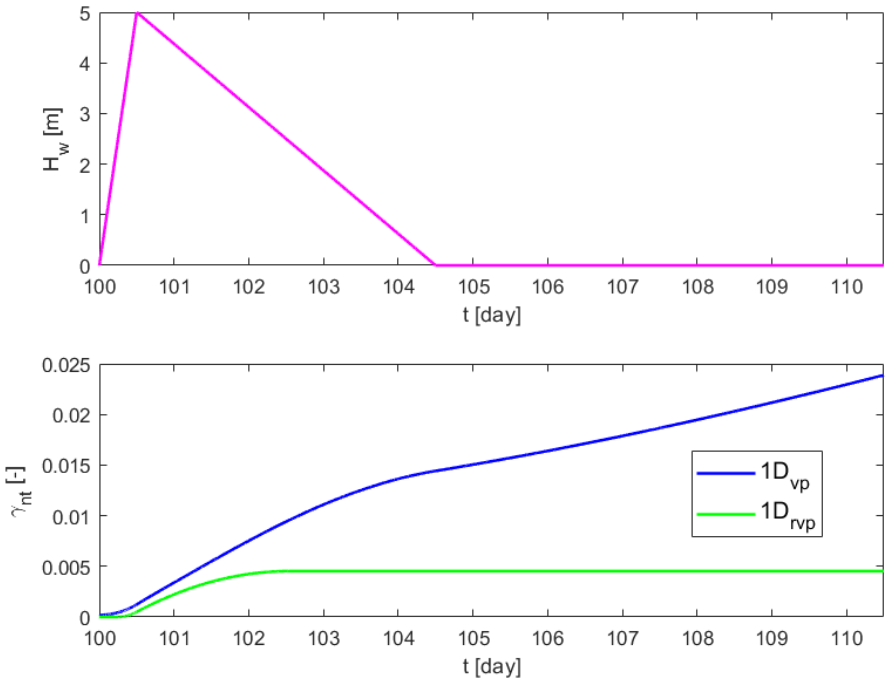

Figure 4.28: 1D viscoplastic and rigid-viscoplastic model comparison in the case of unstable system

Chapter 5

Parameter variability: from the REV to the slope scale

Despite the usual hypothesis of system homogeneity, natural soils are actually very heterogeneous. They are naturally variable because of the way they are formed; then they are then altered by the continuous process of the environment. After deposition of initial formation, they are continuously modified by the external stresses, weathering and chemical reactions.
In [Phoon et al., 2006] three different levels of soils heterogeneity are distinguished:

- *stratigraphic heterogeneity*: it is the result of large-scale geologic and geomorphological processes. This heterogeneity is usually addressed at site-scale; stratigraphies may be extremely complex and heterogeneous;
- *lithological heterogeneity*: can be manifested, for instance, in the form of thin soft/stiff layers embedded in a stiffer/softer medium or the inclusion of pockets of different lithology within a relatively uniform soil mass;
- *inherent soil variability*: it is the variation of properties from one spatial location to another inside a soil mass which could be regarded as being significantly homogeneous for geotechnical purpose.

For the nature of the studied materials, in this chapter the *inherent soil variability* will be considered.
Until now the problem has been studied referring to the REV scale, so the material point response has been considered and the employed "micro" parameters were assumed to be representative for the whole slope. Moreover, both the 1D equivalent model and the SSC model had the implicit assumption of no parameters variation along the slope direction so the aim of this chapter is to understand whether the mean parameters are representative of the mean slope response. To do so, a numerical strain control condition is assumed: simple shear tests were performed.
Actually, a variability of parameters along the t direction exists and to study its

influence on the system response a scale passage also in the t direction must be done. A variability of parameters along t is assumed and in particular an in parallel system, whose mechanical properties change along the t direction, is assumed (Figure5.1).
The assumption of parameters spatial variability along t implies the loss of symmetry in this direction, so each point expected to reach failure in a different moment with respect to the others.
The system will be studied through four different constitutive relationships and for each of those a different parameters variability is assumed. The following constitutive laws are assumed:

1. elastic constitutive law: in this case only the spatial variation of the shear modulus G will be considered;

2. elastic perfectly plastic constitutive law: in this case both spatial variation of cohesion and shear stiffness will be considered. In particular, the variation of shear stiffness will be directly related to cohesion;

3. strain softening elastic-plastic constitutive law: in this case a variation of G, c' and of the non dimensional parameter m is introduced;

4. strain softening elastic-viscoplastic constitutive law: in this case the viscous coefficient η varies in the simulations with also G, c' and m.

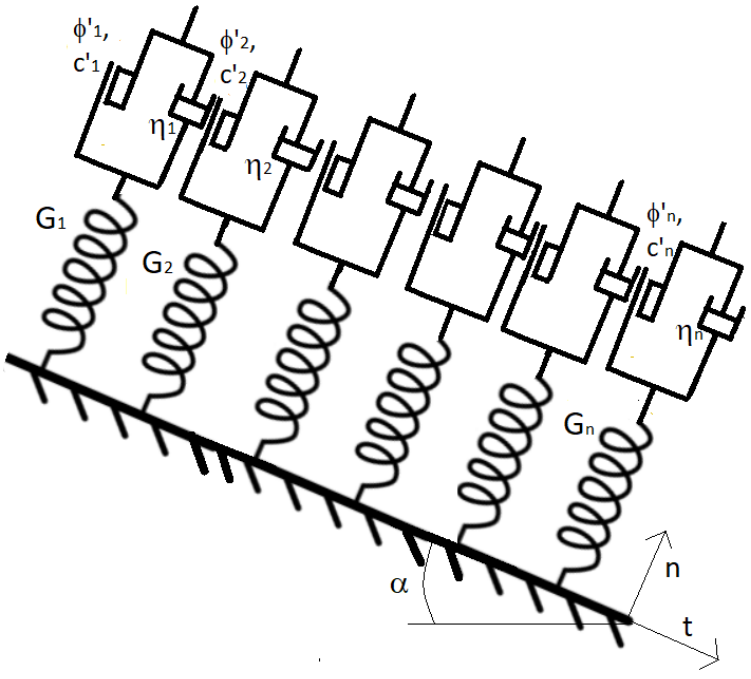

Figure 5.1: Sketch of infinite slope with variable properties

As the system is in parallel, the response of the whole slope in terms of stresses will be the sum of the stress of each part, divided by the number of the elements in which the system is subdivided.
As seen in [Alegre et al., 2001], cementation influences both cohesion and elastic parameters of the material. In fact all the parameters that will be used in this chapter are supposed to be dependent on the degree of cementation. For this reason a unique coefficient of variation has been chosen.
For each case two parallel analyses are performed:

1. an analysis in which the *mean value* of the parameters is used;

2. an analysis in which the parameters vary along t according to a Gaussian distribution and the *mean slope response* is obtained by averaging all the results.

5.1 Spatial variability of natural soils

To study the soil variability different probability distribution models exist. Typically the probability distribution is site and parameter specific, so there is no universally "best" distribution for soil properties. For this study a normal distribution (Figure5.2) has been chosen. The normal (or Gaussian) distribution has a probability density function given by:

$$f_{\psi}(\psi) = \frac{1}{\sigma\sqrt{2\pi}} exp\left[-\frac{1}{2}\left(\frac{\psi-\mu}{\sigma}\right)^2\right], \tag{5.1}$$

where μ and σ are respectively the mean and the standard deviation of the variable ψ. The normal distribution is defined in the range $-\infty < \psi < \infty$ and is symmetric around the mean value. As this distribution allows the presence of negative values, a correction of the parameter is performed each time a negative value occurs from the random variables distribution: is this case the parameter is set equal to zero. Anyway, the probability to obtain negative values is very low and this correction does not significantly modify the results.

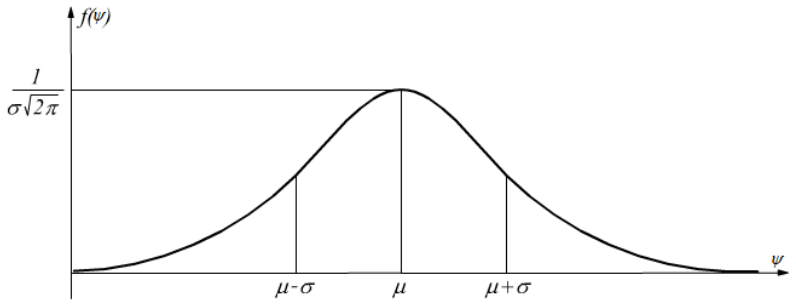

Figure 5.2: Representation of Gaussian distribution

Typically in slope stability analysis a mean value for the parameters is used. The standard deviation is a measure of how much each parameter is far from the mean value. It is defined as:

$$\sigma = \sqrt{\frac{\sum_{i=1}^{N}(\psi_i - \mu)^2}{N}} \tag{5.2}$$

The coefficient of variation is obtained dividing the standard deviation for its mean value. It provides a concise measure of the relative dispersion of data around the central tendency estimator (μ).

$$COV = \frac{\sigma}{\mu} \tag{5.3}$$

From the Gaussian distributions some random values for each parameter are obtained. Each set of random variables will be supposed to vary along the slope direction.
In a slope in cemented materials, different degrees of cementation may coexist. As the first parameter directly related to cement content is cohesion, a coefficient of variation for it has been searched in literature.[Harr, 1985] proposed as an upper bound limit for "low dispersion" in soil parameters a value of COV equal to 0.1. Different values are proposed in literature, in particular [Phoon et al., 1999], from an exhaustive study of cone penetration tests and triaxial tests results, suggested that the coefficient of variation of the cohesion could vary from 0.1 to 0.55. According to this proposed range, a variation coefficient for cohesion equal to 0.4 has been chosen, in order to simulate a quite variable soil.

5.2 Cohesion and shear stiffness distribution

Stability of slopes in cemented materials may be favoured by the presence of intergranular bonds between grains. These bonds are possible thanks to the presence

of bonding agents that act as a cement for the particles. Nevertheless there may be different distributions of these agents that bring to different degrees of cementation. So a change in the mechanical behaviour of cemented materials is expected according to the difference in cement content.
As already outilned, a correlation between degree of cementation and other parameters exists. In particular, an increase in the degree of cementation provokes an increase in cohesion and, subsequently, an increase in the shear stiffness. Due to this fact, the two parameters are necessarily correlated.
Starting from the triaxial tests on cemented materials performed on artificial cemented soil samples by [Alegre et al., 2001] shown in AppendixA, it is possible to extrapolate a relationship between cohesion a shear stiffness G_{50} (EquationA.5).

5.3 Elastic law

For the elastic case the only parameter playing a role is the shear stiffness G, as the variability of the Poission ratio ν is very limited.
Some tests under SSC conditions are performed: the initial state of stress corresponds to the one of a slope inclined of an angle α at a depth $z = H$.
Considering n springs the increment of shear stress in elastic regime of each spring will be given by:

$$d\tau_i = G_i d\gamma, \tag{5.4}$$

where $d\gamma$ is the imposed shear strain increment.
The resultant force will be:

$$R = \sum_{i=1,n} d\tau_i L_i, \tag{5.5}$$

where $L_1, L_2 ... L_n$ are the portions of the slope, characterized by shear stiffness $G_1, G_2 ... G_n$, on which the shear stress is acting.
Substituting Equation5.4 in Equation5.5:

$$R = \sum_{i=1,n} G_i L_i d\gamma \tag{5.6}$$

the increment of equivalent stress giving the average response of the system is:

$$d\tau_{eq} = \frac{R}{\sum_{i=1,n} L_i} = \frac{\sum_{i=1,n} G_i L_i d\gamma}{\sum_{i=1,n} L_i} = G_{eq} d\gamma. \tag{5.7}$$

The only variable following a Gaussian distribution is in this case the shear stiffness G; the various values of the shear stiffness are defined as:

$$G_i = G_0 + COV_G G_{mean} rand_i = G_0 + \Delta G, \tag{5.8}$$

where G_0 is the shear stiffness of the material without bonds, ΔG is the term related to the presence of bonds in the material, depending on the Gaussian distribution and $rand_i$ is a random number generated by the code.
In the table below the parameters used for the analysis in elastic field are reported. The value $G_{mean\,val}$ is evaluated from EquationA.5 starting from an assumed mean value of cohesion.

α [°]	H [m]	G_0 [kPa]	$G_{mean\,val}$ [kPa]	ν [$-$]	$\gamma_{nt,fin}$ [kPa]	COV_G [$-$]
10	5	10000	13000	0.25	0.005	0.4

As was expected, in case of elastic conditions the resulting equivalent $\tau_{nt} - \gamma_{nt}$ curve is the same as the one evaluated using the mean value of G (Figure5.3).

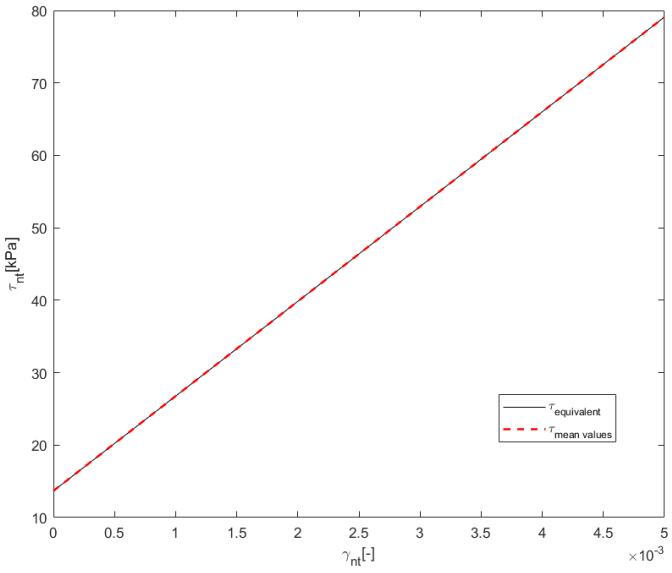

Figure 5.3: $\tau_{nt} - \gamma_{nt}$ curves for equivalent shear stiffness and mean shear stiffness in the elastic case

5.4 Elastic perfectly plastic law

As previously outlined, a relationship between cohesion and shear modulus exists and it is defined by EquationA.5.
The values of cohesion defined according to the Gaussian distribution can be written

as:

$$c'_i = c'_{mean\,val} + c'_{mean\,val} COV_c rand_i \tag{5.9}$$

Al already remarked, an increase/decrease in cohesion (i.e. of cement content) brings to a increment/decrement of shear stiffness. As in the elastic case, the random variable is the increment in elastic stiffness due to the interparticle bonding:

$$\Delta G_i = \Delta G_{mean} + \Delta G_{mean\,val} COV_{\Delta G} rand_i, \tag{5.10}$$

where ΔG_{mean} is defined as:

$$\Delta G_{mean} = a c'^2_{mean} + b c'_{mean}, \tag{5.11}$$

so at each step, the shear stiffness will be defined as:

$$G_i = G_0 + \Delta G_i. \tag{5.12}$$

The Mohr Coulomb failure criterion is adopted and the yield function is expressed as:

$$f = \tau_{nt} - \left(\sigma'_n tan\phi' + c'\right). \tag{5.13}$$

Similarly to the elastic case, for this case and for the following, the equivalent stress is evaluated as the mean of the stresses as:

$$\tau_{eq} = \frac{R}{L_{tot}} = \frac{\sum_{i=1,n} \tau_i}{n}. \tag{5.14}$$

In the table below the parameters used for the elastic-perfectly plastic analysis are reported. The friction angle is maintained constant, because from [Alegre et al., 2001] studied emerged that ϕ' is not very influenced by cement content and thus it can be approximately constant.
Due to the fact that cohesion and shear stiffness are strictly related, is assumed that $COV_{c'} = COV_{\Delta G}$.

α [°]	H [m]	ν [−]	ϕ [°]	m [−]	$c'_{mean\,val}$ [kPa]	$\gamma_{nt,fin}$ [−]	$COV_{\Delta G}$ [−]	$COV_{c'}$ [−]
15	5	0.25	30	0	50	0.01	0.4	0.4

In Figure5.4 the resulting equivalent $\tau_{nt} - \gamma_{nt}$ curve and the one evaluated using the mean values of G and c' are compared. From the curve can be stated that the system response with mean values is different from the mean system response. In particular, as far as the average slope response is concerned, if the constitutive

law is elastic-perfectly plastic, the system response is characterized by a pseudo-hardening response, due to the fact that each point reaches failure in a different imposed strain values with respect to the others.

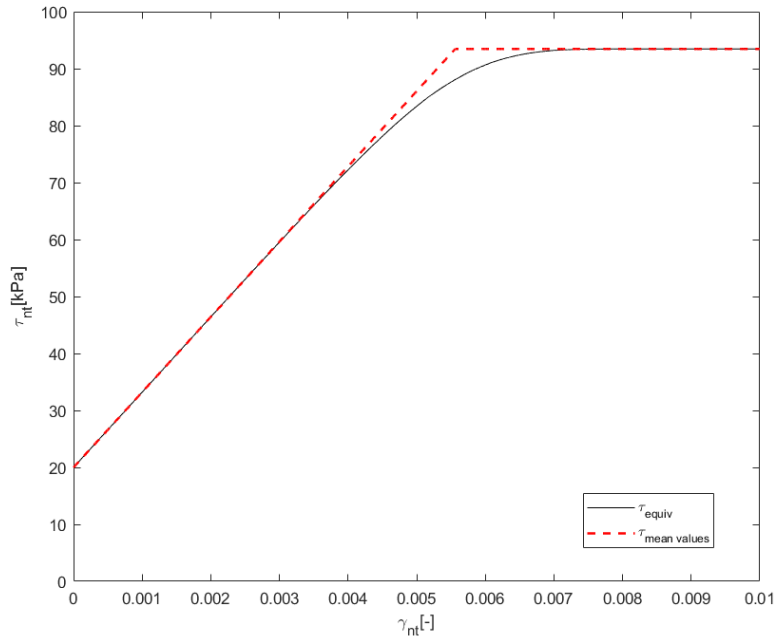

Figure 5.4: $\tau_{nt} - \gamma_{nt}$ curves for equivalent shear stiffness and mean shear stiffness in the elastic-perfectly plastic case

5.5 Elastoplastic law with softening regime

In case softening regime is introduced, a reduction of cohesion with shear strains is expected.
All the procedures describing the increment in stiffness and the subsequent stiffness variation are the same for parameter E.
For softening regime a non dimensional parameter m^* is introduced; according to [di Prisco and Flessati, 2019] it is defined as:

$$m^* = m\frac{\gamma_d z}{E} \tag{5.15}$$

The parameter m is a sort of fragility index of the system and indicates how fast the cohesion reduction will occur. For the study of parameters spatial evolution, m^* is assumed to be constant, implying a spacial variability of m depending on the Young modulus E. The Young modulus is defined according starting from the shear modulus G and m can be simply retrieved from Equation5.15.

For this case and the following strain softening viscoplastic case the numerical code integrating the equations in SSC will be used. The yield function and plastic potential are again defined according to the Mohr Coulomb failure criterion with Equations 3.7 and 3.8.
Two different analyses varying the initial value of cohesion and m^* are performed. In the first analysis $c'_{mean\,val} = 30kPa, m^* = 0.1$ and in the second $c'_{mean\,val} = 50kPa, m^* = 0.3$
In the table below all the other parameters used for the elastoplastic analyses with softening are reported.

α [°]	H [m]	ν [−]	ϕ [°]	$\gamma_{nt,fin}$ [−]	$COV_{\Delta E}$ [−]	$COV_{c'}$ [−]
20	5	0.25	30	0.05	0.4	0.4

In Figure5.5a the resulting equivalent $\tau_{nt} - \gamma_{nt}$ curve and the one evaluated using the mean values of E and c' are compared. As can be noticed, there is not a so marked difference between the mean response and the response with mean values.

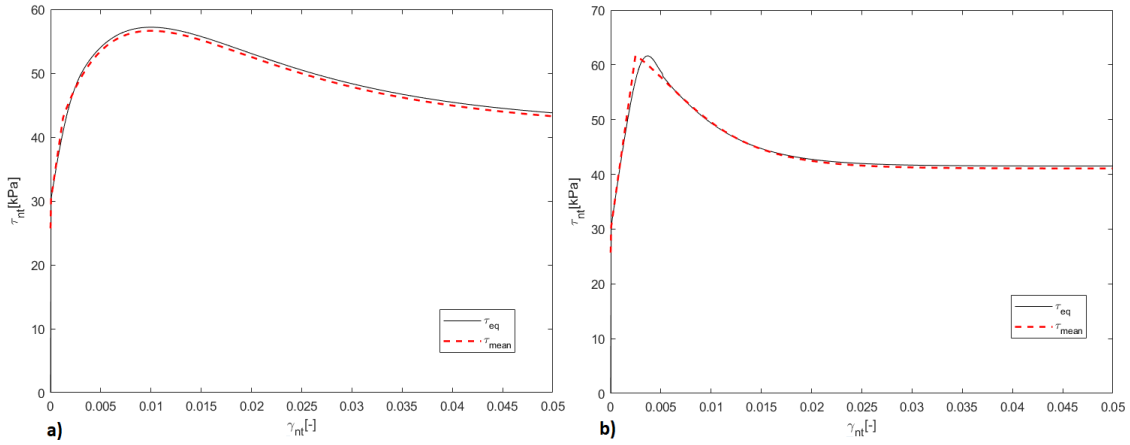

Figure 5.5: $\tau_{nt} - \gamma_{nt}$ for equivalent system response and mean response in case of softening regime a) $c'_{mean\,val} = 30kPa, m^* = 0.1$ b) $c'_{mean\,val} = 50kPa, m^* = 0.3$

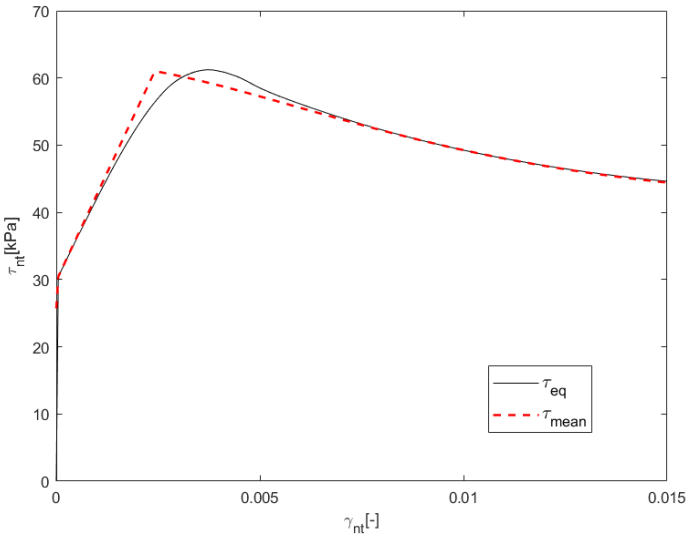

Figure 5.6: Magnified $\tau_{nt} - \gamma_{nt}$ to remark the pre-peak response in the case $c'_{mean\,val} = 50kPa, m^* = 0.3$

Even in this case, in case of mean slope response, irreversible strains start earlier; in addition, the mean slope response shows a more ductile behaviour due to the parameters spatial variability (Figure5.6).
As can be seen from Figure5.6, the peak of the mean response preceds the one of the equivalent response; in addition, a sort of pseudo-hardening regime seems to verify in the equivalent case. This behaviour can be justified with the spatial variability of the yielding shear stress and with the subsequent spatial variation of structural hardening phenomenon. Finally, the post peak branch of the equivalent response is nearly equal to the mean post peak branch.

5.6 Strain softening viscoplastic law

At the microscale (i.e. at the grain scale) defects are present and evolve in time. At the macro scale this is accounted for by introducing a viscous response, governed by the parameter η. So, in general, η is a viscous parameter governing the time response of the system. For high values of η the system response is very quick, while for low values of η, the system response will be delayed in time.
All this considered, η is expected to depend on the degree of cementation: the presence of defetcs is related to the damage in time of the bonds between grains, which is directly related to cement content.
As already outlined, the bond strength is responsible of the increment of cohesion and of material stiffness, while the presence of defects modifies the viscous behaviour of the material.

Being both cohesion and viscous coefficient dependent on the degree of cementation, the same range of COV (i.e. the one proposed by [Phoon et al., 1999]) for all the parameters is assumed.
In the table below the parameters used for the viscoplastic case with softening are reported. In this first analysis the variation coefficient of the viscous parameter is mantained equal to the COV of cohesion and of stiffness increment.

α [°]	H $[m]$	ν [–]	ϕ [°]	m^* [–]	$c'_{mean\,val}$ $[kPa]$	$\eta_{mean\,val}$ $[\frac{1}{kPas}]$	$\gamma_{nt,fin}$ [–]	T_{fin} $[hours]$	$COV_{\Delta E}$ [–]	$COV_{c'}$ [–]	COV_{η} [–]
20	5	0.25	30	0.1	30	$4 \cdot 10^{-7}$	0.05	1	0.4	0.4	0.4

In Figure5.7 the resulting equivalent $\tau_{nt} - \gamma_{nt}$ curve and the one evaluated using the mean values of E, c' and η are compared.
What can be noticed is that, due to spatial variability, the maximum allowable stress for the system is higher considering the equivalent response and the equivalent response is quite different because the softening branch is not present.
The parameters used in this viscoplastic analysis are the same used in the elastoplastic analysis taking into account of softening of Figure5.5 and from the two $\tau - \gamma_{nt}$ curves can be noticed that the two systems behave in a completely different way. This is due to the fact that in the viscous case a delayed in time response is expected.

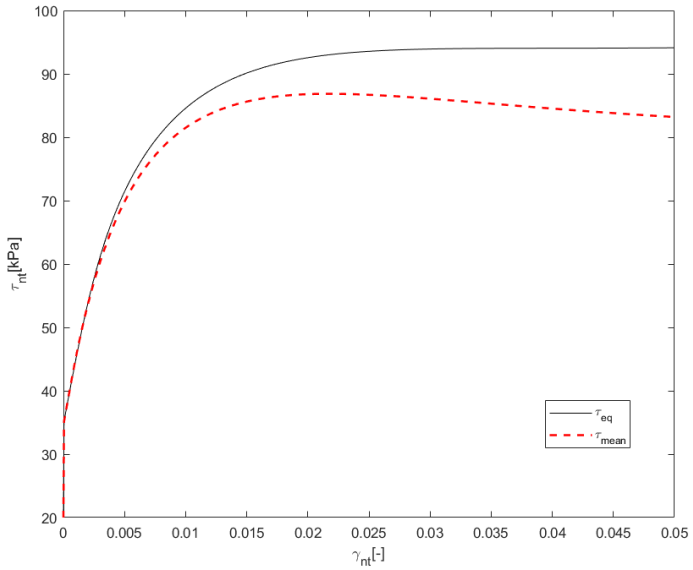

Figure 5.7: $\tau_{nt} - \gamma_{nt}$ curves for equivalent system response and mean response in case of viscoplastic constitutive law

It is interesting to notice that if another analysis is performed with the same parameters of the one in Figure5.7, but using an higher variation coefficient for η (so a greater variability for this parameters), the mean response of the system may be completely different from the one of the system with mean values. The correlation coefficient for η is set equal to 0.55, which is the limit value of the range proposed by [Phoon et al., 1999] and corresponds to a great variability in space. The response of in terms of $\tau_{nt} - \gamma_{nt}$ can be seen in Figure5.8. For the great variability of η, there are some points behaving in an elastic way and others behaving in an viscoplastic way (Figure5.9) and the mean response may result as an hardening behaviour instead of softening.

Considering the obtained results, in the elastoplastic case there is no significant

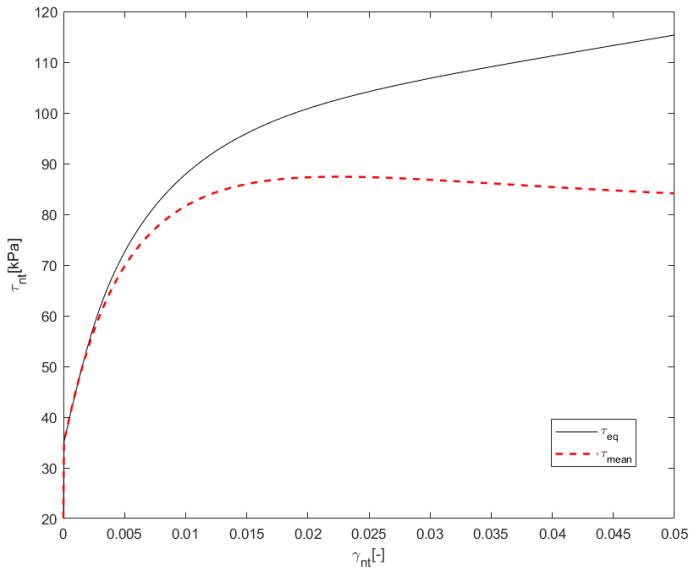

Figure 5.8: $\tau_{nt} - \gamma_{nt}$ viscoplastic curves for equivalent system response and mean response in case $COV_\eta = 0.55$

change in the system response with spatial variability, but for the strain-softening elastoplastic and strain-softening viscoplastic cases, to correctly study the system response, it is not sufficient to use the parameters mean values, but it is necessary to properly take into account their spatial variability.

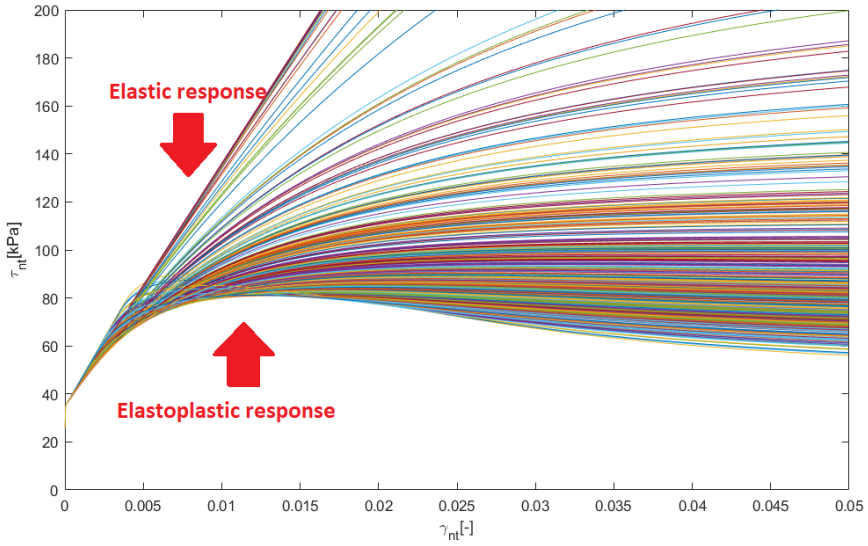

Figure 5.9: $\tau_{nt} - \gamma_{nt}$ viscoplastic curves used to obtain the mean response of the system in case $COV_\eta = 0.55$

Conclusions

In this thesis the response of infinite slopes in naturally bonded materials has been analyzed. Among all the possible perturbations, only water table level change has been studied, being a frequent triggering factor for creeping landslides.
The two main aspects to take into account in the problem are the static redundancy of the infinite slope configuration and the progressive reduction in material strength induced by the accumulation of irreversible strains. The first is fundamental to take into account of all the plastic resources of the system and the second is necessary to properly simulate cemented materials behaviour.
The introduced 1D strain softening elastic-viscoplastic equivalent model overcomes the limits of other simplified models present in literature, taking into account both these aspects. It is essential to remark the importance of considering a strain-softening-viscoplastic constitutive model, because only with mechanical properties reduction the landslide inception phase and tertiary creep phenomenon can be properly reproduced.
The definition of the strain-softening-viscoplastic model passes through the development of an elastoplastic constitutive model, that is subsequently extended to the viscous case.
In the elastic plastic case, to introduce the structural hardening, a condensation procedure of the hyperstatic variable into "macro" constitutive parameters is performed; this method abruptly simplifies the computational costs, by reducing the number of static/kinematic variables (degrees of freedom) to be considered, but implies the introduction of a strain hardening elastic plastic model, even if initially an elastic perfectly plastic constitutive relationship is adopted to reproduce the material mechanical behaviour.
As far as the simulations results are concerned, the equivalent strain hardening elastoplastic model very satisfactorily reproduces the numerical solution obtained by integrating all the constitutive equations under simple shear conditions.
In the viscoplastic case, a simple condensation procedure is no more sufficient to reproduce the numerical behaviour. For this reason, an internal variable and its evolution law have been introduced. In the framework of viscoplasticity it was also possible to introduce the softening regime to describe the mechanical properties degradation with strain accumulation. Considering both softening and structural hardening, the model is capable of reproducing the first failure stage of creeping landslides, characterized by strain acceleration even when the perturbation is reducing (i.e. the water table level is decreasing after a rapid increase). The performed simulations very well reproduce the numerical results.

The new model depends on micro parameters (geometry, material mechanical properties) and on macro parameters; the expression to calculate the values of the macro parameters were provided. For the sake of brevity, a unique stress path (oscillation in the water table level) has been studied, but the adopted procedure is totally general and may be also be tailored to other different stress paths. In bonded soils the main aspect governing the mechanical behaviour is "degree of cementation": from the literature emerged that elastic parameters, cohesion and viscous parameter are particularly influenced by the degree of cementation and consequently, varying this quantity, the mechanical response is expected to be different.
Since along slopes, the "degree of cementation" is expected not to be constant, a study about parameter spatial variability was performed, in order to understand its main implications on the slope response. The infinite slope response with different constitutive laws (elastic, elastic plastic and strain softening visco plastic) was analyzed under simple shear conditions. The results show that with a strain-softening elastoplastic and strain-softening viscoplastic constitutive law the employment of mean parameters could lead to a significantly different response with respect to the mean slope response. So in these situations, it is recommended to properly take into account the material properties spatial variability and to evaluate the average slope response, as more representative of the real behaviour of an heterogeneous soil.

Appendix A

Cemented materials: influence of cement content - Experiemental characterization

In literature many studies to describe the influence of the cement content on the mechanical behviour of cemented materials are present. In this section, particular attention will be given to the one in [Alegre et al., 2001]. The authors studied the influence of cement content on the mechanical behaviour of artificially cemented sands subjected to an experimental program including unconfined compression tests and drained triaxial compression tests.
From a mechanical point of view, cemented soils, weak rocks and similar bonded materials constitute an intermediate class of geomaterials placed between classical soil mechanics and rock mechanics.
In general can be assumed that, for a given range of stresses and for low cement content, shear strength of naturally and artificially cemented sands can be represented by straight Mohr-Coulomb envelope defined by cohesion intercept c', which is a unique function of cementation, and the friction angle ϕ', which seems not to be significantly affected by the cement content.
As to deformability, cemented soils are characterized by a very stiff behaviour before yielding, basically governed by cementation. The brittle behaviour changes to a ductile soil response when the stress level changes from low to high.
In [Leroueil, 1990] is proposed a conceptual approach to describe the stress-strain behaviour of soils with common bonded structure. The effects of structure on soil behaviour are similar to the effects produced by overconsolidation in clays. These effects are basically characterized by an initial stiff behaviour, followed by increasingly plastic deformation as the soil approaches failure.
Following the same concept [Coop and Atkinson, 1994] described an idealized behaviour of cemented soils. They divided cemented materials idealized behaviour in three different classes (FigureA.1):

- the first class (1) represents a behaviour occurring when the soil reaches its yielding stress during isotropic compression; in this case shearing will produce a behaviour similar to the one of the equivalent non-structured soil;

- the second class (2) represents a behaviour occurring for intermediate state of stress, in which the bonds will be broken during shearing; the strength is controlled by the frictional component of the equivalent non-structured soil and the stress-strain curve shows a well defined yield point after an apparent linear behaviour;

- the third class (3) describes a behaviour occurring when the soil is sheared at low confining stresses with respect to the bond strength; a peak in stress-strain curve occurs at small strains and for stresses outside the limit state surface of equivalent non-structured soil (FigureA.2).

In this thesis the behaviour belonging to class 3 will be analyzed: so a strain softening material will be chosen.
In FigureA.2 the stress paths relative to the different classes are shown. As for class 3, when the loading path reaches a point which is above the critical state line, the stress path must then return on that line. This passage can be defined as a softening phenomenon and it is physically represented by a reduction of stresses.

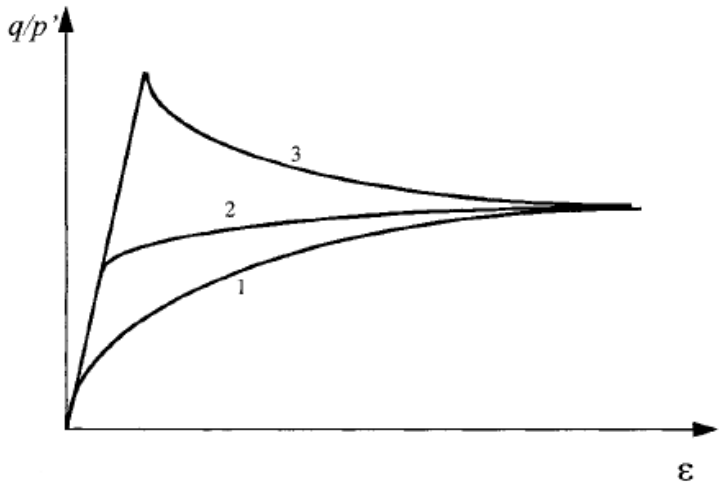

Figure A.1: Stress-strains curves describing th idealized behaviour of of cemented soils

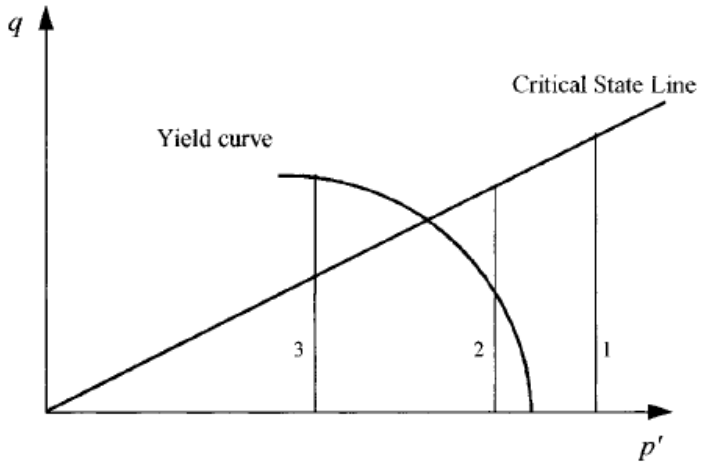

Figure A.2: Effective stress paths describing th idealized behaviour of of cemented soils

A.1 Specimens preparation

In the experimental program specimens made of artificially cemented sands are chosen to reduce the scatter frequently observed from natural soil specimens retrieved in situ.
Specimens were prepared by mixing soil and water with the addition of portland cement 1%, 3% and 5% by weight of dry soil weight. These soil-cement mixtures are characterized as weakly to very strongly cemented soils. The degree of cementation is represented by the cement content added to the soil.
The specimens were compacted in layers into a $50-mm$ diameter, $100-mm$ high cylindrical mold, to a dry unit weight of $17.5kN/m^2$ and at an optimum moisture content of 15.8%.The molds were then wrappened in moisureproof bags and stored in a humid room to cure for 7 days before testing. To approximate full saturation in the unconfined compression test, the specimens were soaked in water during $24h$ of curing, before being tested at a strain rate of $1.141\%min$.

A.2 The experimental program

Some triaxial compression tests at different cement content and at different initial mean effective stress p'_i are performed. The deviatoric stress versus axial strain and thr volumetric versus axial strains are shown in Figure A.3 a) for the uncemented specimens (i.e $C = 0\%$) and FiguresA.3 b) and A.4 c),d) for the artificially cemented

specimens (with $C = 1{,}3{,}5\%$ respectively).
From the analysis of FiguresA.3 and A.4 emerges that stress-strain behaviour of the cemented soil can be described as initially stiff, apparently linear up to a well defined yielding point, beyond which the soil suffers increasingly plastic deformations until failure. As the cement content increases, both peak strength and initial stiffness increase. Differently from the uncemented soil (FigureA.3a), cemented specimens show a marked brittle behaviour at failure with well defined shear bands being formed. This brittle response increases with cement content. As for volumetric response, the cemented specimens show an initial compression followed by a strong dilation with the maximum dilation rate taking place right after the peak strength. Subsequently dilation rate decreases as the soil approaches an ultimate condition.

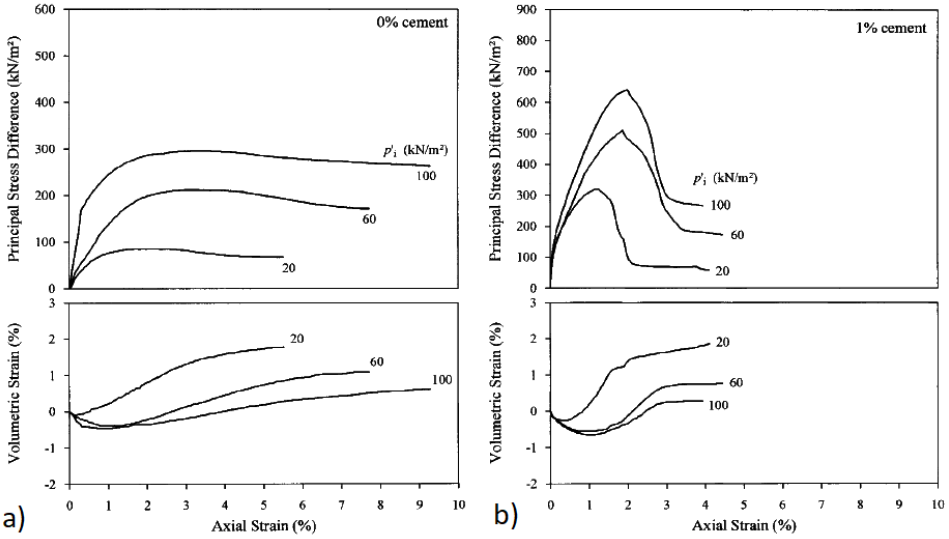

Figure A.3: Stress-Strain-Volumetric response at different initial mean stresses for a) 0% cement content, b) 1% cement content

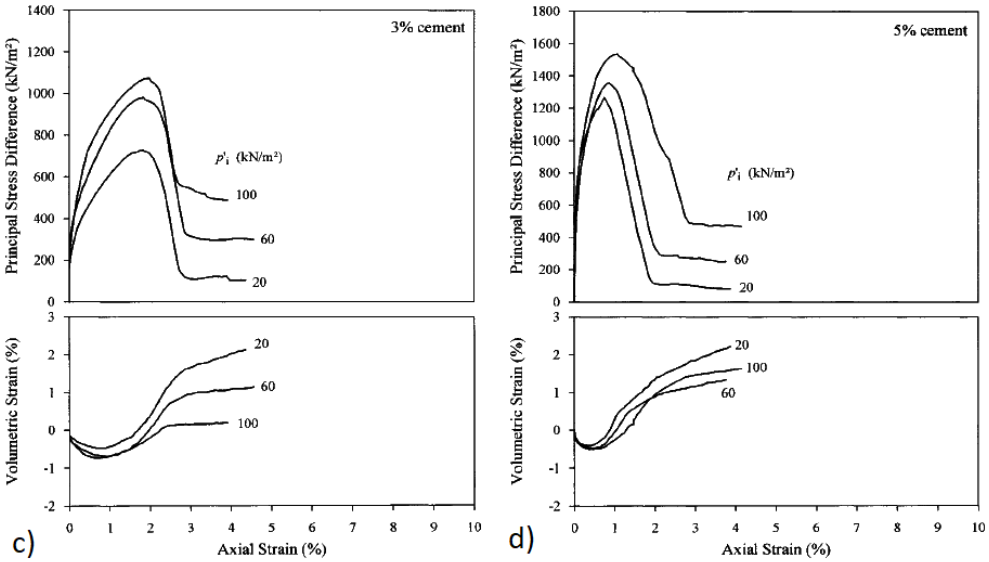

Figure A.4: Stress-Strain-Volumetric response at different initial mean stresses for a) 3% cement content, b) 5% cement content

In FigureA.5 the principal stress difference versus axial strain and volumetric strain versus axial strain curves for different cement contents are shown. The initial mean effective stress is kept constant ($p'_i = 60kN/m^2$). As previously outlined, increasing the cement content the material behaviour passes from ductile to fragile and the dilatancy phenomenon increases.

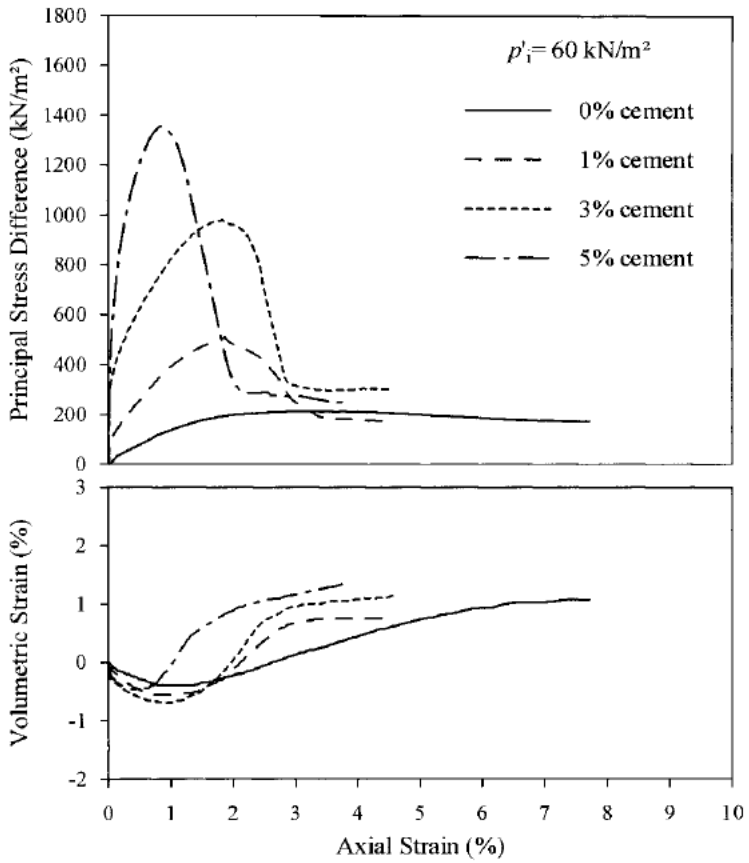

Figure A.5: Stress-strain-volumetric response at different cement contents for $p'_i = 60kN/m^2$

Given the cohesive-frictional nature of the cemented soil, the shear strength can be expressed as a function of the internal friction angle and cohesion intercept. From FigureA.6 can be seen that a well defined linear relationship between cement content and intercept cohesion exists.
From results in literature ([Alegre et al., 2001]) emerges the friction angle varies according to a non-defined pattern that does not allow to establish a clear correlation between cement content and friction angle.

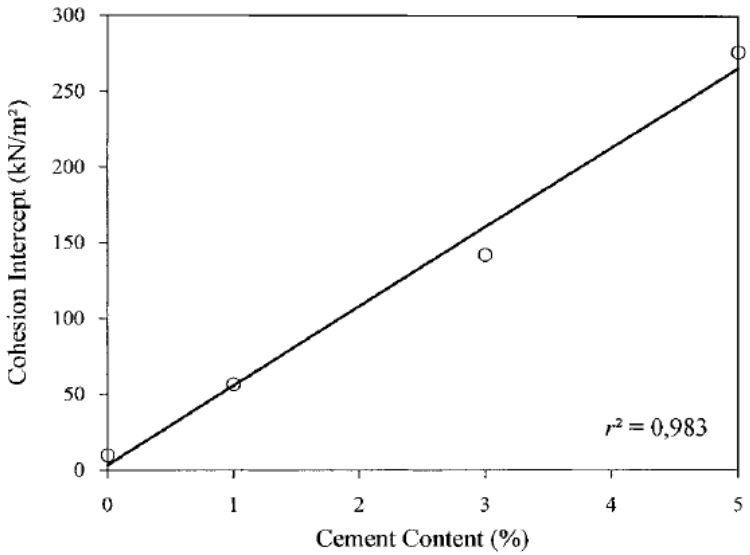

Figure A.6: Effect of cement content on unconfined compressive strength

From the experimental results emerges that a relationship between stiffness and cement content exists; as also cohesion variation is related to cement content, c' and G are necessarily related. An expression relating G and c' extrapolated from experimental results will be hereafter reported.
From the stress-strain behaviour shown in FigureA.5 it is possible to estimate the secant Young modulus at 50% of failure deviatoric load:

$$E_{50} = \frac{0.5 q_f}{\varepsilon_{a,50}} \tag{A.1}$$

Given the volumetric-axial strain curve (FigureA.5) it is possible to determine the radial deformation as follows:

$$\varepsilon_{50,r} = \frac{1}{2}\left(\varepsilon_{a,50} - \varepsilon_{vol,50}\right) \tag{A.2}$$

And from it to estimate the Poisson ratio:

$$\nu_{50} = -\frac{\varepsilon_{r,50}}{\varepsilon_{a,50}} \tag{A.3}$$

So through the relationship between E_{50} and G_{50} coming from theory of elasticity, it is possible to determine the shear modulus:

$$G_{50} = \frac{E_{50}}{2\left(1 + \nu_{50}\right)} \tag{A.4}$$

In FigureA.7 it is possible to see the curves coming from experimental data and from interpolation. Through the interpolation it is possible to determine the following relationship between c' and G_{50} (the subscript $_{50}$ will be hereafter omitted

for sake of brevity):

$$G = G_0 + bc' + ac'^2 \tag{A.5}$$

Where G_0 is the secant shear modulus for $c' = 0kPa$ and a,b are two interpolation constant parameters.
From EquationA.5 can be noticed that the relationship between G and c' is not linear. This expression can be written as the sum of an initial value of G and an increment given by the related to the cementation:

$$G = G_0 + \Delta G \tag{A.6}$$

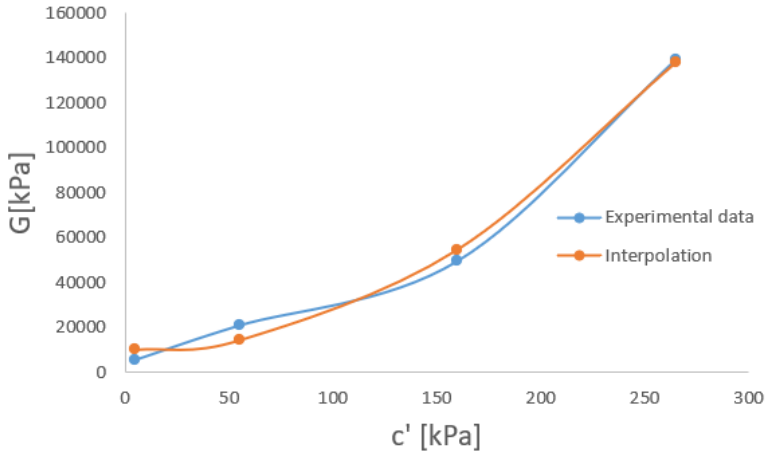

Figure A.7: $G - c'$ curves from experimental data and interpolation

Appendix B

The concept of instability

The concept of instability is founded on the mathematical criterion of stability for elastoplastic constitutive laws elaborated by [Buscarnera et al., 2011] to give a new interpretation to [Nova, 1994] controllability theory. In particular, this deals with the loss of controllability of the incremental response in soil specimens subjected to arbitrary ("mixed") loading programs; Nova remarked that the critical condition is possible even in the hardening regime. The author thus gave an interpretation of the [Hill, 1958] stability criterion assigning to it an alternative mechanical meaning. The drawback of these first approaches is in the fact that they become less powerful when the particular case of hardening regime is abandoned for a more general initial and loading condition. For this reason [Buscarnera et al., 2011] tried to give a more consistent theoretical reference capable of assessing the stability at a given stress state in a more general and flexible manner. Restricting the speech to rate-independent elastoplastic constitutive laws, the aim of the authors was to establish a more explicit link with the notions of existence and uniqueness of the material response, so that to introduce an alternative mathematical indices of stability (defined as moduli of instability) and provide an easier application to brittle materials.

B.1 Material stability and its mathematical definition

Between all the various existing stability criterions, the reference one for this study is [Hill, 1958] stability criterion, which is based on the second order work definition. According to it, a sufficient condition for stability is that second order work is positively defined. This can be written as:

$$dW^2 = \frac{1}{2}\dot{\sigma}_{ij}\dot{\varepsilon}_{ij} > 0, \forall \dot{\varepsilon}_{ij} \tag{B.1}$$

Where $\dot{\sigma}_{ij}$ is the stress tensor and $\dot{\varepsilon}_{ij}$ is the corresponding strain rate tensor.
This criterion can describe diffuse instabilities and shows the loss of uniqueness of incremental response; according to this point of view a contribution was given by [Maier and Hueckel, 1979]: they addressed the evaluation of material stability and the admissibility of incremental stress path for materials characterized by non associative flow rule and strain softening. Starting from Hill's stability criterion they evaluated the minimum value of the quadratic form associated to the second order work dW^2_{min} and they evaluated the sign of this quantity that turned out to be a quadratic function of the hardening modulus H. This last quantity can be defined as:

$$H = -\frac{\partial \tilde{f}}{\partial \mathbf{q}} \frac{\partial \mathbf{q}}{\partial \boldsymbol{\varepsilon}^p} \frac{\partial g}{\partial \boldsymbol{\sigma}} \tag{B.2}$$

Where f is the yield function, $\mathbf{q}$ a vector collecting all the internal variables and g the plastic potential. The tilde of equation above is used to indicate the transpose in matrix notation.
Assuming an associated flow rule, which means that $f = g$, the evolution of dW^2_{MIN} as a function of H in shown in FigureB.1; the stability in the sense of Hill's condition is satisfied when $dW^2_{MIN} > 0$, while the system is unstable if and only if $dW^2_{MIN} \leq 0$. For an associated flow rule it is evident that the material stability is predicted when $H > 0$ and the first point for which instability is reached is $H = 0$. The variabile H_c

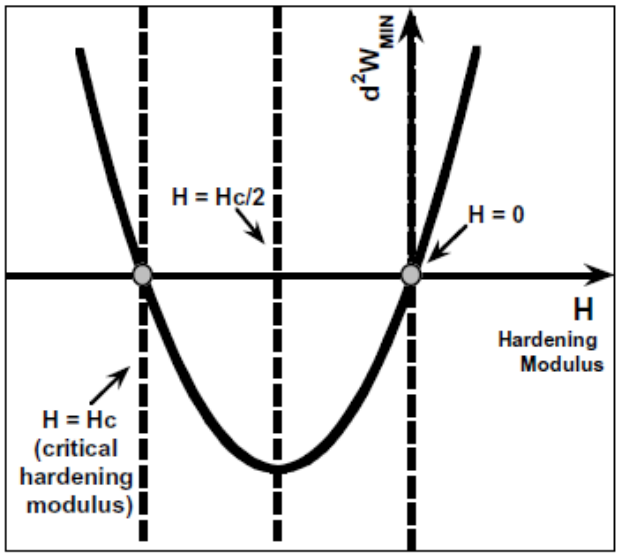

Figure B.1: $H - dW^2_{MIN}$ curve showing the stability criterion in the sense of Hill for an associated flow rule

is called critical hardening modulus and in this particular case it has the following

expression

$$H_c = -\frac{\partial \tilde{f}}{\partial \boldsymbol{\sigma}} \mathbf{D}^e \frac{\partial g}{\partial \boldsymbol{\sigma}}, \tag{B.3}$$

where $\mathbf{D}^e$ is the elastic constitutive stiffness matrix.

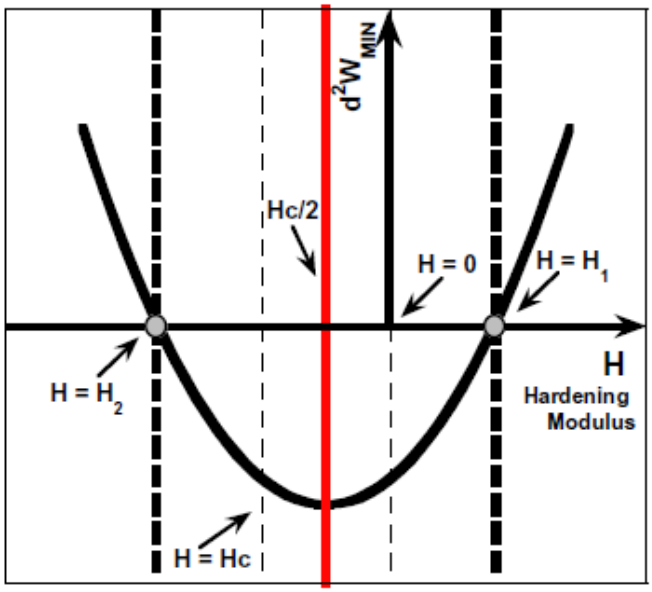

Figure B.2: $H - dW^2_{MIN}$ curve showing the stability criterion in the sense of Hill for a non associated flow rule

For $H < H_c$ a process of subcritical softening develops, characterized by the inception of snap-back process [Maier, 1966].
In FigureB.2 the second order work density varying with H in case of non associative flow rule is shown; two new quantities called H_1 and H_2 can be defined as:

$$H_1 = \frac{1}{2} H_c + \frac{1}{2} \left(\frac{\partial \tilde{g}}{\partial \boldsymbol{\sigma}} \mathbf{D}^e \frac{\partial g}{\partial \boldsymbol{\sigma}} \frac{\partial \tilde{f}}{\partial \boldsymbol{\sigma}} \mathbf{D}^e \frac{\partial f}{\partial \boldsymbol{\sigma}} \right)^{\frac{1}{2}} \tag{B.4}$$

$$H_2 = \frac{1}{2} H_c - \frac{1}{2} \left(\frac{\partial \tilde{g}}{\partial \boldsymbol{\sigma}} \mathbf{D}^e \frac{\partial g}{\partial \boldsymbol{\sigma}} \frac{\partial \tilde{f}}{\partial \boldsymbol{\sigma}} \mathbf{D}^e \frac{\partial f}{\partial \boldsymbol{\sigma}} \right)^{\frac{1}{2}} \tag{B.5}$$

They are the values of hardening modulus for which $dW^2_{MIN} = 0$. As to the stability in the sense of Hill, the non associativeness modifies the range of hardening moduli for which stability is obtained. The first point for which instability is reached is $H = H_1 > 0$ and symmetrically the last point for which the second order work density vanishes is $H = H_2 < H_c$ ([Maier and Hueckel, 1979]); these two points, in

case of associated flow rule, degenerate in $H_1 = 0$ and $H_2 = H_c$.
The conceptual role played by dW^2_{MIN} in showed FigureB.1 and FigureB.2 is not exhaustive, as two crucial aspects are not taken into account, which are the plastic admissibility of the incremental loading and the role of control conditions.
As to the first, an incremental loading path is admissible if these plastic constraints are satisfied:

$$\dot{f} \leq 0, \dot{\Lambda} \geq 0, \dot{f}\dot{\Lambda} = 0, \tag{B.6}$$

where Λ is the plastic multiplier which is obtained imposing the plastic consistency condition. Can be demonstrated that the procedure used to calculate dW^2_{MIN} in FiguresB.1 and B.2 does not enforce the all plastic admissibility constraints in the region of negative hardening moduli and thus part of the information provided by dW^2_{MIN} is not consistent in with the framework of classical elastoplasticity ([Maier and Hueckel, 1979]). In particular, the positive value of dW^2_{MIN}, obtained in the region in which $H < 0$, may lead to the misleading conclusion that stability holds also for $H < H_2$. The second aspect restricts the use of Hill's principle: if it is accepted in its conventional form, the material stability would be seen as an intrinsic characteristic of the material, but it cannot be considered so, as actually both existence and uniqueness are affected by the choice of control parameters and so by the initial state and by the type of external perturbation.

B.2 An alternative mathematical interpretation for test controllability

The new approach for interpretation of instability proposed in [Buscarnera et al., 2011] will be hereafter discussed. To introduce the dependency on control condition of stability for elastic plastic materials, the controllability theory will be used ([Nova, 1994];[Imposimato and Nova, 1998]). According to this new approach a loading program is considered controllable if and only if the predicted incremental response exists and is unique. This new mathematical concept of test controllability provides an anternative definition of stability, that is related to the test controllability.

B.2.1 Link between loss of controllability and definition of the loss of definition of plastic multiplier

According to classical controllability theory ([Nova, 1994]), the study of the stability of the system is done through the study of the determinant of the constitutive

control matrix associated to a specific loading control. The drawback of this approach is that when the control matrix suffers a discontinuous transition, i.e. a plastic yielding or a change in control conditions, which are the major cause of onset of instability, there are some difficulties in the use of the matrix determinant to assess the material stability.
To overcome these limits and to remark the close link between notions of plastic admissibility, existence and uniqueness, the new approach given by the authors is hereafter analyzed.
A laboratory test on a solid specimen in stress control conditions is considered; according to the kind of control, assuming a non singular elastic constitutive matrix, the increment of strains can be obtained as:

$$\dot{\boldsymbol{\varepsilon}} = \mathbf{D}^{-1}\dot{\boldsymbol{\sigma}}. \tag{B.7}$$

Within an elastoplastic constitutive framework the singularity of constitutive matrix coincides with the vanishing of the hardening modulus H and it represents the attainment of failure in classical sense.
The alternative description of the same event is obtained considering the analytical form of the plastic multiplier obtained through the imposition of consistency condition:

$$\dot{\Lambda} = \frac{1}{H}\frac{\partial \tilde{f}}{\partial \boldsymbol{\sigma}}\dot{\boldsymbol{\sigma}}. \tag{B.8}$$

As in classical elastoplasticity, when $H = 0$ failure is reached through the singularity of $\mathbf{D}$, so in this case when $H = 0$, the plastic multiplier is no longer defined and instability is reached. The loss of controllability in the light of this method represents the possibility that, given a single loading control, arbitrary solutions in terms of strains increments exist,bringing to the loss of uniqueness of the solution. Equation B.8 however represents the plastic multiplier under stress control condition and not in a general loading program. Can be demonstrated that the expression of the plastic multiplier is strictly dependent on the imposed loading conditions, as shown also by the expression of Λ obtained under pure strain control conditions:

$$\dot{\Lambda} = \frac{1}{H - H_C}\frac{\partial \tilde{f}}{\partial \boldsymbol{\sigma}}\mathbf{D}^e\dot{\boldsymbol{\varepsilon}}, \tag{B.9}$$

from EquationB.9 emerges that also under this control a particular condition for which instability is reached exists:

$$H = H_C \tag{B.10}$$

When EquationB.10 is satisfied the system is subjected to the so called snap-back process associated with critical softening. Thus this test controllability theory is

capable to describe this sub-critical softening response, which is equivalent to the vanishing of matrix D, but moreover it offers an alternative theoretical support to identify the onset of instabilities. This critical condition can be also identified when a certain scalar quantity called modulus of instability vanishes; it is defined as

$$H_{IN} = H - H_C \tag{B.11}$$

This instability modulus plays a similar role of the hardening modulus in the case of stress control condition: when it goes to zero the instability condition and loss of uniqueness of the solution are reached. Critical values of the plastic hardening modulus can be indeed associated with the loss of positiveness of second order work ([Hueckel and Maier, 1977]; [Maier and Hueckel, 1979]) or to the onset of shear strain localization ([Bigoni and Hueckel, 1991]).
As previously mentioned the plastic multiplier Λ depends on the imposed loading path, so each instability index has to be associated with a specific loading program.

B.2.2 Mixed stress-strain control conditions: definition of the moduli of instability

Laboratory tests are often done in mixed stress strain control conditions, in particular these mixed constraints can often be the cause of instability and
[Imposimato and Nova, 1998] gave a mathematical interpretation for this issue. The authors showed that a general loss of controllability may be studied observing the evolution of certain minors of the constitutive stiffness matrix. If a particular set of control parameters is governed, control matrices may become singular and potential instabilities can be activated even before classical failure. These instability modes are due to specific control conditions and they would not be induced under different constraints: so they are represent a proper form of latent instability. As for the previous case a relation between loss of controllability and loss of definition of the plastic multiplier can be found also for mixed stress strains controls. To reach this aim a particular strategy has to be followed to calculate the plastic multiplier ([Buscarnera et al., 2011]). Considering the following partition of the incremental constitutive law:

$$\begin{bmatrix} \dot{\boldsymbol{\sigma}}_\alpha \\ \dot{\boldsymbol{\sigma}}_\beta \end{bmatrix} = \begin{bmatrix} \mathbf{D}_{\alpha\alpha} & \mathbf{D}_{\alpha\beta} \\ \mathbf{D}_{\beta\alpha} & \mathbf{D}_{\beta\beta} \end{bmatrix} \begin{bmatrix} \dot{\boldsymbol{\varepsilon}}_\alpha \\ \dot{\boldsymbol{\varepsilon}}_\beta \end{bmatrix} \tag{B.12}$$

Assuming to perform an incremental loading path under mixed stress-strain control conditions, taking for instance $\dot{\boldsymbol{\sigma}}_\alpha$ and $\dot{\boldsymbol{\varepsilon}}_\beta$ as control variables, being $\dot{\boldsymbol{\varepsilon}}_\alpha$ and $\dot{\boldsymbol{\sigma}}_\beta$ the corresponding response variables.
The consistency condition, expressed in terms of stress rates, takes the following form:

$$\frac{\partial \tilde{f}}{\partial \boldsymbol{\sigma}_\alpha}\dot{\boldsymbol{\sigma}}_\alpha + \frac{\partial \tilde{f}}{\partial \boldsymbol{\sigma}_\beta}\dot{\boldsymbol{\sigma}}_\beta - H\dot{\Lambda} = 0 \tag{B.13}$$

introducing the elastic part of the incremental constitutive law

$$\begin{bmatrix} \dot{\boldsymbol{\sigma}}_\alpha \\ \dot{\boldsymbol{\sigma}}_\beta \end{bmatrix} = \begin{bmatrix} \mathbf{D}^e_{\alpha\alpha} & \mathbf{D}^e_{\alpha\beta} \\ \mathbf{D}^e_{\beta\alpha} & \mathbf{D}^e_{\beta\beta} \end{bmatrix} \begin{bmatrix} \dot{\boldsymbol{\varepsilon}}^e_\alpha \\ \dot{\boldsymbol{\varepsilon}}^e_\beta \end{bmatrix} \tag{B.14}$$

using EquationB.14 it is possible to express stress and strain measures appearing in the previous matrix partition as follows:

$$\dot{\boldsymbol{\sigma}}_\beta = \mathbf{D}^e_{\alpha\beta}\dot{\boldsymbol{\varepsilon}}^e_\alpha + \mathbf{D}^e_{\beta\beta}\dot{\boldsymbol{\varepsilon}}^e_\beta \tag{B.15}$$

$$\dot{\boldsymbol{\varepsilon}}^e_\alpha = \left(\mathbf{D}^e_{\alpha\alpha}\right)^{-1}\dot{\boldsymbol{\sigma}}_\alpha - \left(\mathbf{D}^e_{\alpha\alpha}\right)^{-1}\mathbf{D}^e_{\alpha\beta}\dot{\boldsymbol{\varepsilon}}^e_\beta \tag{B.16}$$

in which $\mathbf{D}^e_{\alpha\alpha}$ has been assumed not singular. Combining Equation B.15 and B.16 the following expression of $\dot{\boldsymbol{\sigma}}_\beta$ is obtained:

$$\dot{\boldsymbol{\sigma}}_\beta = \mathbf{D}^e_{\beta\alpha}\left(\mathbf{D}^e_{\alpha\alpha}\right)^{-1}\dot{\boldsymbol{\sigma}}_\alpha + \left(\mathbf{D}^e_{\beta\beta} - \mathbf{D}^e_{\beta\alpha}(\mathbf{D}^e_{\alpha\alpha})^{-1}\mathbf{D}^e_{\alpha\beta}\right)\dot{\boldsymbol{\varepsilon}}^e_\beta \tag{B.17}$$

as a consequence Equation B.13 becomes:

$$\frac{\partial \tilde{f}}{\partial \boldsymbol{\sigma}_\alpha}\dot{\boldsymbol{\sigma}}_\alpha + \frac{\partial \tilde{f}}{\partial \boldsymbol{\sigma}_\beta}\mathbf{D}^e_{\beta\alpha}(\mathbf{D}^e_{\alpha\alpha})^{-1}\dot{\boldsymbol{\sigma}}_\alpha + \frac{\partial \tilde{f}}{\partial \boldsymbol{\sigma}_\beta}\left(\mathbf{D}^e_{\beta\beta} - \mathbf{D}^e_{\beta\alpha}(\mathbf{D}^e_{\alpha\alpha})^{-1}\mathbf{D}^e_{\beta\alpha}\right)\dot{\boldsymbol{\varepsilon}}^e_\beta - H\dot{\Lambda} = 0 \tag{B.18}$$

if the trial stress increments (i.e. the stress increment that would be obtained for the considered control conditions if the material was purely elastic) are used, a simpler expression can be obtained. If the partition given by B.12 is considered, being $\dot{\boldsymbol{\sigma}}_\alpha$ and $\dot{\boldsymbol{\varepsilon}}_\beta$ the control variables, the trial stress is given by:

$$\begin{bmatrix} \dot{\boldsymbol{\sigma}}^{tr}_\alpha \\ \dot{\boldsymbol{\sigma}}^{tr}_\beta \end{bmatrix} = \begin{bmatrix} \dot{\boldsymbol{\sigma}}_\alpha \\ \mathbf{D}^e_{\beta\alpha}(\mathbf{D}^e_{\alpha\alpha})^{-1}\dot{\boldsymbol{\sigma}}_\alpha + \left(\mathbf{D}^e_{\beta\beta} - \mathbf{D}^e_{\beta\alpha}(\mathbf{D}^e_{\alpha\alpha})^{-1}\mathbf{D}^e_{\alpha\beta}\right)\dot{\boldsymbol{\varepsilon}}_\beta \end{bmatrix} \tag{B.19}$$

if it is considered that $\dot{\boldsymbol{\varepsilon}}^e_\beta = \dot{\boldsymbol{\varepsilon}}_\beta - \dot{\boldsymbol{\varepsilon}}^p_\beta$ and $\dot{\boldsymbol{\varepsilon}}^p_\beta = \dot{\Lambda}\frac{\partial g}{\partial \boldsymbol{\sigma}_\beta}$ Equation B.18 leads to an expression for the plastic multiplier $\dot{\Lambda}$.

$$\dot{\Lambda} = \frac{1}{H - H_\chi}\frac{\partial \tilde{f}}{\partial \boldsymbol{\sigma}}\dot{\boldsymbol{\sigma}}^{tr} \tag{B.20}$$

For a given set of control parameters, the value H_χ in EquationB.20 is given by the following expression:

$$H_\chi = -\frac{\partial \tilde{f}}{\partial \boldsymbol{\sigma}_\beta}\left(\mathbf{D}^e_{\beta\beta} - \mathbf{D}^e_{\beta\alpha}(\mathbf{D}^e_{\alpha\alpha})^{-1}\mathbf{D}^e_{\alpha\beta}\right)\frac{\partial g}{\partial \boldsymbol{\sigma}_\beta} \tag{B.21}$$

which under pure strain control coincides with the critical hardening modulus H_C. H_χ represents a family of scalar quantities which, together with the hardening modulus, control the inelastic response. Given the scalar nature of such quantities

and their control dependency, they are defined as *moduli of controllability*.
An equivalent controllability modulus can be written in mixed conditions also in terms of compliance matrix.
The elastic law can be rewritten as:

$$\begin{bmatrix} \dot{\boldsymbol{\varepsilon}}^e_\alpha \\ \dot{\boldsymbol{\varepsilon}}^e_\beta \end{bmatrix} = \begin{bmatrix} \mathbf{C}^e_{\alpha\alpha} & \mathbf{C}^e_{\alpha\beta} \\ \mathbf{C}^e_{\beta\alpha} & \mathbf{C}^e_{\beta\beta} \end{bmatrix} \begin{bmatrix} \dot{\boldsymbol{\sigma}}_\alpha \\ \dot{\boldsymbol{\sigma}}_\beta \end{bmatrix} \tag{B.22}$$

This expression can be written with the assumption that $\mathbf{C}^e_{\beta\beta}$ is not singular.
The consistency condition can thus be rearranged as:

$$\frac{\partial \tilde{f}}{\partial \boldsymbol{\sigma}_\alpha}\dot{\boldsymbol{\sigma}}_\alpha + \frac{\partial \tilde{f}}{\partial \boldsymbol{\sigma}_\beta}\mathbf{C}^{e-1}_{\beta\beta}\dot{\boldsymbol{\varepsilon}}^e_\beta + \frac{\partial \tilde{f}}{\partial \boldsymbol{\sigma}_\beta}\mathbf{C}^{e-1}_{\beta\beta}\mathbf{C}^e_{\beta\alpha}\dot{\boldsymbol{\sigma}}_\alpha - H\dot{\Lambda} = 0 \tag{B.23}$$

From Equations B.22 and B.23 the same formal expression given in Equation B.19 is retreived, in which the correspondent mathematical form of H_χ is given by:

$$H_\chi = -\frac{\partial \tilde{f}}{\partial \boldsymbol{\sigma}_\beta}\mathbf{C}^{e-1}_{\beta\beta}\frac{\partial g}{\partial \boldsymbol{\sigma}_\beta} \tag{B.24}$$

These results show that the loss of controllability and the plastic multiplier loss of definition are linked: loss of definition of the plastic multiplier verifies when

$$H_{IN} = H - H_\chi \leq 0 \tag{B.25}$$

This mathematical variable is given by the difference between the hardening modulus H and the controllability modulus H_χ and can be defined as a generalized instability modulus for that particular loading program.
Starting from EquationB.24 some comments regarding instability phenomena in the hardening regime can be done. The instability modulus coincides with the hardening modulus H in case of pure stress control conditions; in this case the test can be controlled only if $H_{IN} = H$ is strictly positive and failure takes place when $H \leq 0$. So in this particular case the intuitive notions of hardening ($H > 0$) and softening ($H < 0$) are directly linked with the possibility of controlling the material response.
In a more general control conditions, for example in mixed stress strain control conditions, the modulus of instability H_{IN} does not coincide with the hardening modulus, as it is characterized by the additional contribution H_χ. In this case, when an associated flow rule is adopted, Equations B.21 and B.24 are always characterized by a non positive value of H_χ and softening is required to have $H_{IN} < 0$. On the contrary a non associated flow rule, can produce situations in which H_χ is positive and for this reason H_{IN} can vanish even in the hardening regime (with $H = H_\chi > 0$) i.e. before classical failure.

B.3 Elastic-viscoplastic materials

As well know, according to the theory proposed by [Perzyna, 1963] an elastic-viscoplastic constitutive law can not be written in an incremetal form, so the approach described in the section 'Elastic perfectly plastic materials' cannot be used to describe the onset of instability in a elastic-viscoplastic material. For this reason [Pisanò and Prisco, 2016] developed an approach based on the combination of the controllability theory ([Nova, 1994]) and Lyapunov's theory of stability ([Lyapunov, 1892]).
According to this approach, the total ($\dot{\boldsymbol{\varepsilon}}$), the elastic ($\dot{\boldsymbol{\varepsilon}}^{el}$) and the irreversible viscoplastic ($\dot{\boldsymbol{\varepsilon}}^{irr}$) strain rate vectors can be partitioned considering the controlled strains and the measured strains.

$$\begin{bmatrix}\dot{\boldsymbol{\varepsilon}}_\beta\\ \dot{\boldsymbol{\varepsilon}}_\beta\end{bmatrix} = \begin{bmatrix}\dot{\boldsymbol{\varepsilon}}^{el}_\alpha\\ \dot{\boldsymbol{\varepsilon}}^{el}_\beta\end{bmatrix} + \begin{bmatrix}\dot{\boldsymbol{\varepsilon}}^{irr}_\alpha\\ \dot{\boldsymbol{\varepsilon}}^{irr}_\beta\end{bmatrix} = \begin{bmatrix}\mathbf{C}^{el}_{\alpha\alpha} & \mathbf{C}^{el}_{\alpha\beta}\\ \mathbf{C}^{el}_{\beta\alpha} & \mathbf{C}^{el}_{\beta\beta}\end{bmatrix}\begin{bmatrix}\dot{\boldsymbol{\sigma}}'_\alpha\\ \dot{\boldsymbol{\sigma}}'_\beta\end{bmatrix} + \Phi\begin{bmatrix}\frac{\partial g}{\partial \boldsymbol{\sigma}'_\alpha}\\ \frac{\partial g}{\partial \boldsymbol{\sigma}'_\beta}\end{bmatrix} \tag{B.26}$$

where $\Phi \geq 0$ is the non negative viscous nucleus.
To describe the relationship between the variables describing the system response (X) and their time derivative ($\dot{X}$) EquationB.26 is derived with respect to time. The previously mentioned relationship is linear ([Pisanò and Prisco, 2016]) and can be written as:

$$\dot{\mathbf{X}} = \mathbf{A}\mathbf{X} + \mathbf{F}, \tag{B.27}$$

where $\mathbf{F}$ is a 'forcing' term related to the control variables and $\mathbf{A}$ is a matrix depending on the constitutive relationship and controlled variables and is defined as:

$$\mathbf{A} = \begin{bmatrix}\mathbf{A}_{\alpha\alpha} & \mathbf{A}_{\alpha\beta}\\ 0 & \mathbf{A}_{\beta\beta}\end{bmatrix}. \tag{B.28}$$

If a generalised creep test is considered, for which $\dot{\boldsymbol{\sigma}}_\alpha = \ddot{\boldsymbol{\sigma}}_\alpha = \dot{\boldsymbol{\varepsilon}}_\beta = \ddot{\boldsymbol{\varepsilon}}_\beta = 0$, which also imply $\mathbf{F} = 0$, the terms of matrix $\mathbf{A}$ depend only on the constitutive relationship and can be expressed as follows ([Pisanò and Prisco, 2016]):

$$\mathbf{A}_{\alpha\alpha} = -\frac{\partial \phi}{\partial f}\big(H - H_\chi\big)\mathbf{I}_{\alpha\alpha} \tag{B.29}$$

$$\mathbf{A}_{\beta\beta} = -\frac{\partial \Phi}{\partial f}\big(H - H_\chi\big)\mathbf{I}_{\beta\beta} - \Phi\mathbf{C}^{el-1}_{\beta\beta}\frac{\partial^2 g}{\partial \boldsymbol{\sigma}'_\beta \otimes \partial \boldsymbol{\sigma}'_\beta} \tag{B.30}$$

$$\mathbf{A}_{\alpha\beta} = \Phi\left(\frac{\partial^2 g}{\partial \boldsymbol{\sigma}'_\alpha \otimes \partial \boldsymbol{\sigma}'_\beta} - \mathbf{C}^{el}_{\alpha\beta}\mathbf{C}^{el-1}_{\beta\beta}\frac{\partial^2 g}{\partial \boldsymbol{\sigma}'_\beta \otimes \partial \boldsymbol{\sigma}'_\beta}\right) \tag{B.31}$$

where $\mathbf{I}$ is the identity matrix.
From Lyapunov's stability theory ([Lyapunov, 1892]), in case $\mathbf{F} = 0$, if all the

eigenvalues of $\mathbf{A}$ are negative, a stable response is obtained. According to [Pisanò and Prisco, 2016], in case of a convex plastic potential in the stress space, all the eigenvalues of the matrix are negative in case $H > H_\chi$: which means that a process is unstable if:

$$H - H_\chi \leq 0 \tag{B.32}$$

Appendix C

Theoretical instability under simple shear conditions

In this chapter the local instability of an infinite slope under simple shear conditions will be discussed in the case of an elastoplastic material (Section C.1) and of an elastic-viscoplastic material (Section C.2).

C.1 Local instability condition for an elastoplastic material in simple shear conditions

The local response of an infinite stratum of an homogeneous cemented material of thickness H and slope α resting on a rigid bedrock will be hereafter theoretically discussed.
The reference system shown in Figure3.1 is given by the vector n, normal to the bedrock, the vector t, parallel to it and the vector y, which is the out of plane vector.
A simple shear condition is here analyzed, so the vectors of controlled Y variables and measured variables X are respectively:

$$\mathbf{Y} = \begin{bmatrix} \dot{\sigma}'_n & \dot{\tau}_{nt} & \dot{\varepsilon}_t = 0 & \dot{\varepsilon}_y = 0 \end{bmatrix}^T \tag{C.1}$$

$$\mathbf{X} = \begin{bmatrix} \dot{\varepsilon}_n & \dot{\gamma}_{nt} & \dot{\sigma}'_t & \dot{\sigma}'_y \end{bmatrix}^T \tag{C.2}$$

To describe the problem in the elastoplastic case, some ingredients are needed:

- an elastic constitutive law;
- a yield function, obeying the Mohr-Coulomb failure criterion, used to assess the starting of plastic strains;
- a plastic potential, to describe the development of plastic deformation;

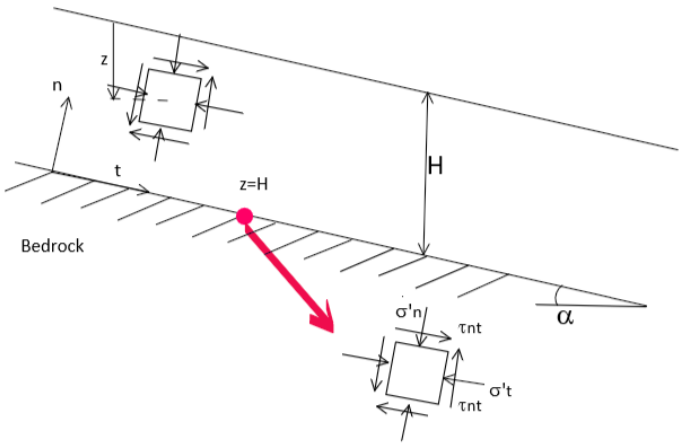

Figure C.1: Geometry of infinite slope configuration

- a softening law, to describe the variation of cohesion with deformation.

The following expression of f has been used.

$$f = \frac{1}{2}\left[\sqrt{4\tau_{nt}^2 + (\sigma'_n - \sigma'_t)^2} - (\sigma'_n + \sigma'_t)sin\phi' - 2c'cos\phi'\right] \tag{C.3}$$

The plastic potential is defined as:

$$g = \frac{1}{2}\left[\sqrt{4\tau_{nt}^2 + (\sigma'_n - \sigma'_t)^2} - (\sigma'_n + \sigma'_t)sin\psi - 2c'cos\psi\right] \tag{C.4}$$

The softening law is defined as:

$$\dot{c}' = -c'm\left(\left|\dot{\varepsilon}_n^{irr}\right| + \left|\dot{\varepsilon}_t^{irr}\right| + \left|\dot{\gamma}_{nt}^{irr}\right|\right) \tag{C.5}$$

This law describes the decrease of cohesion as deformation increases; the non-dimensional constitutive parameter m defines the brittleness of the material response. The cohesion progressively nullifies, starting from an initial value c'_0 and decreasing until $c' = 0$: in this case the material has been completely destructured and softening stops evolving.

C.1.1 Onset of shear band in simple shear conditions

Under simple shear condition the non dimensional controllability modulus previously described can be written in the following simplified way:

$$H_\chi = -\frac{\partial f}{\partial \sigma'_t}\frac{E}{1-\nu^2}\frac{\partial g}{\partial \sigma'_t} \tag{C.6}$$

In case of an elastic perfectly plastic material (i.e. $m = 0$ and $H = 0$), the instability conditions occurs if:

$$\frac{\partial f}{\partial \sigma'_t}\frac{\partial g}{\partial \sigma'_t} \leq 0 \tag{C.7}$$

C.2 Local instability condition for an elastic viscoplastic material in simple shear conditions

In this section the local response of an infinite slope in case of elastic-viscoplastic material will be theoretically discussed.
The elastic-viscoplastic constitutive relationship is characterized by:

- An isotropic linear elastic law
- A viscous nucleus defined as:

$$\Phi(f) = \begin{cases} 0 & if \quad f < 0 \\ \eta f & if \quad f \geq 0 \end{cases} \tag{C.8}$$

- A yield function, a plastic potential and a softening law equally defined as Equations C.3 ,C.4, C.5

The theoretical condition for onset of instability is now discussed; considering a generalized creep test with the assumption of simple shear conditions, EquationB.27 of Section B.3 becomes:

$$\dot{\mathbf{X}} = \begin{bmatrix} \ddot{\varepsilon}_n \\ \ddot{\gamma}_{nt} \\ \ddot{\sigma}'_t \\ \ddot{\sigma}'_y \end{bmatrix} = \begin{bmatrix} A_{11} & 0 & A_{13} & 0 \\ 0 & A_{22} & A_{23} & 0 \\ 0 & 0 & A_{33} & 0 \\ 0 & 0 & 0 & A_{44} \end{bmatrix} \begin{bmatrix} \dot{\varepsilon}_n \\ \dot{\gamma}_{nt} \\ \dot{\sigma}'_t \\ \dot{\sigma}'_y \end{bmatrix} = \mathbf{A}\mathbf{X} \tag{C.9}$$

The terms of matrix $\mathbf{A}$ are hereafter reported

$$A_{11} = A_{22} = -\frac{\partial \Phi}{\partial f}\big(H - H_\chi\big) \tag{C.10}$$

$$A_{33} = A_{44} = -\frac{\partial \Phi}{\partial f}\big(H - H_\chi\big) - \Phi\frac{E}{1-\nu^2}\frac{\partial^2 g}{\partial \sigma'_t} \tag{C.11}$$

$$A_{13} = \Phi\left(\frac{\partial^2 g}{\partial \sigma'_n \partial \sigma'_t} - \frac{\nu}{1-\nu}\frac{\partial^2 g}{\partial \sigma'^2_t}\right) \tag{C.12}$$

$$A_{23} = \Phi\frac{\partial^2 g}{\partial \tau_{nt} \partial \sigma'_t} \tag{C.13}$$

Since in this case the matrix $\mathbf{A}$ is an upper triangular matrix, its eigenvalues are the terms on the main diagonal:

$$\lambda_1 = \lambda_2 = A_{11} = A_{22} \tag{C.14}$$

$$\lambda_3 = \lambda_4 = A_{33} = A_{44} = \lambda_1 - \Phi \frac{E}{1-\nu^2} \frac{\partial^2 g}{\partial \sigma_t^2} \tag{C.15}$$

As E, Φ and $\frac{\partial \Phi}{\partial f}$ are positive, $\lambda_1 \geq \lambda_3$, so the instability condition is given by:

$$\lambda_1 \geq 0 \iff H - H_\chi \leq 0 \tag{C.16}$$

In the elastoplastic case, loss of controllability in terms of γ_{nt} and ε_{nt} is simultaneous ($\lambda_1 = \lambda_2$). But when λ_1 nullifies, λ_3 is still negative. This suggests that the loss of controllability in terms of strains anticipates the loss of controllability in terms of stresses. This time lag depends on the η value. In fact, increasing η, the difference between λ_1 and λ_3 value decreases. For $\eta \to \infty$ the difference vanishes and all the response variables become simultaneously unstable, as it is obtained in the elasto-plastic case.

References

[Alegre et al., 2001] Alegre, P., Grande, R., and Fe, R. (2001). of C Emented S and in. *Manager*, 127(October):857–868.

[Amini and Hamidi, 2014] Amini, Y. and Hamidi, A. (2014). Triaxial shear behavior of a cement-treated sand-gravel mixture. *Journal of Rock Mechanics and Geotechnical Engineering*, 6(5):455–465.

[Atkinson, 1984] Atkinson, B. K. (1984). Subcritical Crack Growth in Geological Materials. *Journal of Geophysical Research*, 89(B6):4077–4114.

[Baud and Meredith, 1997] Baud, P. and Meredith, P. G. (1997). Damage accumulation during triaxial creep of Darley Dale sandstone from pore volumometry and acoustic emission. *International journal of rock mechanics and mining sciences & geomechanics abstracts*, 34(3-4):371.

[Baynes and Dearman, 1978] Baynes, F. J. and Dearman, W. R. (1978). The relationship between the microfabric and the engineering properties of weathered granite. *Bulletin of the International Association of Engineering Geology - Bulletin de l'Association Internationale de Géologie de l'Ingénieur*, 18(1):191–197.

[Bigoni and Hueckel, 1991] Bigoni, D. and Hueckel, T. (1991). Uniqueness and localization—I. Associative and non-associative elastoplasticity. *International Journal of Solids and Structures*, 28(2):197–213.

[Bigot-Cormier et al., 2005] Bigot-Cormier, F., Braucher, R., Bourlès, D., Guglielmi, Y., Dubar, M., and Stéphan, J.-F. (2005). Chronological constraints on processes leading to large active landslides. *Earth and Planetary Science Letters*, 235(1-2):141–150.

[Bishop, 1970] Bishop, A. W. (1970). The influcence of progressive failure on the choice of the method of stability analysis. (1967):168–172.

[Bjerrum, 1973] Bjerrum, L. (1973). Problems of soil mechanics and construction on soft clays and structurally unstable soils. page 193.

[Bonzanigo et al., 2007] Bonzanigo, L., Eberhardt, E., and Loew, S. (2007). Long-term investigation of a deep-seated creeping landslide in crystalline rock. Part I. Geological and hydromechanical factors controlling the Campo Vallemaggia landslide. *Canadian Geotechnical Journal*, 44(10):1157–1180.

[Bouissou et al., 2012] Bouissou, S., Darnault, R., Chemenda, A., and Rolland, Y. (2012). Evolution of gravity-driven rock slope failure and associated fracturing:

Geological analysis and numerical modelling. *Tectonophysics*, 526:157–166.

[Buscarnera et al., 2011] Buscarnera, G., Dattola, G., and Prisco, C. (2011). International Journal of Solids and Structures Controllability , uniqueness and existence of the incremental response : A mathematical criterion for elastoplastic constitutive laws. *International Journal of Solids and Structures*, 48(13):1867–1878.

[Cascini et al., 2014] Cascini, L., Calvello, M., and Grimaldi, G. M. (2014). Displacement trends of slow-moving landslides: Classification and forecasting. *Journal of Mountain Science*, 11(3):592–606.

[Castellanza, 2002] Castellanza, R. (2002). Weathering effects on the mechanical behaviour of bonded geomaterials: an experimental, theoretical and numerical study. *PhD Thesis, Politecnico di Milano.*

[Castellanza et al., 2002] Castellanza, R., Nova, R., and Tamagnini, C. (2002). Mechanical effects of chemical degradation of bonded geomaterials in boundary value problems. *Revue Française de Génie Civil*, 6(6):1169–1192.

[Chandler, 1984] Chandler, R. (1984). Recent european experience of landslides in over-consolidated clays and soft rocks (state-of-the-art lecture). In *Proc. 4th Int. Symp. Landslides Toronto*, volume 1, pages 61–81.

[Ciantia and Castellanza, 2016] Ciantia, M. O. and Castellanza, R. (2016). Modelling weathering effects on the mechanical behaviour of rocks. *European Journal of Environmental and Civil Engineering*, 20(9):1054–1082.

[Ciantia and Di Prisco, 2016] Ciantia, M. O. and Di Prisco, C. (2016). Extension of plasticity theory to debonding, grain dissolution, and chemical damage of calcarenites. *International Journal for Numerical and Analytical Methods in Geomechanics*, 40(3):315–343.

[Coop and Atkinson, 1994] Coop, M. R. and Atkinson, J. H. (1994). The mechanics of cemented carbonate sands. *Geotechnique*, 44(3):533–537.

[Coop and Cuccovillo, 1997] Coop, M. R. and Cuccovillo, T. (1997). Yielding and pre-failure deformation of structured sands. *Geotechnique*, 47(3):491–508.

[Crosta et al., 2014] Crosta, G., Frattini, P., Frigerio, G., and Castellanza, R. (2014). Chasing a complete understanding of the triggering mechanisms of a large rapidly evolving rockslide Chasing a complete understanding of the triggering mechanisms of a large rapidly evolving rockslide. (October).

[Crosta et al., 2006] Crosta, G. B., Chen, H., and Frattini, P. (2006). Forecasting hazard scenarios and implications for the evaluation of countermeasure efficiency for large debris avalanches. *Engineering Geology*, 83(1-3):236–253.

[Dapples, E., 1972] Dapples, E., C. (1972). Some concepts of cementation and lithification of sandstones. *American Association of Petroleum Geologists Bulletin*, 56(1):3–25.

[D'Elia, B.,Picarelli, L., Leroueil, S., Vaunat, 1998] D'Elia, B.,Picarelli, L., Leroueil, S., Vaunat, J. (1998). Geotechnical characterization of slope movements in structurally complex caly soils and stiff jointed clays.

[di Prisco, 2012a] di Prisco, C. (2012a). Creep versus transient loading effects in geotechnical problems. *CISM International Centre for Mechanical Sciences, Courses and Lectures*, 534:227–261.

[di Prisco and Flessati, 2019] di Prisco, C. and Flessati, L. (2019). Progressive failure in elastic – viscoplastic media : from theory to practice. pages 0–2.

[di Prisco, 2012b] di Prisco, C. G. (2012b). in Materiali Cementati. *Slope stability*, pages 73–92.

[Emery, 1978] Emery, J. J. (1978). *Simulation of slope creep*, volume 14. Elsevier Scientific Publishing Company.

[Freitas et al., 2013] Freitas, T. M., Potts, D. M., and Zdravkovic, L. (2013). Some strengths and weaknesses of overstress based elastic viscoplastic models. *Springer Series in Geomechanics and Geoengineering*, pages 107–114.

[Harr, 1985] Harr, M. E. (1985). Reliability-Based Design in Civil Engineering. 3:619–623.

[Helmstetter et al., 2004] Helmstetter, A., Sornette, D., Grasso, J.-R., Andersen, J. V., Gluzman, S., and Pisarenko, V. (2004). Slider block friction model for landslides: Application to Vaiont and La Clapière landslides. *Journal of Geophysical Research: Solid Earth*, 109(B2).

[Hill, 1958] Hill, R. (1958). A general theory of uniqueness and stability in elastic-plastic solids. *Journal of the Mechanics and Physics of Solids*, 6(3):236–249.

[Hueckel and Maier, 1977] Hueckel, T. and Maier, G. (1977). Incremental boundary value problems in the presence of coupling of elastic and plastic deformations: A rock mechanics oriented theory. *International Journal of Solids and Structures*, 13(1):1–15.

[Hutchinson, 1987] Hutchinson, J. (1987). Mechanisms producing large displacements in landslides on pre-existing shears.

[Imposimato and Nova, 1998] Imposimato, S. and Nova, R. (1998). An investigation on the uniqueness of the incremental response of elastoplastic models for virgin sand. 3(December 1996):65–87.

[Kimmance, 1988] Kimmance, J. P. (1988). *Computer aided risk analysis of open pit mine slopes in kaolin mined deposit*. PhD thesis.

[Lagioia and Nova, 1995a] Lagioia, R. and Nova, R. (1995a). An experimental and theoretical study of the behaviour of a calcarenite in triaxial compression. *Geotechnique*, 45(4):633–648.

[Lagioia and Nova, 1995b] Lagioia, R. and Nova, R. (1995b). An experimental and theoretical study of the behaviour of a calcarenite in triaxial compression. *Géotechnique*, 45(4):633–648.

[Leroueil, 2001] Leroueil, S. (2001). Natural slopes and cuts: Movement and failure mechanisms. *Geotechnique*, 51(3):197–243.

[Leroueil et al., 1996] Leroueil, S., Locat, J., Vaunat, J., Picarelli, L., and Lee, H. (1996). Geotechnical characterization of slope movements. In *Landslides*, pages 53–74.

[Leroueil, 1990] Leroueil, S. P. V. (1990). The general and congruent effects of structure in natural soils and weak rocks. Géotechniq(3):467–488.

[Lyapunov, 1892] Lyapunov (1892). The General Problem of the Stability of Motion. 31(2).

[Maier, 1966] Maier, G. (1966). Sui legami associati tra sforzi e deformazioni incrementali in elastoplasticità. *Rendiconti dell'Istituto Lombardo di Scienze e Lettere*, 100:809–838.

[Maier and Hueckel, 1979] Maier, G. and Hueckel, T. (1979). Nonassociated and coupled flow rules of elastoplasticity for rock-like materials. *International Journal of Rock Mechanics and Mining Sciences and*, 16(2):77–92.

[Morgenstern, 1990] Morgenstern, N. (1990). Instability mechanisms in stiff soils and weak rocks. In *Proc 10th Southeast Asian Geotechnical Conf*, pages 27–36.

[Morgenstern, 1967] Morgenstern, N. R. (1967). Microscopic Structures in Kaolin Subjected To. *Science*, (1965).

[Nova, 1977] Nova, R. (1977). on the Hardening of Soils. *Arch Mech*, 29(3):445–458.

[Nova, 1986] Nova, R. (1986). Soil models as a basis for modelling the behaviour of geophysical materials. *Acta Mechanica*, 64(1-2):31–44.

[Nova, 1992] Nova, R. (1992). Mathematical modelling of natural and engineered geomaterials. general lecture 1st ecsm munchen. *Eur. J. Mech. A/Solids*, 11:135–154.

[Nova, 1994] Nova, R. (1994). Controllability of the Incremental Response of Soil Specimens Subjected. *Journal of the Mechanical Behavior of Materials*, 5(2):193–202.

[Nova et al., 2003] Nova, R., Castellanza, R., and Tamagnini, C. (2003). A constitutive model for bonded geomaterials subject to mechanical and/or chemical degradation. *International Journal for Numerical and Analytical Methods in Geomechanics*, 27(9):705–732.

[Perzyna, 1963] Perzyna, P. (1963). The constitutive equations for rate sensitive plastic materials. *Quarterly of Applied Mathematics*, 20(4):321–332.

[Phoon et al., 1999] Phoon, K., Nadim, F., Uzielli, M., and Lacasse, S. (1999). Soil variability analysis for geotechnical practice. *Characterisation and Engineering Properties of Natural Soils*, (December).

[Phoon et al., 2006] Phoon, K., Nadim, F., Uzielli, M., and Lacasse, S. (2006). Soil variability analysis for geotechnical practice. *Characterisation and Engineering Properties of Natural Soils*, (December).

[Pisanò and Prisco, 2016] Pisanò, F. and Prisco, C. (2016). A stability criterion for elasto-viscoplastic constitutive relationships. (June 2015):141–156.

[Prisco and Imposimato, 1996] Prisco, C. and Imposimato, S. (1996). Time dependent mechanical behaviour of loose sands. 1(September 1995):45–73.

[Puzrin and Schmid, 2011] Puzrin, A. M. and Schmid, A. (2011). Progressive failure of a constrained creeping landslide. In *Proceedings of the Royal Society A:*

Mathematical, Physical and Engineering Sciences, volume 467, pages 2444–2461.

[Riedel, 1929] Riedel, W. (1929). Zur mechanik geologischer brucherscheinungen ein beitrag zum problem der fiederspatten. *Zentbl. Miner. Geol. Palaont. Abt.*, pages 354–368.

[Scoppettuolo et al., 2020] Scoppettuolo, M. R., Cascini, L., and Babilio, E. (2020). Typical displacement behaviours of slope movements. *Landslides*.

[Secondi et al., 2011] Secondi, M., Crosta, G., di Claudio Giulio, Frigerio, G., Frattini, P., and Agliardi, F. (2011). Landslide motion forecasting by a dynamic visco-plastic model. pages 1–6.

[Secondi et al., 2013] Secondi, M. M., Crosta, G., Prisco, C., Frigerio, G., Frattini, P., and Agliardi, F. (2013). Landslide Science and Practice. *Landslide Science and Practice*, 3(1):151–159.

[Sharma and Fahey, 2003] Sharma, S. S. and Fahey, M. (2003). Degradation of stiffness of cemented calcareous soil in cyclic triaxial tests. *Journal of Geotechnical and Geoenvironmental Engineering*, 129(7):619–629.

[Singh, 1966] Singh, A. (1966). *Creep phenomena in soils*. PhD thesis, University of California, Berkeley.

[Skempton et al., 1966] Skempton, A. et al. (1966). Some observations on tectonic shear zones. In *1st ISRM Congress*. International Society for Rock Mechanics and Rock Engineering.

[Tavenas et al., 1971] Tavenas, F., Chagnon, J.-Y., and Rochelle, P. L. (1971). The Saint-Jean-Vianney Landslide: Observations and Eyewitnesses Accounts. *Canadian Geotechnical Journal*, 8(3):463–478.

[Taylor, 1948] Taylor, D. W. (1948). Fundamentals of soil mechanics.

[Terzaghi, 1950] Terzaghi, K. (1950). *Mechanism of Landslides*. Number November.

[Terzaghi K., 1948] Terzaghi K., P. R. B. (1948). *Soil mechanics in engineering practice*.

[Van Eekelen, 1980] Van Eekelen, H. (1980). Isotropic yield surfaces in three dimensions for use in soil mechanics. *International Journal for Numerical and Analytical Methods in Geomechanics*, 4(1):89–101.

[Vaughan and Hamza, 1977] Vaughan, P. and Hamza, M. (1977). Clay embankments and foundations: Monitoring stability by measuring deformations. In *Specialty session*, volume 8, pages 37–48.

[Wang, 2015] Wang, J. (2015). *Landslide risk assessment in Wanzhou County, Three Gorges Reservoir*. PhD thesis, Dissertation, China University of Geosciences.

[Wilcox et al., 1981] Wilcox, R. E., Harding, T. t., and Seely, D. (1981). Basic wrench tectonics.

[Xiao et al., 2020] Xiao, L., Wang, J., Zhu, Y., and Zhang, J. (2020). Quantitative Risk Analysis of a Rainfall-Induced Complex Landslide in Wanzhou County,

Three Gorges Reservoir, China. *International Journal of Disaster Risk Science*, 11(3):347–363.